

**Requirements for pre-catalytic B complex formation
during exon- and intron-defined spliceosome assembly**

Dissertation

for the award of the degree

„Doctor rerum naturalium“

of the Georg-August-Universität Göttingen

submitted by

Carsten Boesler

from Homberg (Efze)

Göttingen 2014

Members of the Examination Board:

Prof. Dr. Reinhard Lührmann (1st Referee)

Department of Cellular Biochemistry

Max Planck Institute for Biophysical Chemistry, Göttingen

Prof. Dr. Henning Urlaub (2nd Referee)

Research Group Bioanalytical Mass Spectrometry

Max Planck Institute for Biophysical Chemistry, Göttingen

Prof. Dr. Markus Zweckstetter

Department for NMR-based Structural Biology

Max Planck Institute for Biophysical Chemistry, Göttingen

Prof. Dr. Ralf Ficner

Department for Molecular Structural Biology

Georg-August-Universität Göttingen

Prof. Dr. Holger Stark

Research Group 3D Electron Cryo-Microscopy

Max Planck Institute for Biophysical Chemistry, Göttingen

Dr. Claudia Höbartner

Research Group Nucleic Acid Chemistry

Max Planck Institute for Biophysical Chemistry, Göttingen

Date of oral examination: 19.12.2014

**For my family,
for my friends**

Table of contents

Abstract.....	1
1. Introduction	4
1.1 Pre-mRNA splicing.....	4
1.2 The two step mechanism of splicing	5
1.3 Alternative splicing enhances the proteome post-transcriptionally.....	6
1.4 Composition of spliceosomal snRNPs	7
1.5 Protein inventory of the human snRNPs.....	9
1.6 Stepwise assembly of the spliceosome.....	11
1.7 The dynamic RNA-RNA network in the spliceosome	13
1.8 Dynamics of the spliceosome's protein composition	15
1.9 The role of RNA helicases in splicing.....	17
1.10 Structure of spliceosomal complexes	19
1.11 Exon definition is an alternative pathway to initiate spliceosome assembly	20
1.12 Aims.....	23
2. Materials and methods	25
2.1 Materials	25
2.1.1 Chemicals	25
2.1.2 Chromatography materials and consumables	27
2.1.3 Commerical kits.....	27
2.1.4 Machines	28
2.1.5 Nucleotides.....	29
2.1.6 Radiolabeled nucleotides	29
2.1.7 RNA oligonucleotides	29
2.1.8 Antibodies	30
2.1.9 Enzymes.....	30
2.1.10 Plasmids.....	31
2.1.11 Bacteria strains.....	31
2.1.12 Cell line	31
2.1.13 Buffers	31
2.2 Methods	35
2.2.1 Molecular biology standard methods.....	35
2.2.1.1 Nucleic acid quantification.....	35
2.2.1.2 PCI extraction	35

2.2.1.3 Proteinase K digestion.....	35
2.2.1.4 Generation of templates for run-off <i>in vitro</i> transcriptions.....	36
2.2.1.5 <i>In vitro</i> transcription.....	36
2.2.1.6 Denaturing polyacrylamide gel-electrophoresis	37
2.2.1.7 Silver staining of RNA	37
2.2.1.8 Northern blot	37
2.2.1.9 Radioactive 5'-labeling of RNA oligonucleotides	38
2.2.2 Protein-biochemistry standard methods	38
2.2.2.1 Protein quantification	38
2.2.2.2 Denaturing SDS polyacrylamide gel-electrophoresis (SDS-PAGE).....	38
2.2.2.3 Coomassie staining.....	39
2.2.2.4 Silver staining of proteins.....	39
2.2.2.5 Western blot.....	39
2.2.2.6 Purification of MS2-MBP	40
2.2.2.7 Purification of recombinant hPrp28 proteins	40
2.2.2.8 Purification of antibodies	41
2.2.3 Special methods	42
2.2.3.1 Cell culture	42
2.2.3.2 Preparation of splicing active HeLa nuclear extract.....	42
2.2.3.3 <i>In vitro</i> splicing reactions.....	42
2.2.3.4 Analysis of splicing complexes by native agarose gel-electrophoresis	43
2.2.3.5 MS2 affinity-selection of splicing complexes	43
2.2.3.6 Psoralen-mediated RNA-RNA crosslinking	44
2.2.3.7 UV crosslinking of spliceosomal complexes	44
2.2.3.8 Immunoprecipitation of protein-RNA crosslinks.....	44
2.2.3.9 Two-dimensional gel-electrophoresis of spliceosomal complexes.....	45
2.2.3.10 Electron microscopy	45
2.2.3.11 Mass spectrometry.....	46
3. Results.....	47
3.1 A stable 45S B-like complex is formed upon addition of a 5'splice site-containing RNA oligonucleotide.....	47
3.1.1 Stabilization of U4/U6.U5 tri-snRNP integration is not induced by removing U1 snRNP from the downstream 5'ss.....	49
3.2 Formation of the 45S B-like complex is accompanied by the recruitment of B complex-specific proteins	49

3.3 EM reveals a major structural difference between the 37S exon and the 45S B-like complex..	53
3.4 Interaction of the 5'ss oligonucleotide with affinity-purified 37S exon complexes induces a structural change resulting in stable U4/U6.U5 tri-snRNP binding	55
3.4.1 ATP hydrolysis is not required for the shift in the S-value from 37S to 45S	58
3.4.2 Phosphorylation of hPrp31 is not required for transforming the 37S exon complex into a 45S complex	58
3.5 EM reveals a structural change in the purified 37S exon complex after addition of the 5'ss oligonucleotide.....	59
3.6 Sequence requirements of the 5'ss oligonucleotide for U4/U6.U5 tri-snRNP stabilization during B-like complex formation	61
3.6.1 The exon-intron junction of the 5'ss oligonucleotide interacts with the U5 protein hPrp8 in stably-assembled 45S B-like complexes.....	61
3.6.2 Base pairing interactions between 5'ss and U6 ACAGAG box are not absolutely required for stable B-like complex formation	63
3.6.3 Mutations of nucleotides at the exon-intron junction that contact hPrp8 abolish formation of a stable 45S B-like complex.....	65
3.6.4 Double mutations at the intron-exon boundary abolish binding of 5'ss oligonucleotide to the exon complex.....	66
3.6.5 Recruitment of B complex-specific proteins is independent of complex stability in presence of heparin	68
3.7 A dominant-negative mutant of the DEAD-box helicase hPrp28 stalls spliceosome assembly prior to stable B complex formation	70
3.8 Isolation and characterization of a novel intron-defined spliceosome assembly intermediate.	72
3.9 The 37S cross-intron and 37S exon complexes have nearly identical protein compositions	78
3.10 Analysis of the RNA-RNA network in the 37S cross-intron complex.....	80
3.11 Electron microscopy investigation of the 37S cross-intron complex.....	82
3.12 The 37S cross-intron complex is converted into a stable B complex in presence of a 5'ss oligonucleotide.....	85
3.13 EM reveals that the purified 37S cross-intron complexes adopt a B complex appearance after incubation with the 5'ss oligonucleotide	88
4. Discussion	90
4.1 Addition of a 5'ss-containing RNA oligonucleotide transforms the 37S exon complex into a 45S B-like complex with stably-integrated U4/U6.U5 tri-snRNP	91
4.2 B complex-specific proteins are recruited upon formation of the 45S B-like complex, but are not required for stable integration of the U4/U6.U5 tri-snRNP	91
4.3 Stable binding of the U4/U6.U5 tri-snRNP likely depends on the interactions with U2 snRNP proteins	93
4.4 The hPrp4 kinase is abundant solely in the 37S exon complex	93

4.5 The proteins THRAP3 and BCLAF1 are abundant in exon-defined spliceosomes	94
4.6 The 37S exon complex undergoes a major structural change upon interaction with the 5'ss oligonucleotide and adopts the appearance of a cross-intron B complex	95
4.7 Sequence requirements for the 5'splice site to induce stable U4/U6.U5 tri-snRNP binding	97
4.8 Structural implications for the stabilizing effect of a 5'ss sequence on stable U4/U6.U5 tri-snRNP binding	100
4.9 A dominant-negative mutant of the DEAD-box helicase hPrp28 inhibits stable B complex formation	101
4.10 Identification of a novel cross-intron assembly intermediate that is formed prior to hPrp28 action.....	102
4.11 The 37S cross-intron complex can be converted into a stable B complex via addition of a 5'ss oligonucleotide.....	103
4.12 The 37S cross-intron and 37S exon complex adopt an almost identical appearance upon interaction with a 5'ss oligonucleotide.....	104
4.13 Changes in the RNA-RNA network during spliceosome assembly prior to the first catalytic step	106
4.14 The role of hPrp28 in formation of a stable B complex	107
4.15 Perspectives	109
5. References.....	111
6. Appendix.....	119
6.1 Abbreviations	119
6.2 Danksagung	122
6.3 Curriculum vitae	123

Abstract

In eukaryotes, most protein-coding genes are interrupted by non-coding sequences known as introns. The splicing of intronic sequences from a pre-mRNA is catalyzed by the spliceosome, an elaborate molecular machine formed by the interaction of five snRNPs and numerous splicing factors with the pre-mRNA. Initial assembly of the spliceosome can occur across an intron sequence (intron definition) or alternatively across an exon (exon definition). The latter is likely the prominent pathway for pre-mRNAs with long intronic sequences, which is characteristic for most human pre-mRNAs. As splicing catalysis can only occur across introns, a rearrangement from the exon-defined to intron-defined state is required. This rearrangement can be a critical point during the decision whether to include or to skip an exon in the mature mRNA during the process of alternative splicing. Recently exon-defined spliceosomes were shown to contain not only U1 and U2 snRNPs, but also the U4/U6.U5 tri-snRNP (37S exon complex), and evidence was provided that it is possible for a cross-exon complex to be converted directly into an intron-defined B complex.

During my studies, I addressed the question what are the requirements for stable integration of the U4/U6.U5 tri-snRNP and formation of a pre-catalytic B complex during exon- and intron-defined spliceosome assembly, since this is a crucial point in which the alternative assembly pathways converge.

To address this aim, I used a reductionist *in vitro* system to assemble the 37S exon complex on a single exon-containing RNA substrate in HeLa nuclear extract. The addition *in trans* of an RNA oligonucleotide containing a 5'splice site sequence (5'ss oligonucleotide) mimics an adjacent upstream 5'ss and induces the formation of a 45S B-like complex, which shares similarities with the intron-defined B complex. The transition from a 37S exon to a 45S B-like complex is accompanied by the stable integration of the U4/U6.U5 tri-snRNP within the complex and a significant shift in the sedimentation behavior, suggesting structural changes in the complex during its stabilization. Indeed, electron microscopy (EM) revealed major structural differences between 37S exon and 45S B-like complexes, likely due to a different orientation of the U2 snRNP and the U4/U6.U5 tri-snRNP with respect to each other, while the structure of the 45S B-like complex was highly similar to that of an intron-defined B complex. Thus, formation of a B-like complex and consequently the stable integration of the U4/U6.U5 tri-snRNP is indeed accompanied by significant structural remodeling of the spliceosome.

To identify factors that might contribute to the structural remodeling and the stabilization of U4/U6.U5 tri-snRNP binding, we identified highly-abundant proteins associated with the 37S exon

and 45S B-like complexes by 2D gel-electrophoresis. The comparison of their protein compositions showed the recruitment of a distinct set of B complex-specific proteins, namely RED, MFAP1, FBP21, hSmu-1, hPrp38 and hSnu23, upon formation of the 45S B-like complex. These proteins are also recruited during formation of the intron-defined B complex, underlining the compositional and structural similarities of the 45S B-like and B complex. However, the B complex-specific proteins do not appear to contribute to stable U4/U6.U5 tri-snRNP integration, since solely the interaction of the 5'ss oligonucleotide with affinity-purified 37S exon complexes in the absence of splicing extract triggers the structural rearrangement that supports stable U4/U6.U5 tri-snRNP integration.

The defined changes in structure, stability and protein composition during transition from a 37S exon to 45S B-like complex are induced solely by the addition of a 5'ss oligonucleotide to the splicing reaction. Thus, I investigated the requirements for functional interaction of a 5'ss sequence with components of the U4/U6.U5 tri-snRNP to induce the formation of a stable 45S B-like complex. Studies using 5'ss oligonucleotides with mutated sequences indicated that base pairing with the ACAGAG box motif of U6 snRNA is not required to trigger the observed structural rearrangement. But instead, highly conserved guanine residues at the exon-intron junction are essential for the formation of a stable 45S B-like complex and I could show that these residues within the 5'ss oligonucleotide are contacted only by the U5-specific protein hPrp8, pointing to a crucial role of hPrp8 in stabilizing the binding of the U4/U6.U5 tri-snRNP. Further, my studies provide evidence that the stable integration of the U4/U6.U5 tri-snRNP not only depends on the recognition of the exocyclic part of these guanines, but also on interactions with the ribose backbone of the RNA.

Based on the results in the exon-defined assembly pathway and the similarities between the 45S B-like and B complex, I assumed that stable incorporation of the U4/U6.U5 tri-snRNP during intron-defined B complex formation also requires its interaction with the 5'ss of the pre-mRNA. Consequently, I set out to stall intron-defined spliceosome assembly just prior to stable B complex formation in order to test if the stable integration of the U4/U6.U5 tri-snRNP during B complex formation also relies on the interaction with a 5'ss. The DEAD-box helicase hPrp28 is involved in the displacement of U1 snRNP from the 5'ss and was recently shown to be essential for the formation of a stable intron-defined B complex. Thus, I chose hPrp28 as a target to inhibit spliceosome assembly prior to formation of a B complex. The use of a dominant-negative mutant of hPrp28, lacking its ATPase activity, inhibited B complex formation, but not formation of the A complex, and allowed me to affinity-purify a novel intermediate in the intron-defined spliceosome assembly pathway, namely the 37S cross-intron complex. Characterization of this complex showed that it contains all five snRNPs, but in contrast to the pre-catalytic B complex, the U4/U6.U5 tri-snRNP is not yet stably-integrated. Thus, in the absence of hPrp28 function, the U4/U6.U5 snRNP can associate with the spliceosome, while U1 snRNP is still present in the complex. Psoralen-mediated RNA-RNA crosslinking

showed that in the 37S cross-intron complex U1 snRNA is base paired with the pre-mRNA, while the U6 snRNA establishes base pairing interactions with the U2 snRNA. In the B complex, no base pairing interactions between U1 and the pre-mRNA were detected. Instead we detected interactions between the U4/U6.U5 tri-snRNP and the pre-mRNA, while the U4 and U6 snRNA were still base paired. These data suggest that due to the retention of U1 snRNP at the 5'ss of the pre-mRNA, this sequence is not available for interaction with the U4/U6.U5 tri-snRNP and thus the transition to a pre-catalytic B complex is inhibited. Investigations of the protein composition of the 37S cross-intron complex by mass spectrometry and 2D gel-electrophoresis revealed distinct differences compared to the B complex, in particular the lack of the B complex-specific proteins. Surprisingly, the 37S cross-intron complex is compositionally very similar to the 37S exon complex, indicating that the exon- and intron-defined assembly pathways both involve a similar intermediate where U4/U6.U5 tri-snRNP has docked, but is not yet stably-integrated. However, structural investigation of the 37S cross-intron complex identified differences in its appearance in comparison to the 37S exon complex, suggesting that despite their similar protein inventory, the organization of these complexes is different.

The addition *in trans* of an accessible 5'ss in the form of a short RNA oligonucleotide to the splicing reaction resulted in the formation of a stable B complex, even in presence of the dominant-negative hPrp28 mutant. These results show that the 37S cross-intron complex is competent for stable B complex formation, but due to the lack of an accessible 5'ss that can interact with the U4/U6.U5 tri-snRNP, the stable integration of the latter cannot occur. The stable integration of the U4/U6.U5 tri-snRNP is also supported by addition of the 5'ss sequence to an affinity-purified 37S cross-intron complex, showing that all factors required for the stable integration of the U4/U6.U5 tri-snRNP are already present in the this complex. EM analyses of this stabilized cross-intron complex revealed structural features similar to those of the 37S exon complex after addition of the 5'ss oligonucleotide, showing that the conformational remodeling that occurs during stable U4/U6.U5 tri-snRNP binding, leads to a nearly identical architecture of both complexes. These results indicate that the exon- and intron-defined assembly pathway of the spliceosome converge at the stage where the 37S complexes become committed to a 5'ss sequence via interaction with the U4/U6.U5 tri-snRNP. In summary, our studies provide new insights into the mechanisms underlying the stable association of the U4/U6.U5 tri-snRNP during B complex formation, which is a prerequisite for the catalytic activation of the spliceosome.

1. Introduction

1.1 Pre-mRNA splicing

Most eukaryotic genes are first transcribed into a pre-mRNA, which contains protein-coding exon and non-coding intron sequences. During a process called splicing, the intronic sequences are excised from the pre-mRNA and the exons are ligated together in order to generate mature mRNAs. Pre-mRNA splicing is catalyzed by the spliceosome, an elaborate and highly dynamic molecular machine that assembles *de novo* for each round of splicing [reviewed in Wahl *et al.*, 2009, Will and Lührmann, 2011].

The most challenging task of a spliceosome is to identify the precise boundaries of an exon to avoid the production of aberrant mRNAs. Thus, pre-mRNA introns are characterized by short, conserved sequences, so-called splice sites, which define the ends of the intron (Figure 1.1). These conserved motifs are recognized by components of the spliceosome and initiate its assembly on the pre-mRNA. The 5' splice site (5'ss) sequence defines the boundary between an exon and a downstream intron, and is composed of AG/GURAGU in *Homo sapiens* (*H. sapiens*), where R stands for a purine (G or A) and '/' indicates the exon/intron boundary [Zhang, 1998]. In *Saccharomyces cerevisiae* (*S. cerevisiae*) this sequence is composed of GUAUGU and is highly conserved with a sequence identity of more than 90 % [Lopez and Seraphin, 1999]. The 3' splice site (3'ss) sequence defines the boundary between an intron and the downstream exon, and in *H. sapiens* as well as in *S. cerevisiae*, it is composed of YAG, where Y stands for a pyrimidine (C or U) [Lopez and Seraphin, 1999]. Additionally, a conserved sequence element surrounds the adenosine that forms a branched intermediate during the first step of splicing. This sequence is therefore called the branch point sequence (BPS).

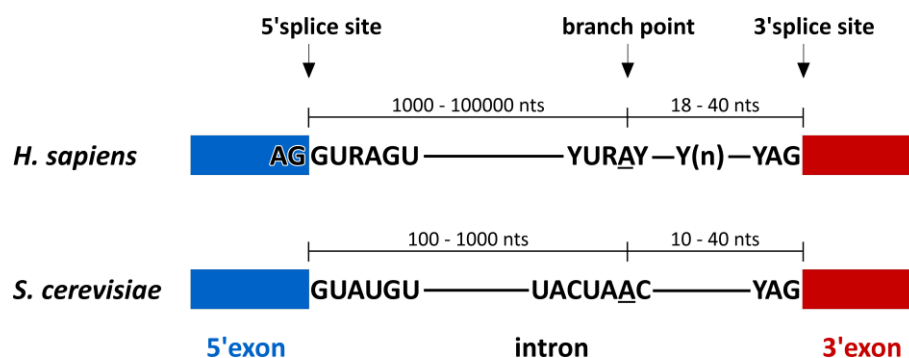


Figure 1.1: Conserved splicing signals from *H. sapiens* and *S. cerevisiae*

Schematic representation of conserved consensus sequences defining an intron. The branch point adenosine is underlined and the polypyrimidine tract is represented by Y(n). Y: pyrimidines (C or T), R: purines (A or G), nts: nucleotides.

In human pre-mRNAs the branch point is usually located 18-40 nucleotides (nts) upstream of the 3'ss and is defined by YURAY, where the branch point adenosine is underlined [Zhang, 1998]. In contrast, the yeast consensus sequence of the BPS is UACUAAC and the BP adenosine is usually located 10-40 nucleotides upstream of the 3'ss [Spingola *et al.*, 1999]. Additionally, most human introns contain a pyrimidine-rich region called the polypyrimidine tract (PPT), which is located between the branch point sequence and the 3'splice site. The PPT helps to recruit and stabilize the binding of spliceosomal factors and is an important splicing element in humans.

1.2 The two step mechanism of splicing

The excision of pre-mRNA introns is facilitated by two consecutive transesterification reactions [Moore and Sharp, 1993]. In the first reaction the 2'hydroxyl group of the branch point adenosine performs a nucleophilic attack at the phosphodiester bond of the 5'ss.

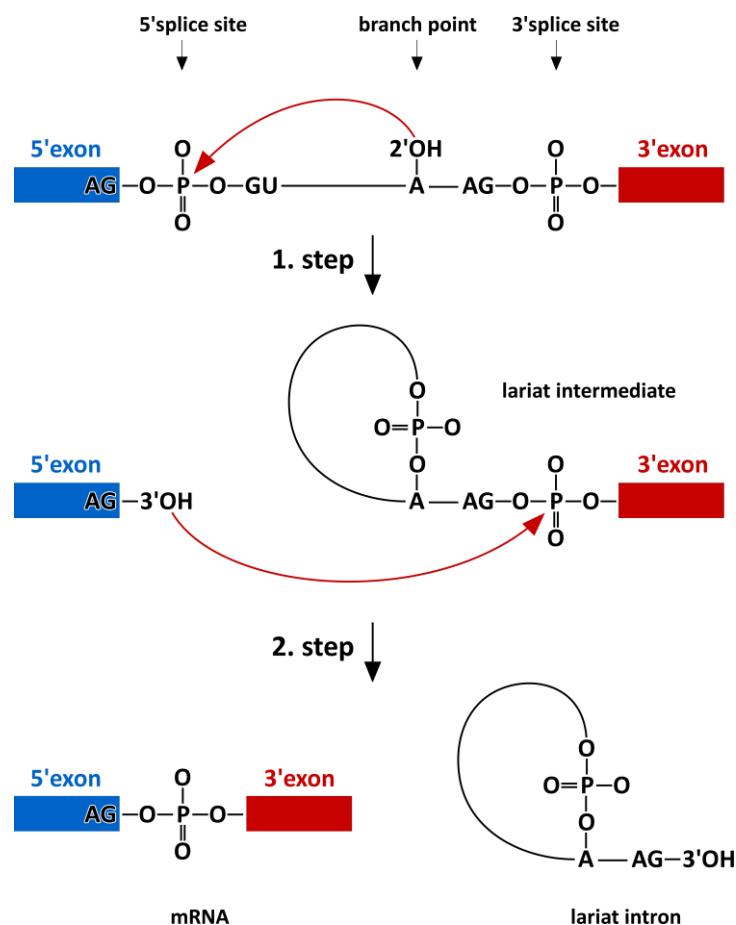


Figure 1.2: Chemistry of the splicing reaction

Two consecutive transesterification reactions lead to the excision of the intron with a lariat structure and the joining of the 5' and 3'exons.

The cleavage of the pre-mRNA generates a free 5'exon and a lariat intermediate, in which the BP adenosine and the guanosine at the 5'end of the intron are connected by a 2'-5'phosphodiester-bond. In the second step, the free 3'hydroxyl group of the 5'exon attacks the 3'ss resulting in the excision of the intron lariat and ligation of the 5' and 3'exon to form the mature mRNA. The same reaction mechanism is used during the splicing of group II introns, since exactly the same intermediates and products are generated. Group II introns are self-splicing ribozymes that catalyze their own excision from pre-mRNAs [Pyle and Lambowitz, 2006]. Although the two step reaction is essentially iso-energetic, splicing is ATP-dependent because several factors necessary for the formation of the spliceosome and its structural rearrangements during catalysis require ATP for their function (see chapter 1.6).

1.3 Alternative splicing enhances the proteome post-transcriptionally

Alternative splicing plays a central role in eukaryotic gene expression and it is a key process in extending the coding potential of a genome post-transcriptionally. In *S. cerevisiae* only ~3 % of the genes contain introns and the majority of these genes contain only a single intron that is usually a few hundred nucleotides in length [Barrass and Beggs, 2003, Spingola *et al.*, 1999]. In contrast, human genes contain on average four introns per gene and a single intron can be one hundred thousand nucleotides in length [Deutsch and Long, 1999]. The average length of vertebrate exons is only ~137 nts and generally does not exceed more than 400 nts [Berget, 1995]. Thus, pre-mRNAs of higher eukaryotes are characterized by a mosaic-like structure, in which short exons are interrupted by much longer introns. In pre-mRNAs with multiple introns, different sets of exons can be joined in a process called alternative splicing. Alternative splicing enhances the number of mature mRNAs that are generated from a single gene and can result in translation of numerous protein variants with different functions. This post-transcriptional modification of the pre-mRNA sequence is a ubiquitous mechanism of pre-mRNA processing in higher eukaryotes, since more than 90 % of the human pre-mRNAs are spliced alternatively [Wang *et al.*, 2008]. The majority of alternative splicing events involve exon skipping (Figure 1.3, 1), in which an exon and its flanking introns are excluded from the mature mRNA by joining the direct upstream and downstream exons instead [reviewed in Keren *et al.*, 2010]. Alternatively, sections of individual exons can be excluded or included from the mRNA by recognition and use of alternative 5'ss or 3'ss within the respective exon (Figure 1.3, 2 & 3). Further, the inhibition of spliceosome assembly or masking of 5'ss and 3'ss signals can result in the retention of intronic sequences within the mature mRNA (Figure 1.3, 4). In rare cases pre-mRNAs contain mutually exclusive exons resulting in splicing products that include either one or another exon, but not both within the same mature mRNA (Figure 1.3, 5).

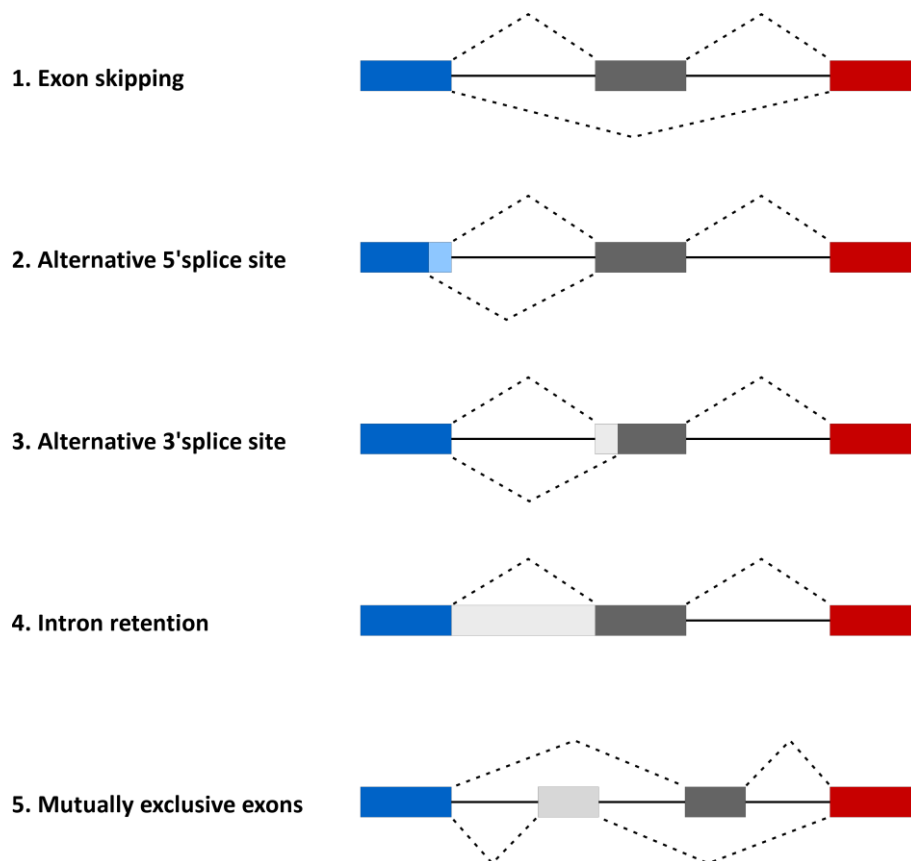


Figure 1.3: Modes of alternative splicing

Schematic representation of different modes of alternative splicing: (1) Exon skipping accounts for the majority of alternative splicing events. In this process an exon and its surrounding introns are spliced out from the pre-mRNA. (2 & 3) An exon can contain more than one 5'ss or 3'ss, respectively. The use of these alternative 5' or 3'ss results in the exclusion or inclusion of partial exon segments in the mature mRNA. (4) Additionally, an entire intron can be retained in the mature transcript. (5) Two exons are mutually excluded from being in the mature mRNA. Constitutively spliced 5' and 3'exons are indicated as blue and red boxes, respectively. Alternatively spliced regions are represented by grey boxes and introns are shown as solid lines. Dashed lines indicate splicing options. The figure was adapted from Keren *et al.* [Keren *et al.*, 2010].

Alternative splicing of pre-mRNAs is modulated by auxiliary regulatory elements that either enhance or inhibit exon recognition. These exonic and intronic splicing enhancers (ESEs and ISEs) and silencers (ESSs and ISSs) are supplementary *cis*-acting elements that recruit regulatory proteins, which then stimulate or repress spliceosome assembly. In addition to their crucial role in alternative splicing, these regulatory elements can also act on constitutive splicing [reviewed in Black, 2003].

1.4 Composition of spliceosomal snRNPs

The major, U2-dependent spliceosome is formed by the interaction of five snRNPs (U1, U2, U4, U5 & U6). Each snRNP particle is comprised of a uridine-rich small nuclear RNA (U snRNA) and a variable number of proteins. Approximately 1 % of all human introns are spliced by the minor, U12-

The major spliceosomal RNAs can be divided into the Sm- and Sm-like (LSm) class of snRNAs based on their biogenesis and maturation. The Sm class is comprised of the U1, U2, U4 and U5 snRNAs. These snRNAs are transcribed by the RNA polymerase II as a precursor molecule containing a m⁷G-cap and undergo multiple maturation steps including export to the cytoplasm [reviewed in Matera *et al.*, 2007, Matera and Wang, 2014]. The maturation of these snRNAs requires export to the cytoplasm, where the Sm-proteins B, D1, D2, D3, E, F and G are assembled on a uridine-rich stretch of the respective snRNA in a ring-like structure. Following the assembly of the Sm-ring, the m⁷G-cap is hypermethylated to a 2, 2, 7-trimethylguanosine-cap and the 3' end of the snRNAs is trimmed. The Sm-core and the hypermethylated-cap induce then the re-import of the spliceosomal snRNAs into the nucleus, where the assembly of snRNA-specific proteins with the respective snRNA occurs.

The U6 snRNA belongs to the LSm-class of snRNAs. It is transcribed by the RNA polymerase III, whose transcripts are characterized by a γ -monomethyl-cap. The U6 snRNA does not contain a Sm-ring, but seven LSm (LSm 2-8) proteins assemble also in a ring-like structure at its 3' end. The biogenesis and maturation of U6 snRNA occurs thereby completely in the nucleus.

The snRNAs are characterized by extensive secondary structures and these structures are highly conserved in higher eukaryotes. The proposed secondary structures of the human snRNAs within their respective snRNPs are shown in figure 1.4, but several of these structures are rearranged during spliceosome assembly (see chapter 1.7). Notably, the U4 and U6 snRNAs are partially complementary to each other and therefore base pair within the U4/U6 di-snRNP via stem I and stem II [Brow and Guthrie, 1988].

1.5 Protein inventory of the human snRNPs

Each U snRNP contains, besides the Sm or LSm proteins, its own specific set of proteins. The human U1 snRNP contains only three additional proteins, namely U1-70K, U1-A and U1-C, and acquires thereby a Svedberg value (S-value) of 12S. U1-C is involved in stabilization of base pairing interactions between U1 snRNA and the 5' splice site of the pre-mRNA [Heinrichs *et al.*, 1990], whereas U1-70K interacts with SR proteins to stabilize the interaction of U1 snRNP with the pre-mRNA [Kohtz *et al.*, 1994].

The 17S U2 snRNP is composed of U2A', U2B'' and the heteromeric subcomplexes SF3a and SF3b. The SF3a and SF3b proteins help to stabilize the base pairing between the U2 snRNA and the BPS by interactions with the pre-mRNA around the branch point [Gozani *et al.*, 1996, Valcarcel *et al.*, 1996], whereas SF3b14a directly interacts with the branch point adenosine [Will *et al.*, 2001]. Furthermore, several factors have been identified as U2-related proteins, which are loosely-associated with the

17S U2 snRNP, including hPrp43, SPF45, SPF30, SPF31, SR140, CHERP, PUF60, hPrp5 and the U2AF65/35 heterodimer [Will *et al.* 2002].

The 20S U5 snRNP contains the eight specific proteins hPrp8, hBrr2, hSnu114, hPrp6, hPrp28, hLin1, 40K and hDib1 [Bach *et al.*, 1989]. The factor hPrp8 is the largest protein in the spliceosome and was shown to contact the 5'ss, 3'ss and the BPS at different points of the splicing cycle [Reyes *et al.*, 1996, Reyes *et al.*, 1999, McPheeters and Muhlenkamp, 2003, Teigelkamp *et al.*, 1995a, b]. The U5-specific proteins hPrp28 and hBrr2 are helicases that were identified to be essential for formation of a pre-catalytic spliceosome and its subsequent activation, respectively [Mathew *et al.*, 2008, Raghunathan and Guthrie, 1998]. The U5-specific proteins hPrp8 and hSnu114 have been shown to regulate hBrr2 activity [Small *et al.*, 2006, Mozaffari-Jovin *et al.*, 2012, Mozaffari-Jovin *et al.*, 2013].

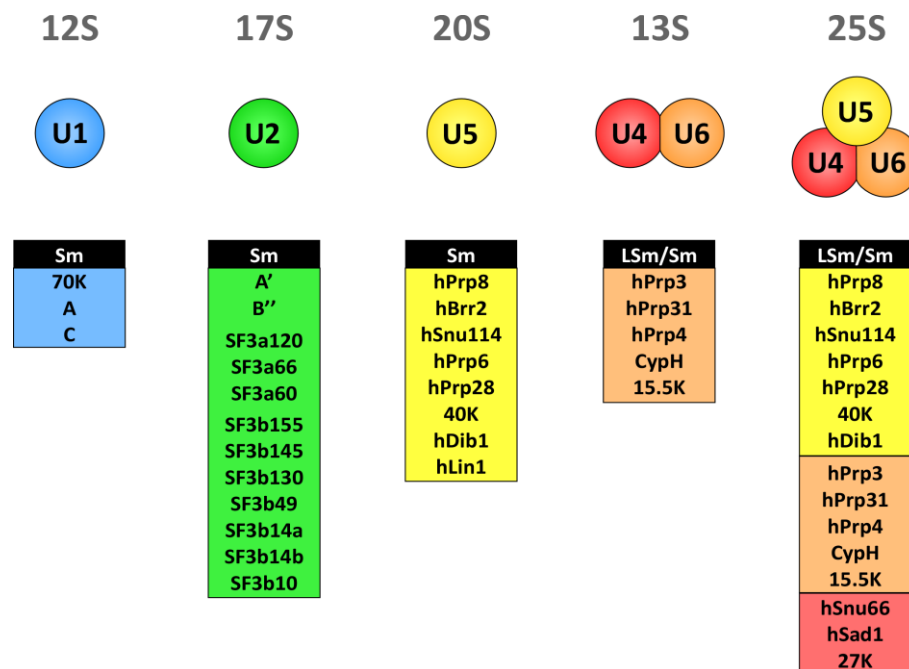


Figure 1.5: Protein composition of the human snRNPs

Typical snRNP complexes are represented as colored circles and the S-value of each snRNP is shown on top. Shown below are the abundant factors associated with the U snRNPs including the Sm or Sm-like proteins.

The U4/U6 di-snRNP is associated with the five specific proteins hPrp3, hPrp31, hPrp4, CypH and 15.5K, resulting in an S-value of 13S [Behrens and Lührmann, 1991, Lauber *et al.*, 1997]. Upon association of the 13S U4/U6 di-snRNP with the 20S U5 snRNP the 25S U4/U6.U5 tri-snRNP is formed, which additionally contains the three proteins hSnu66, hSad1 and 27K [Behrens and Lührmann, 1991]. The U5-specific protein hLin1 is proposed to play a role during assembly of this 25S particle and is not present in the mature U4/U6.U5 tri-snRNP [Laggerbauer *et al.*, 2005]. Since no interactions between the U5 and U4/U6 snRNAs are known, the assembly of the U4/U6.U5 tri-snRNP appears to be based solely on protein-protein interactions. The proteins hPrp6 and hPrp31 play an important

role in assembly of the U4/U6.U5 tri-snRNP, as depletion of either protein abolishes U4/U6.U5 tri-snRNP formation *in vitro* and *in vivo* [Makarova *et al.*, 2002, Schaffert *et al.*, 2004].

1.6 Stepwise assembly of the spliceosome

Spliceosome assembly occurs by the ordered interaction of the five snRNPs and numerous splicing factors with the pre-mRNA and proceeds sequentially with distinct intermediate stages, i.e. the E, A, B, B^{act}, B* and C complex [reviewed in Will and Lührmann, 2011]. Thereby, the spliceosome assembles anew onto each intron and rebuilds its catalytic center during each splicing cycle. The dynamic assembly and disassembly of the spliceosome requires the function of eight conserved DExH/D ATPases/helicases, whose detailed function is described in chapter 1.9.

The stepwise assembly of the spliceosome is initiated by recognition of the 5'ss by the U1 snRNP (Figure 1.6). The U1 snRNA base pairs with the 5'ss of the pre-mRNA and U1 snRNP proteins stabilize this interaction. At the same time, SF1 and U2AF65/35 interact with the BPS and the PPT/3'ss, respectively [Heinrichs *et al.*, 1990, Berglund *et al.*, 1997, Ruskin *et al.*, 1988]. Together, these interactions lead to formation of the E complex and already in this initial state of spliceosome assembly the conserved splicing signals of the pre-mRNA are recognized. The U2 snRNP is also associated with the E complex, but an ATP-dependent rearrangement mediated by the helicase Prp5 is required to establish interactions between U2 snRNP and the BPS, which results then in formation of the A complex [Das *et al.*, 2000, Dalbadie-McFarland and Abelson, 1990, Fleckner *et al.*, 1997]. These interactions involve base pairing of the U2 snRNA with the BPS, which leads to bulging out of the BP adenosine, and interactions of the U2-associated SF3a and SF3b proteins near the BPS. The BP adenosine is directly contacted by the SF3b14a protein [Query *et al.*, 1994, Will *et al.*, 2001]. Moreover, SF3b155 not only interacts with the pre-mRNA, but also with the auxiliary factor U2AF65 to stabilize the binding of U2 snRNP to the pre-mRNA [Gozani *et al.*, 1998]. Thus, multiple recognitions of splicing signals is a general mechanism of spliceosome assembly and splicing catalysis that ensures the accuracy of this process.

The spliceosomal B complex is formed upon association and stable binding of the pre-assembled U4/U6.U5 tri-snRNP with the A complex. The stable integration of the U4/U6.U5 tri-snRNP is mediated by the DEAD-box helicase Prp28, which destabilizes the interaction between the 5'ss and U1 snRNP, and enables an interaction of the 5'ss and the ACAGAG box of U6 snRNA [Staley and Guthrie, 1999, Mathew *et al.*, 2008]. During stabilization of the B complex the U4/U6.U5 tri-snRNP associated factors hPrp31 and hPrp6 are phosphorylated by the hPrp4 kinase, which was shown to be essential for pre-mRNA splicing *in vitro* [Schneider *et al.*, 2010b]. Although all spliceosomal snRNPs are present in this complex, the spliceosome is still in a catalytically inactive state.

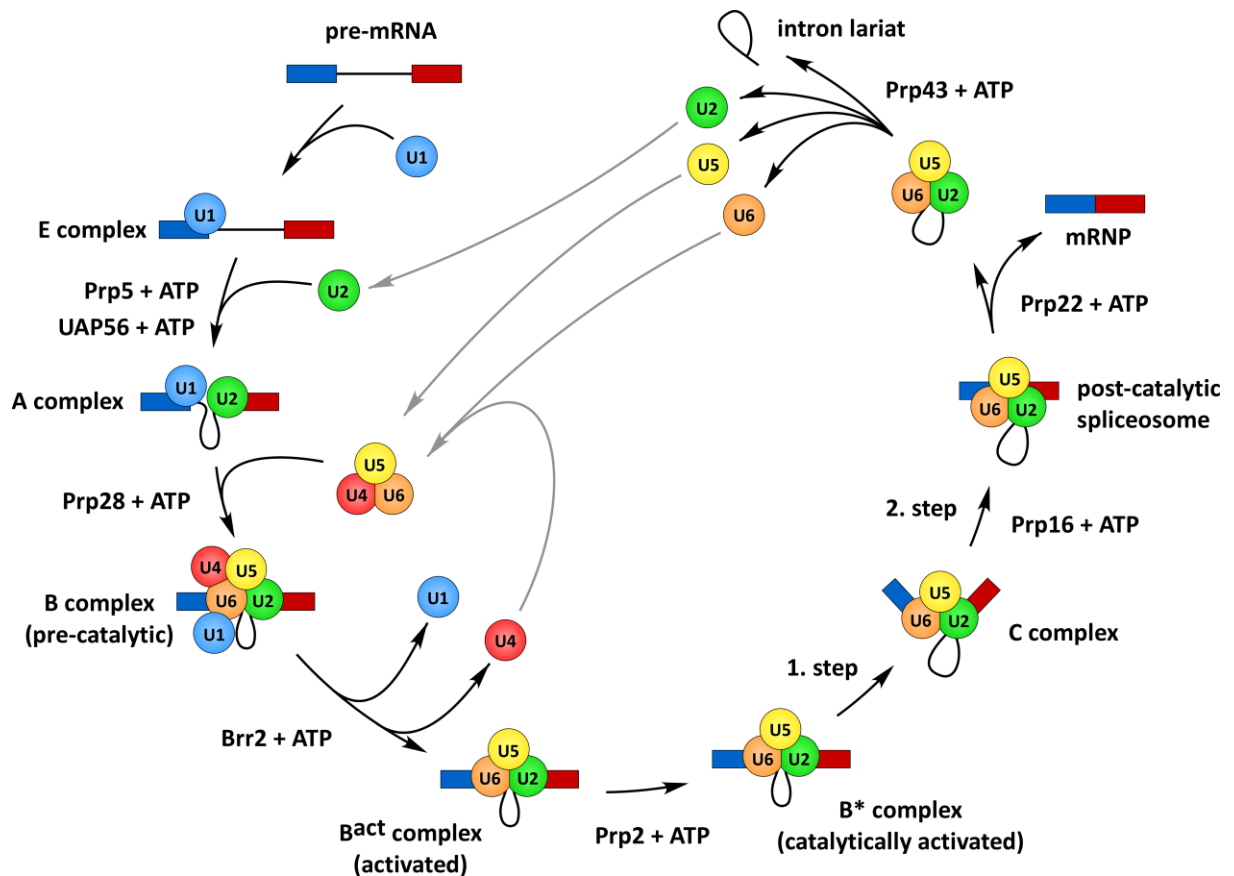


Figure 1.6: Stepwise assembly of the human spliceosome

Schematic representation of spliceosome assembly and disassembly during one splicing cycle. For simplicity the U snRNPs are represented as circles labeled with its respective U snRNA. The spliceosomal complexes are named according to the metazoan nomenclature. The eight conserved DExD/H-box ATPases/helicases, which are required for important RNP remodeling events, are indicated and their function is described in detail in chapter 1.9. Exons and introns are indicated as colored boxes or bold lines, respectively. Recycling of snRNPs is indicated by grey arrows [modified from Will and Lührmann, 2011].

During activation of the spliceosome the B complex undergoes major conformational and compositional rearrangements, which are accompanied by the release of the U1 and U4 snRNPs and recruitment of additional factors to form the B^{act} complex. The action of Prp2 transforms the spliceosome into a catalytically activated state, forming the B* complex that carries out the first step of splicing. The first step of splicing results in formation of the C complex, which contains the cleaved 5' exon and the exon-intron lariat intermediate. Upon action of Prp16, the spliceosome undergoes a second structural rearrangement, which activates the complex for the second step of splicing. During the second step, the lariat intron is excised and the 5' and 3' exons are ligated. Subsequently, the post-catalytic spliceosome is disassembled by Prp22 and the mRNA is released in form of an mRNP, which is then exported to the cytoplasm. The snRNPs associated with the excised intron are

displaced by the action of Prp43 and recycled for additional rounds of splicing, whereas the intron is degraded.

1.7 The dynamic RNA-RNA network in the spliceosome

The stepwise assembly of the spliceosome requires major structural rearrangements during the formation of its catalytic site. These conversions involve extensive changes in pre-mRNA-snRNA and snRNA-snRNA interactions underlining the highly dynamic nature of the RNA network within the spliceosome [reviewed in Wahl *et al.*, 2009, Will and Lührmann, 2011]. Spliceosome assembly is initiated by the recognition of the 5'ss through base pairing interactions with the 5'end of U1 snRNA (Figure 1.7, blue). Subsequently, the U2 snRNA forms a short helix with the BPS (U2/BPS helix, turquoise), in which the BP adenosine is branched out (A complex). Then, the pre-assembled U4/U6.U5 tri-snRNP is recruited to the A complex resulting in formation of a pre-catalytic spliceosome. At this time the 3'end of U6 snRNA forms a short helix (U2/U6 helix II, purple) with the 5'end of U2 [Nilsen, 1998]. The U4 and U6 snRNAs are still extensively base paired via U4/U6 stem I and stem II within the U4/U6.U5 tri-snRNP [Brow and Guthrie, 1998].

Upon activation of the spliceosome, a major remodeling of RNA-RNA interactions occurs in order to position the 5'ss and the branch point in a proper orientation for the first catalytic step of splicing. First, the U1 snRNA interaction with the 5'ss is replaced by base pairing of the 5'ss with the conserved ACAGAGA box of U6 snRNA (orange) [Staley and Guthrie, 1999]. Next the extensive base pairing of U4 and U6 snRNA is disrupted. Consequently, the U4 snRNA is displaced and a complex network of interactions between the U2 and U6 snRNA is formed (U2/U6 helix Ia and Ib, red) [Anokhina *et al.*, 2013]. Thus, especially U2/U6 interactions appear to be highly dynamic and the RNA-RNA network mainly established by these snRNAs is believed to play a crucial role in splicing catalysis [Fica *et al.*, 2013]. At this time, the U6 snRNA also forms an intramolecular stem-loop (U6 ISL, green), which is essential for the binding of a catalytically important metal ion [Yean *et al.*, 2000]. The contribution of the U6 ISL to splicing catalysis underscores the importance of the initial U4/U6 base pairing interaction, since catalytically important sequences of U6 snRNA are delivered in an inactive form, while still base paired. Thus, the U4 snRNA may act as a chaperone for U6 snRNA to prevent premature catalysis. Furthermore, the stem loop I of U5 snRNA interacts with the 5'exon and at a later stage of splicing additional interactions with the 3'exon are established [reviewed by Turner *et al.*, 2004]. Thus, the U5 snRNA keeps both exons in close proximity and might align them for the second catalytic step [Sontheimer and Steitz, 1993].

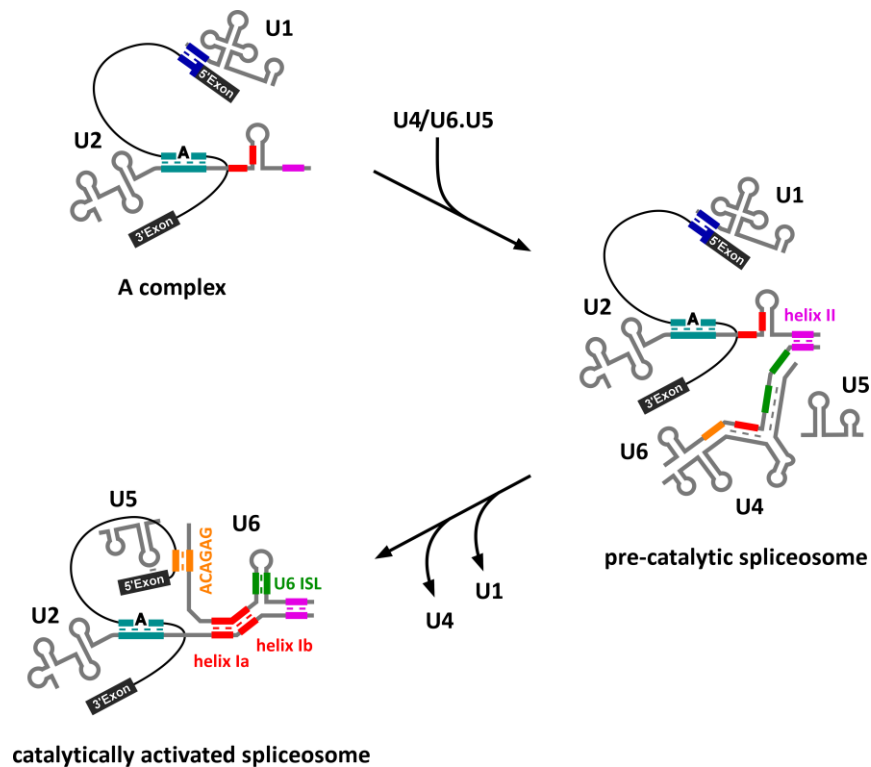


Figure 1.7: Rearrangements of the RNA-RNA network during formation of a catalytically activated spliceosome

Schematic representation of the rearrangement of RNA-RNA interactions during formation of a catalytically activated spliceosome. In the pre-spliceosome, U1 snRNA is base paired with the 5'ss (blue), while U2 snRNA interacts with the BPS (turquoise). The branch point adenosine is bulged out (bold). Upon recruitment of the U4/U6.U5 tri-snRNP, initial contacts between U6 and U2 snRNA via helix II (pink) are established. Subsequently, the base pairing between U1 snRNA and the 5'ss is disrupted and replaced by interactions of the 5'ss with the conserved ACAGAG motif of U6 snRNA (orange). Furthermore, the base pairing between U4 and U6 snRNA is disrupted, leading then to an extensive base pairing between U2 and U6 snRNA via helix Ia and Ib (red), as well as formation of an internal-stem loop (ISL) of U6 snRNA (green). The U2 snRNA remains base paired with the BPS and U5 snRNA contacts nucleotides of the exon. Exons are represented as dark grey boxes and introns are shown as a black line.

The reaction mechanism of the spliceosome is identical to self-splicing group II introns, which do not require *trans*-acting factors for catalysis of splicing. However, spliceosome-mediated excision of introns requires proteins and ATP to facilitate splicing catalysis. Until recently it was not clear if the spliceosome uses an RNA-based or protein-mediated splicing mechanism. Compelling evidence that the spliceosome's active site is composed of RNA first came from the crystal structure of a self-splicing group II intron [Toor *et al.*, 2008]. These studies revealed that the structural motifs shared by U6 snRNA and group II introns form the basis of the group II intron active site. Most recently, an elegant biochemical approach using metal rescue experiments provided compelling evidence that structures formed by U2/U6 snRNA, in particular U6 snRNA, are important for both steps of pre-mRNA splicing [Fica *et al.*, 2013].

1.8 Dynamics of the spliceosome's protein composition

Spliceosome assembly and recycling of spliceosomal components involves not only extensive remodeling of RNA-RNA interactions, but also the protein composition of the spliceosome undergoes dramatic changes. Initial characterization of the spliceosome's protein inventory via mass spectrometry indicated that more than 300 proteins interact with the spliceosome during its assembly and catalytic action [Rappsilber *et al.*, 2002]. But these initial experiments analyzed a mixture of all assembly stages, i.e. E, A, B, C and mRNP complexes.

However, characterization of the protein composition of these distinct intermediates is necessary to elucidate the recruitment and exchange of proteins, and assign splicing factors to a particular assembly or functional stage of the spliceosome. The purification of *in vitro* assembled splicing complexes with subsequent analysis of their protein compositions by mass spectrometry allowed a comprehensive insight into distinct human spliceosomal complexes, i.e. the A, B, B^{act} and C complexes, under comparable biochemical conditions [Behzadnia *et al.*, 2007, Deckert *et al.*, 2006, Bessonov *et al.*, 2010]. These analyses revealed for the first time the protein dynamics of the spliceosome, i.e. the exchange of proteins, upon transition from one assembly/functional state to the next, and revealed that approximately 170 proteins are components of the human spliceosome, with individual complexes containing up to 120 proteins [reviewed in Wahl *et al.*, 2009, Will and Lührmann, 2011]. Spliceosome-associated proteins include proteins of the U snRNPs plus a multitude of additional factors, which are not stably bound to purified U snRNPs and interact with the spliceosome either alone or as part of pre-formed protein complexes (Figure 1.8). These non-snRNP proteins interact either with one distinct assembly intermediate of the spliceosome or are integrated into a specific complex and are present throughout several stages of the splicing cycle.

An example of a pre-formed subcomplex of the spliceosome is the Prp19 complex, which was shown to be essential for splicing by genetic studies in yeast [Ruby and Abelson, 1991, Tarn *et al.*, 1994]. The human counterpart of the Prp19 complex is composed of seven proteins and plays an essential role in the activation of the spliceosome for the first step of splicing [Makarov *et al.*, 2002, Makarova *et al.*, 2004]. In the human spliceosome, several factors are considered to be related to the Prp19 complex, because they were found together with Prp19 in the post-spliceosomal 35S U5 snRNP particle [Makarov *et al.*, 2002]. Another non-snRNP protein complex is the trimeric RES (retention and splicing) complex that was identified in *S. cerevisiae* and enhances pre-mRNA splicing and retention of un-spliced pre-mRNA in the nucleus [Dziembowski *et al.*, 2004].

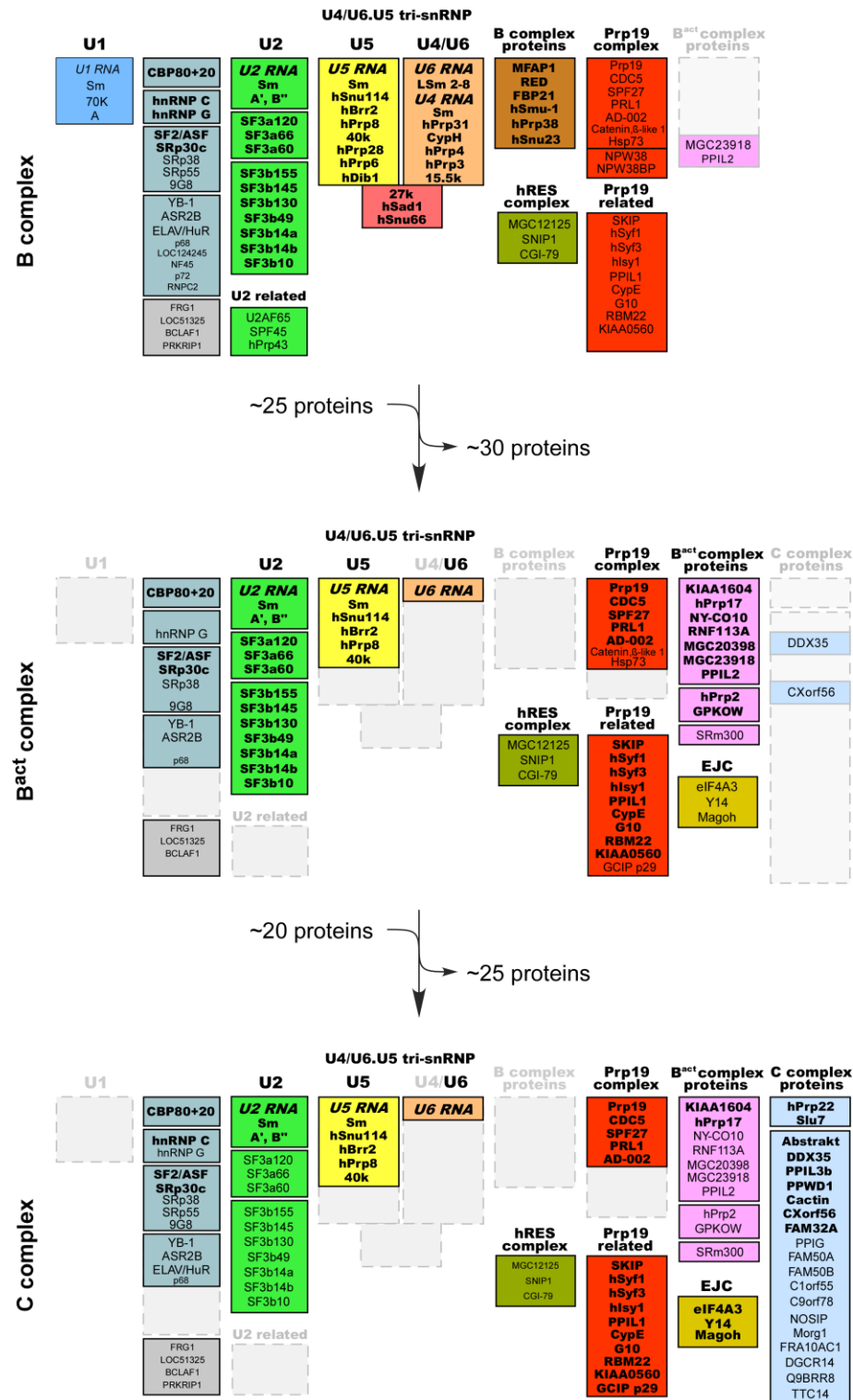


Figure 1.8: Compositional dynamics of the human spliceosome

The protein composition of the human B, B^{act} and C complexes based on 2D gel-electrophoresis and mass spectrometry analysis is shown. The relative abundance of proteins is indicated by bold (stoichiometric amounts) or light (substoichiometric amounts) lettering. Proteins are grouped according to snRNP association, function, presence in a stable heteromeric complex or association with a particular spliceosomal complex, as indicated. This figure was kindly provided by Dr. Sergey Bessonov, Department of Cellular Biochemistry, MPI-BPC.

In human, homologs of the RES complex proteins were shown to be associated with the B, B^{act} and C complex [Bessonov *et al.*, 2010], but their role in the human spliceosome is not yet clear. During the later steps of the splicing cycle, the heteromeric exon junction complex (EJC) is assembled onto the pre-mRNA, approximately 24 nts upstream of the splice junction, and stays bound to the processed mRNA even after its release from the post-catalytic spliceosome [reviewed in Le Hir and Seraphin, 2008]. The EJC is important for the quality control and export of the mature mRNA and is stripped from the mRNA during the first round of translation.

Mass spectrometry and 2D gel-electrophoresis of affinity-purified spliceosomal complexes showed that upon stable integration of the U4/U6.U5 tri-snRNP within the spliceosome and formation of a pre-catalytic B complex, the proteins RED, MFAP1, FBP21, hSmu-1, hPrp38 and hSnu23 are recruited to the complex. These proteins are associated solely with the B complex, i.e. they are B complex-specific proteins, being displaced upon activation of the spliceosome and transition to the B^{act} complex. The role of these proteins in the assembly of the spliceosome is presently not clear. Kinetically-assembled B complexes also contain proteins of the Prp19 complex [Deckert *et al.*, 2006, Bessonov *et al.*, 2010], but these factors are not essential for its formation, since the B complex is also formed in nuclear extract, in which the Prp19 complex was depleted [Makarova *et al.*, 2004].

During transition from the pre-catalytic B complex to an activated spliceosome ~25 proteins are displaced from the spliceosome, among others the B complex-specific proteins along with the U4/U6 snRNP and U4/U6.U5 tri-snRNP-specific proteins. Upon formation of the B^{act} complex ~20 proteins are recruited to the spliceosome, especially proteins associated with or related to the Prp19 complex. During the transition from the B^{act} to the C complex, ~25 proteins leave the complex, while ~20 proteins join the spliceosome, mainly the so-called C complex-specific proteins.

In yeast ~90 proteins were shown to be associated with the spliceosome, while individual assembly intermediates contain ~50-60 proteins [Fabrizio *et al.*, 2009]. Nearly all of these proteins have homologs in human and thus likely represent conserved factors of the spliceosomal core machinery.

1.9 The role of RNA helicases in splicing

During assembly, activation and disassembly of the spliceosome, RNA helicases act as key factors by mediating rearrangements in RNA-RNA or protein-RNA interactions. Eight conserved DExD/H-box ATPases/helicases, namely UAP56, Prp5, Prp28, Brr2, Prp2, Prp16, Prp22 and Prp43, are essential for rearrangements of RNA-RNA interactions and the remodeling of snRNPs during a single splicing cycle [reviewed in Staley and Guthrie, 1998]. These proteins couple the energy of ATP hydrolysis to structural and/or compositional rearrangements in the spliceosome at distinct steps of the splicing cycle. The activity of these enzymes also plays a central role in proofreading the spliceosome

reaction, ensuring the fidelity of the splicing process [Semlow and Staley, 2012]. Most of these enzymes interact only transiently with the spliceosome, but nonetheless act as important molecular switches during spliceosome reaction. Brr2, in contrast, associates already in the B complex and remains associated until the spliceosome dissociates [Makarov *et al.*, 2002]. Thus, a tight regulation of Brr2's activation is required to prevent its pre-mature activation, a task carried out in part by other spliceosomal components and also modulated in some cases by posttranslational modifications.

During the initial stages of the splicing cycle, Prp5 and UAP56 are required for the transition from the E to A complex by displacing SF1 from the BPS and rearranging U2 snRNA to enable its base pairing with the BPS [Dalbadie-McFarland and Abelson, 1990, Fleckner *et al.*, 1997]. Then, Prp28 mediates the transition from the A to B complex, in which the U4/U6.U5 tri-snRNP is stably-integrated within the spliceosome. Genetic studies in *S. cerevisiae* have shown that Prp28 plays an essential role in destabilization of the U1:5'ss duplex, potentially by weakening the interaction of U1-specific proteins with the U1:5'ss helix [Staley and Guthrie, 1999, Chen *et al.*, 2001]. Destabilization of the U1:5'ss interaction is required to allow an exchange of U1 for U6 snRNA interaction with the 5'ss of a pre-mRNA. In *S. cerevisiae*, Prp28 interacts only transiently with the spliceosome, whereas the human homolog, hPrp28, is an integral component of the U4/U6.U5 tri-snRNP. It was shown that SRPK2-mediated phosphorylation of hPrp28 is necessary for its integration into the U4/U6.U5 tri-snRNP and only a U4/U6.U5 tri-snRNP containing hPrp28 is competent for stable B complex formation [Mathew *et al.*, 2008].

After the stable integration of the U4/U6.U5 tri-snRNP within the B complex, the action of Brr2 leads to a subsequent disruption of the U4/U6 base pairing interaction to allow annealing of U6 with U2 snRNA and the formation of the catalytically important U6 ISL [Laggerbauer *et al.*, 1998, Raghunathan and Guthrie, 1998]. Brr2 is an integral component of the U4/U6.U5 tri-snRNP both in human and in yeast and since its substrate, namely the U4/U6 di-snRNP, is also present in the U4/U6.U5 tri-snRNP, the activation of Brr2 has to be precisely regulated to avoid pre-mature disruption of U4/U6 base pairing and thereby pre-mature activation of the U6 snRNA. The activity of Brr2 is regulated by the U5-specific proteins Prp8 and Snu114. The GTPase Snu114 blocks Brr2's helicase activity when it is in a GDP-bound state, whereas Snu114's GTP-bound form promotes helicase activity [Small *et al.* 2006]. Recently, it was shown that the C-terminal end of Prp8 can reversibly block the RNA-binding channel of Brr2 and thereby controls U4/U6 unwinding activity of Brr2 [Maeder *et al.*, 2009, Mozaffari-Jovin *et al.*, 2013]. Additionally, the RNase H domain of Prp8 competes with Brr2 for binding to its substrate, showing that Brr2 activity is regulated in multiple ways [Mozaffari-Jovin *et al.*, 2012].

In a subsequent step, the B^{act} complex is remodeled by Prp2 in cooperation with its co-factors Spp2 and Cwc25 to catalytically activate the spliceosome for the first step of splicing [Kim and Lin, 1996, Warkocki *et al.*, 2009]. Recent studies in *S. cerevisiae* indicate that Prp2 destabilizes and/or rearranges the U2-associated SF3a and SF3b proteins in the spliceosome to position the BP adenosine for its nucleophilic attack on the 5'ss [Warkocki *et al.*, 2009]. The cleavage of the pre-mRNA at the 5'ss results then in formation of the C complex, which contains the free 5'exon and the intron-lariat intermediate. In a subsequent step, Prp16 remodels the catalytic core of the C complex to generate a conformation that can catalyze the second step of splicing [Schwer and Guthrie, 1992, Ohrt *et al.*, 2013]. After excision of the intron, release of the mature mRNA from the post-catalytic spliceosome is facilitated by Prp22 [Fourmann *et al.*, 2013]. In the final step, Prp43 catalyzes the disassembly of the intron-lariat spliceosome. The Ntr1/Ntr2 heterodimer acts as a co-factor of Prp43 to stimulate the release of the excised lariat-intron [Martin *et al.*, 2002, Tsai *et al.*, 2005, Fourmann *et al.*, 2013]. The free intron is then degraded and the spliceosomal factors are recycled for the next round of splicing.

1.10 Structure of spliceosomal complexes

Although the composition of the spliceosome's various assembly and functional states have been characterized in detail, less is known about the structure of the spliceosome. The size and structural variability of the spliceosome make it a particularly challenging object for structural studies [Newman and Nagai, 2010]. In recent years substantial progress has been made towards high resolution structure determination of large multi-component spliceosomal subunits, such as the human U1 snRNP, whose structure has been determined down to the atomic level [Pomeranz Krummel *et al.*, 2009, Weber *et al.*, 2010]. But aside from the U1 snRNP, high resolution structures generated by X-ray crystallography or NMR are restricted to individual proteins or single components of the spliceosome. Due to the complexity of the spliceosome and its highly dynamic character, to date it has not been possible to crystallize any spliceosomal assembly intermediates. Thus, electron microscopy (EM) is still the state of the art method to elucidate the 3D structure of the spliceosome and its structural dynamics during the transition from one intermediate to another [Lührmann and Stark, 2009]. Indeed, cryo-EM has provided valuable insights into the three-dimensional global shape of the splicing machinery [Golas *et al.*, 2010]. Nevertheless, EM investigation of the spliceosome is also challenging as this protein-rich RNP complex is very labile and can easily disintegrate during purification and sample preparation. Therefore a method was established, in which the spliceosomal complexes are fixed under mild conditions during density-gradient centrifugation (GraFix) in order to preserve the structure of the intermediates and overcome the critical limitation of structural disintegration [Kastner *et al.*, 2008]. This GraFix procedure led to substantial improvements in the

structural conservation of the complexes and accelerated the structural investigation of spliceosomal assembly intermediates significantly. For example, human B complexes prepared under GraFix conditions, exhibit a clearly more homogeneous appearance in EM analyses than unfixed B complexes [Boehringer *et al.*, 2004, Deckert *et al.*, 2006]. However, the resolution of EM structures is currently not good enough to allow a determination of their intrinsic complex organization. Thus, the localization of factors within the spliceosomal complexes is required to comprehend how they are arranged. A powerful strategy for topographical localization of relevant sites within the spliceosome is the specific immunolabeling of these factors and subsequent localization by EM. Using this approach, the U2 protein SF3b155 and various sites of the pre-mRNA have been located within the human B and C complex, and a comparison of these structures provides a first insight into how functionally important areas are rearranged within the spliceosome [Wolf *et al.*, 2009, Wolf *et al.*, 2012]. Recently, investigations using cryo-EM revealed the three-dimensional architecture of the catalytically active C complex and its salt-stable core [Golas *et al.*, 2010]. The location of the 5' exon within the C complex was determined by immunolabeling, and by combining different structural data including the 3D structure of the 35S U5 snRNP, it was possible to localize the catalytic core within the C complex. Thus, structural investigations of the spliceosome provide valuable insights into the architecture of functional sites and extend our understanding of how structural rearrangements in the spliceosome contribute to its function.

1.11 Exon definition is an alternative pathway to initiate spliceosome assembly

Pre-mRNAs of higher eukaryotes are characterized by a mosaic-like structure, in which short exons are interrupted by long intronic sequences. But the initial assembly of the spliceosome across an intron (intron definition) is limited to pre-mRNAs containing very short introns, i.e. less than 300 nts [Sternner *et al.*, 1996]. On pre-mRNAs with long intronic sequences, the spliceosome initially assembles via an alternative pathway, in which the earliest spliceosomal complex first forms across an exon (exon definition) [Berget, 1995]. In fact, exon definition is thought to be the prominent pathway of spliceosome assembly for the majority of metazoan pre-mRNAs [Ast, 2004].

The formation of a spliceosome across an exon is initiated upon base pairing of U1 snRNP to a downstream 5' splice site (5'ss), while U2 snRNP and U2AF65/35 interact with an upstream branch point sequence (BPS) and pre-mRNA 3' splice site (3'ss), respectively. During this process the boundaries of an exon are initially defined in contrast to the intron-defined assembly pathway, in which the boundaries of a single intron are recognized.

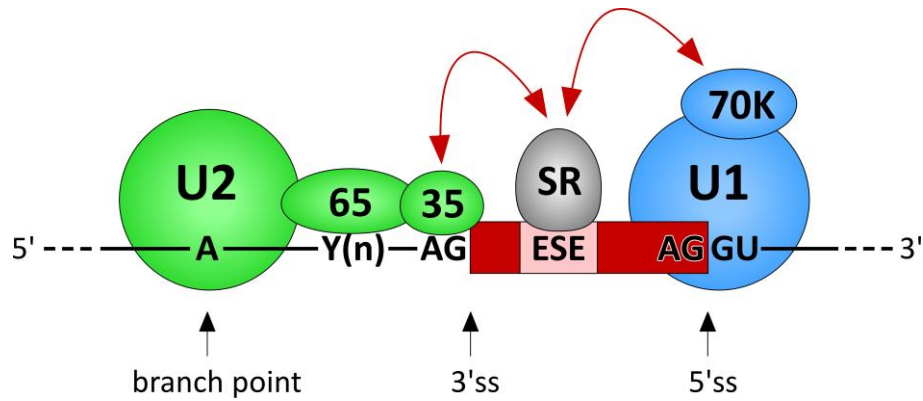


Figure 1.9: Molecular interactions during initial spliceosome assembly across an exon

During initial assembly of an exon-defined, A-like complex, U2 snRNP binds to an upstream BPS and U1 snRNP to the downstream 5'ss, while the U2AF65/35 heterodimer interacts with the PPT/3'ss. SR proteins bind to exonic splicing enhancers (ESEs) within the exon sequence and bridge interactions with components of the general splicing machinery (indicated by red arrows). The polypyrimidine tract is represented by Y(n).

In addition, auxiliary factors, namely SR and hnRNP proteins, bind to ESE or ESS sequences within the exon sequence and either support or inhibit exon recognition, respectively [Busch and Hertel, 2012]. SR proteins bind to ESE sequences within the exon and support spliceosome assembly by recruiting spliceosomal factors to the splice sites or by establishing protein-protein interactions with these factors to stabilize their interaction with the pre-mRNA [Lam and Hertel, 2002]. The SR proteins are characterized by consecutive RS-rich repeats (RS domain) and these RS domains interact with RS domains of spliceosomal factors to enable protein-protein interactions in the initial stages of spliceosome assembly. Thus, SR proteins establish a protein-protein network likely involving U1-70K and U2AF65/35 that bridges the interaction between U1 and U2 snRNP within the exon-defined A-like complex (Figure 1.9). In contrast, hnRNP proteins bind to ESS sequences and exhibit in general an inhibitory effect on spliceosome assembly by impairing the recruitment of spliceosomal factors to the splice sites or inhibiting protein-protein interactions. The antagonistic effect of the activating SR and inhibitory hnRNP proteins on spliceosome assembly modulates the probability of inclusion or exclusion of an exon during alternative splicing. SR and hnRNP proteins are conserved in higher eukaryotes such as *H. sapiens*, *Drosophila melanogaster* (*D. melanogaster*) and *Caenorhabditis elegans* (*C. elegans*), but not in *S. cerevisiae*, and their abundance correlates with the amount of alternative splicing events that occur in these organisms [Busch and Hertel, 2012].

The chemical steps of splicing can only occur across an intron, and thus a rearrangement from the exon-defined state to an intron-defined organization must occur to pair the 5'ss and 3'ss of an intron (Figure 1.10). Previous studies indicated that commitment to splice site pairing occurs upon formation of the A complex [Lim and Hertel, 2004], which suggested that the switch from exon- to

intron-definition occurs likely prior to the recruitment of the U4/U6.U5 tri-snRNP. But recent studies showed that the U4/U6.U5 tri-snRNP can associate with the exon-defined A-like complex resulting in formation of a cross-exon complex [Schneider *et al.*, 2010a]. Elegant biochemical data showed that the addition of a short RNA oligonucleotide containing a 5'ss induces the formation of a B-like complex, which shares similarities with an intron-defined B complex [Schneider *et al.*, 2010]. This suggests that the transition to an intron-defined organization can also occur when the U4/U6.U5 tri-snRNP of the cross-exon complex directly engages an upstream 5'ss and thereby leads to the pairing of splice sites across an intron (Figure 1.10). Thus, the exon- and intron-defined pathways of spliceosome assembly can converge at later stages of splicing, likely upon formation of a pre-catalytic B complex. Afterwards, splicing proceeds with the catalytic activation of the spliceosome and catalysis of both splicing reactions to generate a mature mRNA.

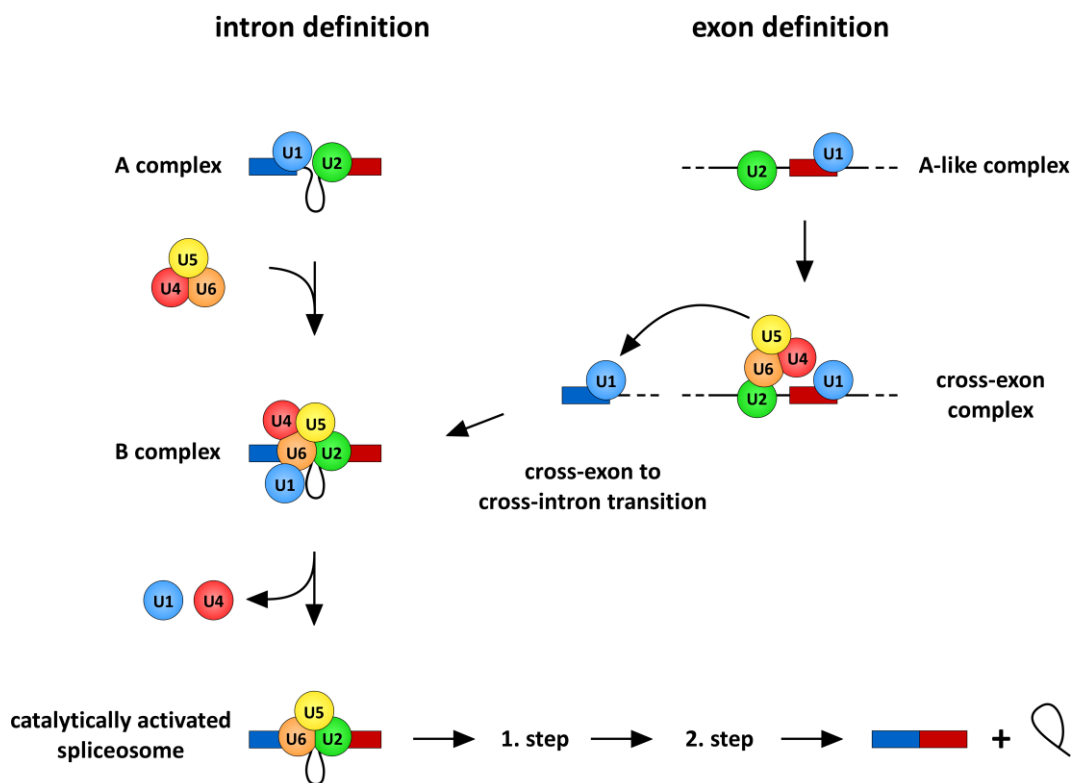


Figure 1.10: Alternative assembly pathways of the spliceosome

Intron and exon definition during spliceosome assembly. In the intron-defined pathway, U1 and U2 snRNPs bind to the 5'ss and BPS of the same intron. Upon association of the U4/U6.U5 tri-snRNP a fully-assembled B complex is formed. During exon-definition, U2 snRNP interacts with an upstream BPS and the U1 snRNP with the downstream 5'ss of an exon. The recruitment of the U4/U6.U5 tri-snRNP results in formation of a cross-exon complex. After transition to an intron-defined organization, spliceosome assembly proceeds with the canonical splicing pathway described in chapter 1.6.

Various studies showed that assembly of an exon-defined spliceosomal complex and the transition to an intron-oriented organization is an important point for the decision whether an exon is included or excluded from a mature mRNA during the process of alternative splicing [Bonnal *et al.*, 2008, Izquierdo *et al.*, 2005, House and Lynch, 2006, Sharma *et al.*, 2008]. Inhibition of either exon recognition or the switch to an intron-defined organization results directly in exon skipping. However, the mechanism of the cross-exon to cross-intron transition remains for the most part unclear.

1.12 Aims

One of the most fascinating design principles of the spliceosome is that it forms its catalytic core anew during each round of splicing by the stepwise assembly of five snRNPs and numerous additional proteins. The B complex is an assembly intermediate, in which the pre-formed U4/U6.U5 tri-snRNP is first stably-integrated into the spliceosome. Although much progress has been made in characterizing the protein dynamics that occur during splicing, further investigations are necessary to elucidate the role of many factors in splicing and their exact time of recruitment to the spliceosome. Little is known about which factors are minimally required to stably integrate the U4/U6.U5 tri-snRNP within the spliceosome and in which order they act to ensure formation of a pre-catalytic B complex.

The U5-specific protein hPrp28 was identified to be essential for the integration of the U4/U6.U5 tri-snRNP into the B complex and studies from *S. cerevisiae* provide evidence that this DEAD-box helicase enables RNA-RNA interactions between the U4/U6.U5 tri-snRNP and the 5' ends of the pre-mRNA, which are important for its stable association within the spliceosome [Mathew *et al.*, 2008, Staley and Guthrie, 1999]. Upon formation of the human B complex the proteins RED, MFAP1, FBP21, hSmu-1, hPrp38 and hSnu23 associate with the spliceosome [Agafonov *et al.*, 2011]. Nevertheless, the function of these B complex-specific proteins is currently unknown, in particular whether they play a role in stable binding of the U4/U6.U5 tri-snRNP. The U4/U6.U5 tri-snRNP-specific proteins hPrp31 and hPrp6 are phosphorylated by the hPrp4 kinase upon stable B complex formation [Schneider *et al.*, 2010b]. The depletion of the hPrp4 kinase from the splicing reaction inhibits assembly of a stable B complex, suggesting that the phosphorylation of hPrp31 and hPrp6 might be necessary for stable association of the U4/U6.U5 tri-snRNP with the spliceosome. However, the detailed hierarchy of assembly, i.e. order in which factors are recruited, and the prerequisites for stable binding of the U4/U6.U5 tri-snRNP during B complex formation, remain unclear.

Recently exon-defined spliceosomes were shown to contain the U4/U6.U5 tri-snRNP, providing evidence that it is possible for an exon-defined complex to be converted directly into an intron-

defined B complex [Schneider *et al.*, 2010a]. The addition of a RNA oligonucleotide containing a 5'ss induces the formation of a stabilized B-like complex, which shares similarities with an intron-defined B complex, including a stably-integrated U4/U6.U5 tri-snRNP. This transformation of the exon complex likely mimics the switch from an exon-defined to an intron-defined organization of the spliceosome. However, the prerequisites and order of events that occur during the transition from an exon-defined to an intron-defined B complex are only poorly understood.

Thus, I addressed the question which factors constitute the minimum requirement to induce the stable integration of the U4/U6.U5 tri-snRNP and assembly of a pre-catalytic B complex. The aim of this study was to dissect B complex formation and spliceosome remodeling during the conversion from an exon- to intron-defined organization in terms of protein composition and particle architecture at the electron microscopy level. Results of these studies will help to elucidate at which point exon- and intron-defined assembly pathway converge and will provide valuable insights into this decisive step of the spliceosome assembly pathway. Results of this study are expected to provide important information about the structural and compositional changes that occur during stable integration of the U4/U6.U5 tri-snRNP and B complex formation, which is a prerequisite for the activation of the spliceosome.

2. Materials and methods

2.1 Materials

2.1.1 Chemicals

Acetic acid	Merck, Germany
Agarose (low melting point)	Invitrogen, Netherlands
Agarose	Invitrogen, Netherlands
Ammonium peroxodisulphate (APS)	Merck, Germany
Ampicillin	Sigma-Aldrich, Germany
AMT (4'-aminomethyl-4,5',8-trimethylpsoralen hydrochloride)	Sigma-Aldrich, Germany
Boric acid	Merck, Germany
Bovine serum albumin (BSA), acetylated	Sigma-Aldrich, Germany
Bromphenol blue	Merck, Germany
Coomassie brilliant blue G-250	Serva, Germany
Creatine phosphate	Sigma-Aldrich, Germany
Dimethylsulphoxide (DMSO)	Roth, Germany
Dipotassiumhydrogenphosphate	Merck, Germany
Dithiothreitol (DTT)	Roth, Germany
DNA molecular weight marker	Gibco, New Zealand
EDTA (Disodium salt dihydrate)	Roth, Germany
Ethanol	Merck, Germany
Ethidium bromide	Roche, Germany
Ficoll	Sigma-Aldrich, Germany
Fish sperm DNA (10 mg/ml)	Roche, Germany
Formaldehyde	Merck, Germany
Formamide	Merck, Germany
Glutaraldehyde	Electron Microscopy Sciences, USA
Glycerol	Merck, Germany
Glycine	Merck, Germany
Glycoblu	Ambion, USA
Heparin (sodium salt)	Roth, Germany

HEPES (N-2-Hydroxyethylpiperazin-N-2-ethansulfonic acid)	Calbiochem, USA
Imidazole	Merck, Germany
IPTG	Merck, Germany
Lithium chloride	Merck, Germany
Maltose	Merck, Germany
Magnesium acetate	Merck, Germany
Magnesium chloride	Merck, Germany
Methanol	Merck, Germany
β -Mercaptoethanol	Roth, Germany
Milk powder	Heirler, Germany
MOPS	Invitrogen, Netherlands
Nonidet P-40 (Igepal CA-630)	Sigma-Aldrich, Germany
PMSF (Phenylmethylsulfonylfluoride)	Roche, Germany
Polyvinylpyrrolidone	Sigma-Aldrich, Germany
Potassium acetate	Merck, Germany
Potassium chloride	Merck, Germany
Potassium dihydrogen phosphate	Merck, Germany
Pre-stained protein-molecular weight marker	Bio-Rad, Germany
Roti phenol-chloroform-isoamyl alcohol (PCI)	Roth, Germany
Rotiphorese gel 30 solution	Roth, Germany
Rotiphorese gel 40 solution	Roth, Germany
Silver nitrate	Merck, Germany
Sodium acetate	Merck, Germany
Sodium carbonate	Merck, Germany
Sodium chloride	Merck, Germany
Sodium dodecyl sulfate (SDS)	Serva, Germany
Sodium thiosulfate	Merck, Germany
Spermidine	Sigma-Aldrich, Germany
TEMED (N, N, N', N'-Tetramethylethylenediamine)	Sigma-Aldrich, Germany
Tris [Tris-(hydroxymethyl)aminomethane]	Roth, Germany
Triton X-100	Merck, Germany
tRNA from <i>E. coli</i>	Boehringer, Germany
Tween-20	Sigma-Aldrich, Germany

Uranyl formate	in-house
Urea	Merck, Germany
Xylene cyanol	Fluka, Switzerland

2.1.2 Chromatography materials and consumables

Amylose resin	New England Biolabs, Germany
Cassettes for film exposure	Kodak, USA
Centrifuge tubes	Beraneck, Germany
Chromatography columns	Bio-Rad, Germany
Concentrator	Millipore, USA
Dialysis membranes (MWCO 6000-8000 Da)	SpektraPor, USA
HisTrap HP, Ni-NTA-Sepharose (5 ml)	GE Healthcare, UK
NuPAGE™ gels (1.5 mm, 4-12%)	Invitrogen, Netherlands
Nylon membrane Hybond XL	GE Healthcare, UK
Parafilm	Roth, Germany
Poly-Prep columns	Bio-Rad, USA
Protein A-Sepharose CL 4B0	GE Healthcare, UK
Protran BA 83 nitrocellulose	Whatman, UK
ProbeQuant™ G-25/ G-50 micro columns	GE Healthcare, UK
Slide-A-Lyzer dialysis units (MWCO 6 kDa)	Pierce, USA
Sterile filters (0.2 µm or 0.45 µm)	Sarstedt, Germany
Superdex 200 (16/60) oder (10/30)	GE Healthcare, Germany
Surgical blades	Martin, Germany
Whatman 3MM paper	Whatman, UK
X-ray films (BioMax MR)	Kodak, USA

2.1.3 Commercial kits

BCA™ protein assay kit	Pierce, USA
ECL Western Blot Detection Kit	GE Healthcare, USA
Prime-It II Random Primer Labeling Kit	Stratagene, USA
QIAGEN Plasmid Maxi Kit	Qiagen, Germany
QIAquick® Gel Extraction Kit	Qiagen, Germany

2.1.4 Machines

ÄKTA Explorer	GE Healthcare, UK
ÄKTA Prime	GE Healthcare, UK
Autoclaves	H+P Labortechnik, Germany
Biofuge fresco	Kendro, USA
Biofuge pico	Kendro, USA
Gel documentation unit	Bio-Rad, Germany
Gel electrophoresis apparatus	in-house
Gel dryer model 583	Bio-Rad, Germany
Gradient master model 106	BioComp Instruments, Canada
Head-over-tail rotor	Cole-Parmer, USA
Heating blocks	Eppendorf, Germany
Hybridization oven	Hybaid Biometra, UK
LTQ Orbitrap XL	Thermo Fisher Scientific, Germany
Megafuge 1.0R	Kendro, USA
Milli-Q-water supply apparatus	Millipore, USA
PerfectBlue semi-dry electro blotter	PeqLab, Germany
pH-Meter	Mettler Toledo, Switzerland
Phosphorimager Typhoon 8600	Amersham Pharmacia, Germany
Power supply EPS 2A200	Hoefer Pharmacia Biotech, USA
Power supply EPS 3501/XL	Amersham Pharmacia, Germany
Q-ToF Ultima mass spectrometer	Waters, USA
Scintillation counter LS 1701	Packard, USA
Sorvall HB-6 rotor	Kendro, USA
Sorvall SA800 AT4 rotor	Kendro, USA
Sorvall SS-34 rotor	Kendro, USA
Sorvall TH660 rotor	Kendro, USA
Sorvall TST41.14 rotor	Kendro, USA
Speed Vac Konzentrator 5301	Eppendorf, Germany
Spectrophotometer Nanodrop ND-1000	Thermo Fisher Scientific, Germany
Spectrophotometer Ultrospec 3000 pro	Amersham Pharmacia, Germany
SS-34 rotor	Kendro, USA
Tabletop centrifuge 5415D	Eppendorf, Germany

Trans-Blot Cell	Bio-Rad, USA
Ultracentrifuge Discovery 90	Sorvall/Kendro, USA
Ultracentrifuge Discovery M150	Sorvall/Kendro, USA
UV-Stratalinker 2400	Stratagene, USA
UV lamps (365 nm)	Bachofer, Germany
Vortex	Janke & Kunkel, Germany
X-ray film developer X-Omat 2000	Kodak, USA

2.1.5 Nucleotides

Nucleoside-5'-triphosphate (100 mM): ATP, CTP, UTP, GTP	Pharmacia, Germany
Deoxynucleoside-5'-triphosphate (100 mM): dATP, dCTP, dTTP, dGTP	Pharmacia, Germany
7-monomethyl-diguanosine triphosphate (m ⁷ G(5')ppp(5')G-cap)	Kedar, Poland
AMP-PNP	Sigma-Aldrich, Germany

2.1.6 Radiolabeled nucleotides

α - ³² P-UTP [10 μ Cl/ μ l, 3000 Ci/mmol]	Perkin-Elmer, Germany
γ - ³² P-ATP [10 μ Cl/ μ l, 6000 Ci/mmol]	Perkin-Elmer, Germany
α - ³² P-dATP [10 μ Cl/ μ l, 3000 Ci/mmol]	Perkin-Elmer, Germany

2.1.7 RNA oligonucleotides

RNA oligonucleotides were purchased from Eurofins MWG Operon or Sigma-Aldrich. Modifications are indicated by brackets.

<u>Name</u>	<u>Sequence</u>
5'ss oligonucleotide (wildtype)	AAGGUAAGUAU
2'O-ribose methylated 5'ss oligonucleotide	[AAGGUAAGUAU]
U5:5'ss	UUUGUAAGUAU
U6:5'ss	AAGGUAACUA
U5:5'ss + U6:5'ss	UUUGUAACUA
-1G \rightarrow A	AAAGUAAGUAU
+1G \rightarrow A	AAGAUAAGUAU
+2U \rightarrow A	AAGGAAAGUAU

GG → AA	AAAAUAAGUUAU
GU → AA	AAGAAAAGUUAU
GG → rIrl	AA[ribo-inosine][ribo-inosine]UAAGUA
(-1) 6-thio-G	AA[6-thio-G]GUAAGUUAU
(+1) 6-thio-G	AAG[6-thio-G]UAAGUUAU
(+2) 4-thio-U	AAGG[4-thio-U]AAGUUAU

2.1.8 Antibodies

Anti-hPrp8	Dept. Lührmann [Lauber <i>et al.</i> , 1996]
Anti-hSnu66	Dept. Lührmann [Makarova <i>et al.</i> , 2001]
Anti-hPrp31, phospho-specific	Dept. Lührmann [Schneider <i>et al.</i> , 2010b]
Anti-RED	Dept. Lührmann
Anti-MFAP1	Dept. Lührmann
Anti-FBP21	Santa Cruz Biotechnology, USA
Anti-hSmu-1	Santa Cruz Biotechnology, USA
Anti-hPrp38	Dept. Lührmann
Anti-hSnu23	Dept. Lührmann
Anti-His ₆ -tag	Abcam, UK
Goat-anti-rabbit (horseradish peroxidase coupled)	Jackson ImmunoResearch, USA

2.1.9 Enzymes

Complete protease inhibitor, EDTA-free	Roche, Germany
Klenow fragment of DNA polymerase I [5 U/μl]	New England Biolabs, Germany
Proteinase K	Fluka, Switzerland
Restriction endonucleases	New England Biolabs, Germany
RNase A [1 mg/ml]	Ambion, USA
RNase T1 [1 U/μl]	Ambion, USA
RNasin (RNase inhibitor) [40 U/μl]	Promega, USA
RQ1 DNase [1 U/μl]	Promega, USA
T4 Polynucleotide kinase (PNK) [10 U/μl]	New England Biolabs, Germany
T7 RNA polymerase [20 U/μl]	New England Biolabs, Germany
Yeast inorganic pyrophosphatase (YIPP) [0.1 U/μl]	New England Biolabs, Germany

2.1.10 Plasmids

pMINX	U2-dependent pre-mRNA construct (MINX) in pSP65-vector under control of SP6 promoter, Amp ^R . [Zillman <i>et al.</i> , 1988].
pMINX-exon	MINX exon-RNA construct in pSP65-vector under control of T7 promoter, Amp ^R . [Schneider <i>et al.</i> , 2010].
pMS2-MBP	MS2-MBP fusion protein in pMAL vector (NEB), Amp ^R .
pET21a-hPrp28	His ₆ -tagged hPrp28 wildtype protein in pET21a vector (S. Möhlmann).
pET21a-hPrp28-AAAD	His ₆ -tagged hPrp28 ^{AAAD} protein in pET21a vector (S. Möhlmann).

2.1.11 Bacteria strains

<i>E. coli</i> DH5 α	Novagen, Germany
<i>E. coli</i> Rosetta 2 (DE3)	Novagen, Germany

2.1.12 Cell line

HeLa S3 cells (human cervical cancer cells)	GBF, Germany
---	--------------

2.1.13 Buffers

Commonly used media, buffers and solutions were prepared with deionized water (Millipore) and autoclaved if necessary (121 °C, 20 min, 1 bar). Solutions with heat-labile components were filter-sterilized (0.22 μ m).

Coomassie staining solution:	100 μ M Coomassie brilliant blue G-250 0.13 mM (v/v) HCl
100x Denhardt's solution:	2 % (w/v) Ficoll 400 2 % (w/v) Polyvinylpyrrolidone 2 % (w/v) BSA
6x DNA loading dye:	60 % (v/v) glycerol 10 mM Tris-HCl, pH 7.5 60 mM EDTA, pH 8.0 0.05 % (w/v) bromphenol blue 0.05 % (w/v) xylene cyanol
10x G-75 buffer:	200 mM HEPES 0.75 M KCl 15 mM MgCl ₂ adjust to pH 7.9

10x G-150 buffer:	200 mM HEPES 1.5 M KCl 15 mM MgCl ₂ adjust to pH 7.9
1x MC buffer:	10 mM HEPES-KOH, pH 7.6 10 mM KOAc 0.5 mM MgOAc 5 mM DTT (add one Complete EDTA-free protease inhibitor cocktail tablet to 50 ml of 1x MC buffer)
5x Native gel loading dye:	90 mM Tris 90 mM boric acid 2.5 mM EDTA, pH 8.0 30 % (v/v) glycerol 0.05 % (w/v) bromphenol blue
10X PBS:	1.3 M NaCl 200 mM Na ₂ HPO ₄ adjust to pH 7.4 or 8.0
2x PK buffer:	200 mM Tris-HCl, pH 7.5 25 mM EDTA, pH 8.0 2 % (w/v) SDS
Pre-/Hybridisationsbuffer: (for Northern blot)	25 mM Na ₂ HPO ₄ , pH 6.5 5x Denhardt's solution 6x SSC 50 % (v/v) deionized formamide 0.5 % (w/v) SDS 100 µg/ml fish sperm DNA
2x RNA loading dye:	80 % (v/v) formamide 1 mM EDTA, pH 8.0 0.05 % (w/v) bromphenol blue 0.05 % (w/v) xylene cyanol

1x Roeder C buffer:	25 % (v/v) glycerol 20 mM HEPES-KOH, pH 7.9 420 mM NaCl 1.5 mM MgCl ₂ 0.2 mM EDTA, pH 8.0 0.5 mM DTT 0.5 mM PMSF
1x Roeder D buffer:	10 % (v/v) glycerol 20 mM HEPES-KOH, pH 7.9 100 mM KCl 1.5 mM MgCl ₂ 0.2 mM EDTA, pH 8.0 0.5 mM DTT 0.5 mM PMSF
6x SDS loading dye:	750 mM Tris-HCl, pH 6.8 6 % (w/v) SDS 30 % (v/v) glycerol 0.03 % (w/v) bromophenol blue 60 mM DTT
SDS-PAGE Running buffer:	25 mM Tris-HCl, pH 6.8 192 mM glycine 1 % (w/v) SDS
4x Separating gel buffer:	1.5 M Tris 0.4 % (w/v) SDS adjust to pH 8.8
20x SSC:	3 M NaCl 0.3 M sodium citrate
4x Stacking gel buffer:	0.5 M Tris 0.4 % (w/v) SDS adjust to pH 6.8
Stripping buffer:	62.5 mM Tris-HCl, pH 6.7 100 mM β-mercaptoethanol 2 % (w/v) SDS

10x TBE:	0.89 M Tris 0.89 M boric acid 25 mM EDTA, pH 8.0
10x TBS:	200 mM Tris 1.37 M NaCl adjust to pH 7.6
10x TBS-T:	500 mM Tris 1.5 M NaCl 1 % (v/v) Tween-20 adjust to pH 7.5
TNES (RNA extraction buffer):	20 mM Tris-HCl pH 7.5 150 mM NaCl 0.2 mM EDTA, pH 8.0 0.5 % (w/v) SDS
5x TRO buffer:	1 M HEPES-KOH, pH 7.5 200 mM DTT 160 mM MgCl ₂ 10 mM spermidine
10x Western transfer buffer:	200 mM Tris 1.5 M glycine

2.2 Methods

2.2.1 Molecular biology standard methods

2.2.1.1 Nucleic acid quantification

To determine the concentration of nucleic acids the extinction coefficient in an aqueous solution was measured at a wavelength of 260 nm and 280 nm in comparison to the corresponding buffer without nucleic acids. The ratio of OD₂₆₀/OD₂₈₀ determined the purity of a nucleic acid solution: 2.0 corresponded to pure RNA or oligonucleotides and 1.8 to pure DNA. The following equations were used to determine the concentrations:

$$1 \text{ OD}_{260}: 50 \text{ }\mu\text{g/ml double-stranded DNA}$$

$$1 \text{ OD}_{260}: 33 \text{ }\mu\text{g/ml single-stranded DNA}$$

$$1 \text{ OD}_{260}: 40 \text{ }\mu\text{g/ml single-stranded RNA}$$

Lower ratios show contamination with proteins or phenol, which requires an additional PCI extraction (2.2.1.2).

2.2.1.2 PCI extraction

The phenol-chloroform-isoamyl alcohol (PCI) extraction was used to separate nucleic acids from proteins. Phenol and chloroform denature proteins and keep them in the organic phase, while nucleic acids stay in the aqueous phase. Reactions were first adjusted to 200 μ l final volume. Subsequently an equal volume of PCI was added and samples were thoroughly mixed on a rotational shaker for 10 min at room temperature. To separate the aqueous from the organic phase, the suspension was centrifuged for 10 min at room temperature and 13000 rpm in a microfuge. The nucleic acids in the aqueous phase were precipitated by addition of 0.1 volume 3 M NaOAc pH 4.7 and 3 volumes absolute ethanol. Samples were kept at -20 °C for at least 30 min and precipitates were sedimented by centrifugation for 30 min at 4 °C and 13000 rpm in a microfuge. The pellet was washed once with 70 % (v/v) ethanol, vacuum dried and finally resuspended in the desired solution.

2.2.1.3 Proteinase K digestion

To facilitate RNA recovery from protein rich samples, proteinase K treatment was performed prior to PCI extraction. Samples were incubated in 1x PK buffer in the presence of 0.2 μ g/ μ l proteinase K for 45 min at 45 °C. The RNA was recovered by PCI extraction (2.2.1.2) followed by ethanol precipitation in the presence of 0.3 M NaOAc pH 4.7. The dried RNA pellet was subsequently resuspended in sterile water and stored at -20 °C.

2.2.1.4 Generation of templates for run-off *in vitro* transcriptions

DNA plasmids encoding the MINX pre-mRNA or exon-RNA were extracted from *E. coli* DH5 α cells using the QIAGEN Plasmid Maxi Kit (Qiagen) according to the manufacturer's protocol. Plasmid DNA was eluted in ddH₂O and used for restriction digestion to generate templates for run-off *in vitro* transcriptions. The reactions were performed with the respective restriction endonuclease (NEB) according to instruction of the manufacturer. Briefly, 10 units of enzyme were used to cut 1 μ g of plasmid DNA for 1 h at 37 °C.

Agarose gel-electrophoresis was then performed to purify preparative amounts of DNA fragments after restriction enzyme digestions. Samples were supplemented with 6x DNA loading dye. Depending on the length of linearized plasmids, gels were prepared using 1-2 % (w/v) agarose and 0.4 μ g/ml ethidium bromide in 1x TBE buffer. Gels were run at 100 V for approximately 1 h in 1x TBE buffer.

In order to isolate DNA from agarose gels, DNA bands visualized with UV-light at a wavelength of 365 nm were cut out from the gel using a sterile surgical blade. DNA was extracted using the QIAquick[®] Gel Extraction Kit (Qiagen) according to the manufacturer's instructions.

2.2.1.5 *In vitro* transcription

RNA *in vitro* transcriptions were carried out using DNA templates derived from linearized plasmids (2.2.1.4). Uniformly ³²P-labeled m⁷G(5')ppp(5')G-capped MINX pre-mRNA was synthesized *in vitro* by T7 run-off transcription. The composition of a standard reaction is shown in Table 2.1. For transcriptions of MINX exon-RNA, the m⁷G(5')ppp(5')G-cap was omitted and the final concentration of GTP was increased to 7.5 mM.

Table 2.1: A standard *in vitro* transcription reaction

	Stock concentration	Minx pre-mRNA		Minx exon-RNA	
		Volume (μ l)	Final concentration	Volume (μ l)	Final concentration
TRO buffer	5x	16	1x	16	1x
ATP	100 mM	6	7.5 mM	6	7.5 mM
CTP	100 mM	6	7.5 mM	6	7.5 mM
GTP	100 mM	1	1.25 mM	6	7.5 mM
UTP	100 mM	1	1.25 mM	1	1.25 mM
m ⁷ G(5')ppp(5')G-cap	151 mM	2.7	5 mM	-	-
Template	1 μ g/ μ l	4	50 ng/ μ l	4	50 ng/ μ l
RNasin	40 U/ μ l	2	1 U/ μ l	2	1 U/ μ l
YIPP	40 U/ μ l	1	0.5 U/ μ l	1	0.5 U/ μ l
T7 RNA polymerase	20 U/ μ l	4	1 U/ μ l	4	1 U/ μ l
α - ³² P-UTP	10 μ Ci/ μ l, 3000 Ci/mmol	10		10	
ddH ₂ O		26.3		24	
total		80		80	

The transcription was carried out at 37 °C for 3 h. The DNA template was removed by addition of 2 µl RQ1 DNase (1U/µl, NEB) and further incubation at 37 °C for 30 min. In order to purify the pre-mRNA from unincorporated NTPs, the synthesized RNA was first separated by denaturing PAGE (2.2.1.6). The RNA bands were detected via autoradiography and cut out of the gel using a sterile razor blade. RNA was eluted from the gel pieces in TNES buffer overnight at 4 °C. Alternatively, the transcription reaction was passed through a ProbeQuant G-50 column (GE Healthcare) according to the manufacturer's protocol to remove unincorporated nucleotides.

2.2.1.6 Denaturing polyacrylamide gel-electrophoresis

Denaturing polyacrylamide gel electrophoresis (PAGE) in the presence of 8 M urea was mainly used to separate snRNAs or intermediates and products of pre-mRNA *in vitro* splicing. Depending on the size of the RNAs, the gels contained 5-14 % (v/v) polyacrylamide, 8 M urea and 1x TBE. Polymerization of the gels was initiated by addition of 300 µl 10 % (w/v) APS and 30 µl TEMED to 50 ml of gel solution. The RNA samples were dissolved in RNA loading dye, denatured for 5 min at 96 °C and briefly chilled on ice before loading. The electrophoresis was performed at 15 W in 1x TBE buffer. The RNA was then visualized by Northern blotting, silver staining or autoradiography.

2.2.1.7 Silver staining of RNA

To stain RNA separated by denaturing PAGE (2.2.1.6), the gel was fixed in 10 % (v/v) acetic acid for 30 min at room temperature. After fixation, the gel was washed three times with water for 5 min each and then treated with a 12 mM AgNO₃ and 0.056 % (v/v) formaldehyde solution for 30 min at room temperature. Again, the gel was briefly washed three times with water for 30 seconds each. For development the gel was treated with a solution containing 280 mM Na₂CO₃, 0.056 % (v/v) formaldehyde and 2.5 mM Na₂S₂O₃ until a clearly visible staining of the RNA was achieved. The staining was stopped by addition of 10 % (v/v) acetic acid solution.

2.2.1.8 Northern blot

Northern blot analyses were performed to detect specific RNAs via radiolabeled DNA probes complementary to the respective RNA. RNAs separated by denaturing PAGE (2.2.1.6) were transferred to a nylon membrane (Hybond XL) using a semi-dry electroblot apparatus. The transfer was carried out in 1x TBE at 2 mA/cm² of the membrane for 2 h. After transfer the blot was UV-irradiated (1200 mJ) using a UV-Stratalinker 2400 in order to crosslink the RNAs to the membrane. The membrane was incubated with pre-hybridization buffer at 42 °C for 2 h. The radiolabeled DNA probes were denatured by heating at 95 °C for 5 min and then added to the pre-hybridization buffer and the membrane was incubated overnight at 42 °C. After hybridization, the membrane was washed

twice with wash buffer 1 [2x SSC, 0.5 % (w/v) SDS] and twice with wash buffer 2 [2x SSC, 0.1 % (w/v) SDS] for 15 min each at room temperature. After washing, signals were detected by autoradiography.

The radiolabeled DNA probes were generated from plasmids encoding the target sequence by using α - 32 P-dATP and a Prime It II Random Labeling Kit (Stratagene) according to the manufacturer's protocol.

2.2.1.9 Radioactive 5'-labeling of RNA oligonucleotides

In order to detect protein-RNA crosslinks, 5' ss RNA oligonucleotides were radioactively labeled at their 5'-end using γ - 32 P-ATP and T4 polynucleotide kinase (PNK). The concentration of RNA oligonucleotides were adjusted to 100 pmol/ μ l. A standard 25 μ l reaction containing 1 μ l of the RNA oligo, 2.5 μ l of 10x PNK buffer (NEB), 2 μ l of T4 PNK (10U/ μ l, NEB) and 10 μ l of γ - 32 P-ATP (6000 Ci/mmol, 10 μ Ci/ μ l) was incubated at 37 °C for 1 h. After incubation, the radiolabeled oligonucleotide was purified from unincorporated γ - 32 P-ATP using ProbeQuant G-25 columns (GE Healthcare) according to the manufacturer's protocol.

2.2.2 Protein-biochemistry standard methods

2.2.2.1 Protein quantification

To measure the concentration of proteins, a BCATM Protein Assay Kit (Pierce) was used according to the manufacturer's protocol. This assay is a detergent-compatible method based on bicinchoninic acid (BCA) for the colorimetric detection. Quantification of total protein was analyzed at an absorption maximum of 562 nm.

2.2.2.2 Denaturing SDS polyacrylamide gel-electrophoresis (SDS-PAGE)

Proteins were resolved by denaturing SDS-PAGE according to Laemmli [Laemmli, 1970]. Protein samples were dissolved in 6x SDS loading dye and denatured for 10 min at 70 °C, before loading onto a 10-13 % step polyacrylamide gel with a 5% stacking gel.

Table 2.2: Compositions of SDS gels

	Stock concentration	Stacking gel	Separation gel	
		5 %	10 %	13 %
		Volume	Volume	Volume
Acrylamide/Bis solution	30 %	2 ml	6.7 ml	8.7 ml
Stacking buffer	4x	3 ml	-	-
Separation buffer	4x	-	5 ml	5ml
SDS	10 % (w/v)	400 μ l	400 μ l	400 μ l
APS	10 % (w/v)	130 μ l	130 μ l	130 μ l
TEMED		14 μ l	14 μ l	14 μ l
ddH ₂ O		ad 12 ml	ad 20 ml	ad 20 ml

The gel was run in 1x SDS running buffer at 30 mA until the samples entered the separating gel and then run at 50 mA until the bromophenol blue reached the bottom of the gel. Proteins were visualized by coomassie or silver staining. For mass spectrometry or western blot analysis, proteins were separated on 4-12 % NuPAGE™ gradient gels (Invitrogen) run in 1x MOPS buffer (Invitrogen) according to the manufacturer's protocol.

2.2.2.3 Coomassie staining

Coomassie staining of proteins was performed according to Sambrook *et al.* [Sambrook *et al.*, 1989]. Proteins in denaturing SDS gels were stained with coomassie staining solution overnight at room temperature and were subsequently destained in water until protein bands were clearly visible.

2.2.2.4 Silver staining of proteins

Silver staining of proteins was performed as described in Blum *et al.*, 1987. Protein gels were fixed in 40 % (v/v) MeOH and 10 % (v/v) acetic acid over night at room temperature while gently shaking. After fixation, the gel was washed twice with 50 % (v/v) ethanol and once with 30 % (v/v) ethanol for 20 min each. The gel was then washed with 0.8 mM Na₂S₂O₃ for exactly 60 seconds, and immediately washed three times with water to remove excessive thiosulfate from the surface. After that, the gel was incubated with a 12 mM AgNO₃, 0.026 % (v/v) formaldehyde solution for 20 min. Again, the gel was briefly washed with water, followed by the development step with 560 mM Na₂CO₃, 0.0185 % (v/v) formaldehyde and 16 μM Na₂S₂O₃ until the desired visualization of protein bands was achieved. The staining was stopped by addition of a 10 % (v/v) acetic acid solution. For detection of radioactive signals by autoradiography the gel was dried at 80 °C for 1 h and exposed to a phosphoimager screen.

2.2.2.5 Western blot

Proteins separated by SDS-PAGE were transferred to a nitrocellulose membrane (Protan BA83 nitrocellulose, 0.2 μm) using a wet electroblot procedure. Therefore, a sandwich of two layers of Whatman 3MM paper, SDS gel, nitrocellulose membrane and again two layers of Whatman 3MM paper were assembled in a Trans-Blot Cell (Biorad). After assembly of the blotting sandwich, the transfer was carried out in 1x western transfer buffer + 5 % (v/v) ethanol by applying a constant current of 65 V for 1 h at room temperature. Subsequently, the membrane was incubated with primary antibodies in 1x TBS-T + 5 % (w/v) milk overnight at 4 °C. Immunoblotting was performed with the antibodies specified in the figures. The membrane was then washed three times with 1x TBS-T for 10 min each. Secondary antibodies (Horseradish peroxidase-conjugated anti-rabbit antibodies diluted 1:30000) were incubated for 1 h at room temperature and the blot washed again

three times with 1x TBS-T. Proteins were detected by enhanced chemiluminescence using an ECL Western Blot Detection Kit (GE Healthcare) according to the manufacturer's instructions.

For the sequential incubation of a membrane with different antibodies, the previous antibodies had to be removed from the blot. Therefore, the membrane was incubated with stripping buffer for 30 min at 50 °C with constant shaking. Afterwards the membrane was washed twice in 1x TBS-T for 15 min each at room temperature.

2.2.2.6 Purification of MS2-MBP

The fusion protein, which was used for affinity-purification of spliceosomal complexes was expressed in an *E. coli* strain containing the plasmid encoding the MS2-MBP protein. Cells were grown to an OD₆₀₀ of 0.3-0.6 in LB medium supplemented with the respective antibiotics. The expression of the MS2-MBP protein was then induced by adding 0.1 M IPTG. The culture was further incubated for 2.5 h at 37 °C. The cells were pelleted by centrifugation in a Cryofuge 6000i (Heraeus) for 10 min at 2000 rpm. The supernatant was discarded and the cell pellet was washed with 40 ml of washing buffer (20 mM Tris-HCl pH 7.6, 0.2 M NaCl) supplemented with one complete EDTA-free protease inhibitor cocktail tablet. Then, the cells were resuspended in 25 ml of washing buffer and subsequently lysed by sonification. The lysate was centrifuged in a SS34 rotor for 30 min at 16000 g. The supernatant was transferred to 2 ml of amylose beads (NEB), which were equilibrated with MBP150 buffer (20 mM HEPES-KOH pH 7.9, 150 mM NaCl, 0.05 % (v/v) NP-40). Afterwards the mixture was incubated head-over-tail for 2 h at 4 °C. The suspension was transferred into a Bio-Spin chromatography column (Biorad) and the amylose resin was washed with 10 column volumes of MBP150 buffer followed by 5 column volumes of 5 mM Na₂HPO₄ pH 7.0. The MS2-MBP protein was then eluted with 5 mM Na₂HPO₄ pH 7.0 containing 20 mM maltose and the eluate was subsequently loaded onto a pre-equilibrated heparin agarose column. The column was washed with 10 volumes of 5 mM Na₂HPO₄ pH 7.0 and the protein was eluted fraction-wise with elution buffer [20 mM HEPES-KOH pH 7.9, 100 mM KCl, 15 % (v/v) glycerol, 0.5 mM DTT]. Peak fractions were pooled, shock frozen in liquid nitrogen and finally stored at -80 °C. The protein concentration was determined using the BCATM Protein Assay Kit (2.2.2.1).

2.2.2.7 Purification of recombinant hPrp28 proteins

To purify recombinant hPrp28 protein, *E. coli* strains containing the plasmids for His₆-tagged hPrp28 wildtype or AAAD mutant were grown in 2xYT medium [1.6 % (w/v) Tryptone, 0.5 % (w/v) NaCl, 1 % (w/v) Yeast extract] supplemented with the respective antibiotics. Cells were grown to an OD₆₀₀ of 0.4-0.8 at 30 °C and the expression of the recombinant protein was then induced by adding 0.3 mM IPTG. The culture was further incubated at 18 °C overnight and cells were harvested by centrifugation

in a Cryofuge 6000i (Heraeus) for 10 min at 2000 rpm and 4 °C. The cell pellet was resuspended in 20-50 ml of lysis buffer [50 mM Tris-HCl pH 7.5, 2 M LiCl, 5 % (v/v) glycerol, 2 mM β -mercaptoethanol] and subsequently subjected to lysis by a microfluidizer (3-7 cycles at 80 psi). The lysate was centrifuged in a SS34 rotor for 30 min at 16000 g and 4 °C. The supernatant was supplemented with 10 mM imidazole and subsequently applied to a pre-equilibrated Ni²⁺-NTA column (pre-packed columns with 5 ml column volume, GE Healthcare). The column was washed with 6 column volumes of buffer A [50 mM Tris-HCl pH 7.5, 500 mM NaCl, 5 % (v/v) glycerol, 2 mM β -mercaptoethanol] containing 5 % (v/v) of buffer B (buffer A + 300 mM imidazol). For elution of the His₆-tagged proteins the column was washed with 6 column volumes of a linear gradient from 5-100 % (v/v) of buffer B. The elution was collected in 1 ml fractions and the fractions containing the recombinant hPrp28 protein were pooled. The eluted sample was concentrated to approximately 10 mg/ml and subjected to a second purification step in order to remove remaining contaminating proteins. Therefore, this sample was loaded to a pre-equilibrated size-exclusion column (Superdex 200, GE Healthcare). Gel-filtration was performed in the presence of a high-salt buffer [10 mM Tris-HCl pH 7.5, 500 mM NaCl, 5 % (v/v) glycerol, 2 mM β -mercaptoethanol] to avoid aggregation of the recombinant protein on the column. The protein was then eluted with one volume of high-salt buffer. The eluted protein was concentrated to 1-5 mg/ml, shock frozen in liquid nitrogen and finally stored at -80 °C.

2.2.2.8 Purification of antibodies

For the purification of antibodies, a 1 ml aliquot of packed PAS beads (GE Healthcare) was washed twice with 10 ml 1x PBS pH 8.0. Then, 3 ml of sera were mixed with 7 ml of 1x PBS pH 8.0 and this mixture was passed through a 0.45 μ m filter to remove particulate material. The filtrate was then incubated with the washed PAS beads for 2 h at RT head-over-tail. After antibody binding, the supernatant was removed and the beads were washed five times with 10 ml 1x PBS pH 8.0 each. Bound antibodies were then eluted via pH shock by successively adding 10 times 500 μ l elution buffer (0.1 M glycine pH 2.7). The eluates were collected in separate fractions and the pH of each fraction was immediately neutralized by the addition of 30 μ l of 1 M Tris pH 9.5. The protein concentration in each fraction was determined by BCATM Protein Assay and the peak fractions were pooled. The purified antibodies were dialyzed in a Slide-A-Lyzer (Pierce) against 500 ml 1x PBS pH 8.0 for five hours with one change of buffer after 2.5 h.

2.2.3 Special methods

2.2.3.1 Cell culture

HeLa S3 cells (Computer Cell Culture Center, Belgium) were grown in suspension in S-MEM media supplemented with 5 % (v/v) newborn calf serum, 50 µg/ml penicillin and 100 µg/ml streptomycin to a density of $2.5\text{-}5 \times 10^5$ cells/ml. Cultivation and harvesting of the cells was essentially done as previously described in Kastner, 1998, and Dignam *et al.*, 1983.

2.2.3.2 Preparation of splicing active HeLa nuclear extract

Splicing active nuclear extract was prepared from HeLa cells as described in Dignam *et al.*, 1983. Six to eight liters of HeLa cells were grown to a density of $2.5\text{-}5 \times 10^5$ cells/ml [Kastner, 1998]. The cells were pelleted by centrifugation in a Cryofuge 6000i (Heraeus) for 10 min at 2000 rpm. The supernatant was discarded and the cells were washed three times with ice-cold 1x PBS pH 7.4. Then, the cell pellet was resuspended in 1.25 volumes of 1x MC buffer supplemented with two complete EDTA-free protease inhibitor cocktail tablets per 50 ml of buffer. After an incubation of 5 min on ice the cells were lysed with 18 strokes of a Dounce homogenizer at 4 °C. The cell suspension was transferred to Corex tubes and the nuclei were pelleted by centrifugation in a SS34 rotor for 5 min at 13000 g. Afterwards the supernatant was discarded and the nuclei were resuspended in 1.3 volumes of 1x Roeder C buffer containing 0.5 mM DTE and 0.5 mM PMSF. For lysis of the nuclei the suspension was again treated with 20 strokes of a Dounce homogenizer at 4 °C. The lysate was stirred for 40 min at 4 °C, followed by centrifugation in a SS34 rotor at 16000 rpm for 30 min to pellet particulate material. The supernatant was recovered and dialyzed against 50 volumes of 1x Roeder D buffer at 4 °C for five hours with one change of buffer after 2.5 h. The dialyzed nuclear extract was recovered and centrifuged in a HB6 rotor at 10000 rpm for 10 min at 4 °C. The supernatant was aliquoted, frozen in liquid nitrogen and stored at -80 °C.

2.2.3.3 *In vitro* splicing reactions

A typical splicing reaction was carried out in the presence of 10 nM MINX pre-mRNA or exon-RNA and 40 % (v/v) HeLa nuclear extract [Dignam *et al.*, 1983] in a buffer containing 20 mM HEPES-KOH pH 7.9, 3 mM MgCl₂, 65 mM KCl, 2 mM ATP and 20 mM creatine phosphate. Spliceosomal complexes were allowed to form at 30 °C for the times indicated in the respective figure (3. Results). 37S exon complexes were assembled on MINX exon-RNA by incubating at 30 °C for 6 min. 45S B-like complexes were formed by first incubation for 3 min and then adding a 100-fold excess of the 5' ss oligonucleotide or mutated oligonucleotide and incubating for an additional 3 min. After splicing, reactions were chilled on ice.

For complex assembly in the presence of recombinant hPrp28 protein, the splicing reaction was first supplemented with the indicated concentration of recombinant protein and was then pre-incubated for 30 min at 30 °C prior to the addition of the pre-mRNA.

2.2.3.4 Analysis of splicing complexes by native agarose gel-electrophoresis

The process of spliceosomal assembly *in vitro* can be analyzed by a mobility retardation assay. Briefly, spliceosomal complexes A, B and C form in a subsequent manner and show decreased mobility on a native agarose gel [Kent and MacMillan, 2002, Lamond *et al.*, 1987].

To resolve spliceosomal complexes by native agarose gel-electrophoresis, 20 µl splicing reactions were incubated at 30 °C for the times indicated in the respective figure (3. Results). Heparin was added to a final concentration of 0.65 µg/µl and the mixtures were incubated for another 1 min at 30 °C before addition of 6 µl of 5x native gel loading dye. The samples were immediately loaded onto a native gel containing 2 % (w/v) low melting point agarose in 0.5x TBE buffer. Electrophoresis was then performed at 50 V for 16 h at room temperature. The gels were dried at 60 °C for 5 h and exposed to a phosphorimager screen to visualize complex formation.

2.2.3.5 MS2 affinity-selection of splicing complexes

Spliceosomal complexes were isolated by MS2 affinity-selection as previously described in [Bessonov *et al.*, 2010]. Pre-mRNA was incubated with 20 mM HEPES-KOH pH 7.9 and a 20-fold molar excess of purified MS2-MBP fusion protein for 30 min at 4 °C prior to splicing. Then, a 1 ml standard splicing reaction containing 20 mM HEPES-KOH pH 7.9, 3 mM MgCl₂, 65 mM KCl, 2 mM ATP, 20 mM creatine phosphate and 10 nM of uniformly ³²P-labeled MINX pre-mRNA or exon-RNA was incubated for 6 min at 30 °C. After 3 min of incubation the splicing reaction was supplemented with 1 µM of 5' splice oligonucleotides as indicated in the respective figure (3. Results).

The splicing reaction was loaded onto a 14 ml linear 10-30 % (v/v) glycerol gradient containing G-150 buffer. Gradients were centrifuged at 25000 rpm for 15 h at 4 °C in a Sorvall TST 41.14 rotor and harvested manually in 500 µl fractions from top to bottom. The distribution of ³²P-labeled MINX pre-mRNA or exon-RNA across the gradient was determined by Cherenkov counting. Peak fractions containing the spliceosomal complexes were pooled and loaded onto a pre-equilibrated column containing 300 µl of amylose beads (NEB). The matrix was then washed with four column volumes of G-75 washing buffer. Finally, spliceosomal complexes were eluted by adding 300 µl of G-75 washing buffer containing 20 mM maltose.

To test the stabilization of the 37S exon or 37S cross-intron complexes, the respective elution fraction containing usually 2-3 pmol of affinity-purified complexes was supplemented with a 100-fold

excess of either the 5' splice oligonucleotide or the 2'-O-ribose methylated 5' splice oligonucleotide. After an incubation of 15 min on ice, the reaction was loaded onto a linear 10-30 % (v/v) analytical glycerol gradient containing G-75 or G-150 buffer as specified in the respective figure (3. Results). Gradients were centrifuged at 60000 rpm for 135 min at 4 °C in a Sorvall TH660 rotor and harvested manually in 175 µl fractions from top to bottom.

2.2.3.6 Psoralen-mediated RNA-RNA crosslinking

Affinity-purified spliceosomal complexes were crosslinked with 4'-aminomethyl-4,5',8-trimethylpsoralen hydrochloride (AMT) to reveal RNA-RNA interactions [Hartmuth *et al.*, 2002]. Crosslinking was initiated by adding 2 mg/ml AMT in DMSO to affinity-purified complexes to a final concentration of 20 µg/ml and incubating for 10 min on ice. Next, samples were irradiated with 365 nm UV-light for 30 min at 4 °C with a distance of 4 cm between the samples and UV lamp. After proteinase K treatment of the samples (2.2.1.3), the RNA was recovered and resolved on a 5 % or 10 % denaturing polyacrylamide gel (2.2.1.6) and analyzed by Northern blotting (2.2.1.8).

2.2.3.7 UV crosslinking of spliceosomal complexes

In order to induce site-specific protein-RNA crosslinks by UV-irradiation, spliceosomal complexes were affinity-purified as described in 2.2.3.5. The elution fraction was pipetted dropwise (30 µl each) onto a pre-cooled metal rack covered with Parafilm. The samples were irradiated at 365 nm for 10 min with a distance of 4 cm between the metal rack and UV lamp. Afterwards, the drops were pooled and subsequently supplemented with 1 µl RNase A (1 mg/ml, Ambion). The crosslinked complexes were then incubated for 20 min at 37 °C to digest RNA.

2.2.3.8 Immunoprecipitation of protein-RNA crosslinks

For the enrichment of hPrp8-specific protein-RNA crosslinks, immunoprecipitation was performed. Purified antibodies were first coupled to PAS beads. For each assay, 20 µl packed PAS beads (GE Healthcare) were washed twice with PBS pH 8.0. Then, 500 µl of PBS pH 8.0 containing 0.5 mg/ml BSA, 0.05 mg/ml tRNA and 5 µg of purified anti-hPrp8 antibodies were added to the beads. In the negative control antibodies were omitted. The beads were then incubated for 1 h at room temperature while rotating head-over-tail. After centrifugation for 2 min at 3000 rpm in a microfuge, the supernatant was removed and the beads were washed twice with 500 µl of ice cold G-150 buffer containing 0.05 % SDS and 0.5 % Triton X-100. Then 250 µl of the elution fraction containing UV-crosslinked spliceosomes disrupted by RNase digestion and treatment with detergent (2.2.3.7) were added and incubated with antibody coupled PAS beads, rotating head-over-tail at room temperature for 2 h. After centrifugation at 3000 rpm for 2 min in a microfuge and removal of the supernatant,

the beads were again washed two times with G-150 buffer containing 0.05 % SDS and 0.5 % Triton X-100. Bound material was eluted by addition of 20 μ l 6x SDS loading dye and incubation at 96 °C for 10 min. Proteins were separated by SDS-PAGE (2.2.2.2) and finally analyzed by western blot (2.2.2.5) and autoradiography.

2.2.3.9 Two-dimensional gel-electrophoresis of spliceosomal complexes

Two-dimensional gel-electrophoresis of spliceosomal complexes was performed as described in [Agafonov *et al.*, 2011]. Briefly, spliceosomal complexes were affinity-purified (2.2.3.5) and subsequently pelleted in a Sorvall SA800 AT400 rotor at 700000g at 4 °C for 6 h. The pellet was dissolved in G-1000 buffer (50 mM HEPES-KOH pH 7.9, 2 mM MgCl₂, 1 M NaCl, 0.1 mM EDTA) and treated with RNase A and T1 (Ambion) under increasing urea concentrations. Then, the sample was dialyzed in a Slide-A-Lyzer (Pierce). Separation of proteins in the first dimension was carried out under very strong denaturing conditions at acidic pH in the extremely large pore matrix. In the second dimension proteins were separated on an 8 % acrylamide gel in the presence of SDS. Proteins were stained with SyproRuby (Life Science) according to the manufacturer's protocol or with Coomassie. For identification of proteins, individual Coomassie-stained protein-spots were cut out from the gel and corresponding proteins were subsequently identified by mass spectrometry (2.2.3.11).

2.2.3.10 Electron microscopy

The structure of isolated spliceosomal complexes was analyzed by electron microscopy (EM). All EM experiments were performed in collaboration with Dr. Norbert Rigo and Dr. Berthold Kastner. For EM investigations, affinity-purified complexes were subjected to a second glycerol gradient centrifugation under mild-fixating GraFix conditions [Kastner *et al.*, 2008]. Briefly, 6-8 pmol of spliceosomes were loaded onto a linear 10-30 % (v/v) glycerol and 0-0.1 % (v/v) glutaraldehyde gradient containing G-75 or G-150 buffer. Gradients were centrifuged at 60000 rpm for 2 h in a TH660 rotor at 4 °C and harvested manually in 175 μ l fractions from top to bottom. The distribution of ³²P-labeled RNA across the gradient was determined by Cherenkov counting and peak fractions were used for EM studies. The spliceosomal complexes from these fractions were allowed to adsorb to a thin carbon film for approximately 2 h. The carbon film was then transferred to a staining solution containing 2 % (w/v) uranyl formate and was stained for 2 min. After staining, the carbon film was applied to a copper EM grid and subsequently covered with a second carbon film.

For visualization of structural features, images were recorded at a magnification of 88000x with a CM200 FEG electron microscope (Philips, Netherlands) equipped with a 4kx4k charge-coupled (CCD) camera (TVIPS) and a room temperature holder (Philips, Netherlands). For each data set 10000-

15000 individual single-particle images were collected. Repeating rounds of image-processing of these images were performed using the software package IMAGIC-5 [van Heel *et al.*, 1996]. After a reference-free alignment, images were subjected to multivariate statistical analysis and classification [Dube *et al.*, 1993, van Heel and Frank, 1981, van Heel, 1989]. The resulting class averages were used as reference images in subsequent rounds of alignment until the class averages were stable.

2.2.3.11 Mass spectrometry

For protein identification via mass spectrometry, proteins recovered from affinity-purified spliceosomal complexes were first separated by 2D gel-electrophoresis as described in 2.2.3.10 and then stained with SyproRuby. Individual protein-spots were cut out and proteins were digested in-gel with trypsin and extracted as described by Shevchenko *et al.* [Shevchenko *et al.*, 1996]. For mass spectrometry of the 37S cross-intron and B complex (approximately 1-2 pmol each), proteins recovered from the complexes were separated on 4-12 % NuPAGE™ gradient gels (Invitrogen) and stained with Coomassie. Entire lanes were cut into 23 slices and proteins were digested in-gel with trypsin and extracted as described by Shevchenko *et al.* [Shevchenko *et al.*, 1996]. The extracted peptides were analyzed in a liquid-chromatography coupled electrospray ionization quadrupole time of flight (Q-ToF) or Orbitrap (LTQ Orbitrap XL) mass spectrometer under standard conditions. Proteins were identified by searching fragment spectra against the NCBI non-redundant (nr) database using Mascot as a search engine.

3. Results

Intron-defined spliceosome assembly occurs by the ordered interaction of spliceosomal components across an intron and proceeds sequentially with distinct intermediate stages. An alternative assembly pathway exists, in which the splicing complex first forms across an exon. This so-called exon definition is thought to be the prominent pathway for pre-mRNAs with long intronic sequences. However, the chemical steps of splicing can only occur across an intron, and therefore a rearrangement from exon-defined to an intron-defined organization must occur. Recent studies showed that exon-defined spliceosomes not only contain U1 and U2 snRNPs, but also the U4/U6.U5 tri-snRNP, providing evidence that it is possible for a cross-exon complex to be converted directly into a cross-intron B complex via interaction with an upstream 5'ss [Schneider *et al.*, 2010a]. Here I have investigated the requirements for stable integration of the U4/U6.U5 tri-snRNP during both exon- and intron-defined spliceosome assembly and factors contributing to this process, as this is a crucial step during which the two spliceosome assembly pathways converge and alternative splice site choices are made.

3.1 A stable 45S B-like complex is formed upon addition of a 5'splice site-containing RNA oligonucleotide

To assemble exon-defined spliceosomes in a splicing reaction containing HeLa nuclear extract, I used a single exon RNA construct derived from the MINX pre-mRNA substrate (Figure 3.1A) [Schneider *et al.*, 2010a]. This MINX exon-RNA contains a single exon flanked by intronic sequences containing an upstream branch site and polypyrimidine-tract, which is essential for U2 snRNP binding, and a downstream 5'ss with which the U1 snRNP interacts. Additionally, three MS2-aptamers are inserted at the 3'end to enable MS2 affinity-selection of splicing complexes as described in chapter 2.2.3.5. Incubation of this RNA substrate under splicing conditions results in the formation of an exon complex with a *S*-value of ~37S as determined by glycerol gradient centrifugation (Figure 3.1C). This 37S exon complex contains all five snRNPs in stoichiometric amounts (Figure 3.1D). Previous investigation of the RNA-RNA network by psoralen-mediated crosslinking showed that the U1 snRNP is base paired with the downstream 5'splice site, while the U2 snRNP interacts with the upstream BPS [Schneider *et al.*, 2010a]. The U4/U6.U5 tri-snRNP is associated with the 37S exon complex via base pairing with the U2 snRNA (U2/U6 helix II) and therefore the U2 snRNP establishes the connection between the MINX exon-RNA and the U4/U6.U5 tri-snRNP. But, in this 37S exon complex the U4/U6.U5 tri-snRNP is loosely-associated in a heparin-sensitive manner, as judged by native gels, where only an A-like complex containing U2 snRNP is detectable (Figure 3.1B, lane 2).

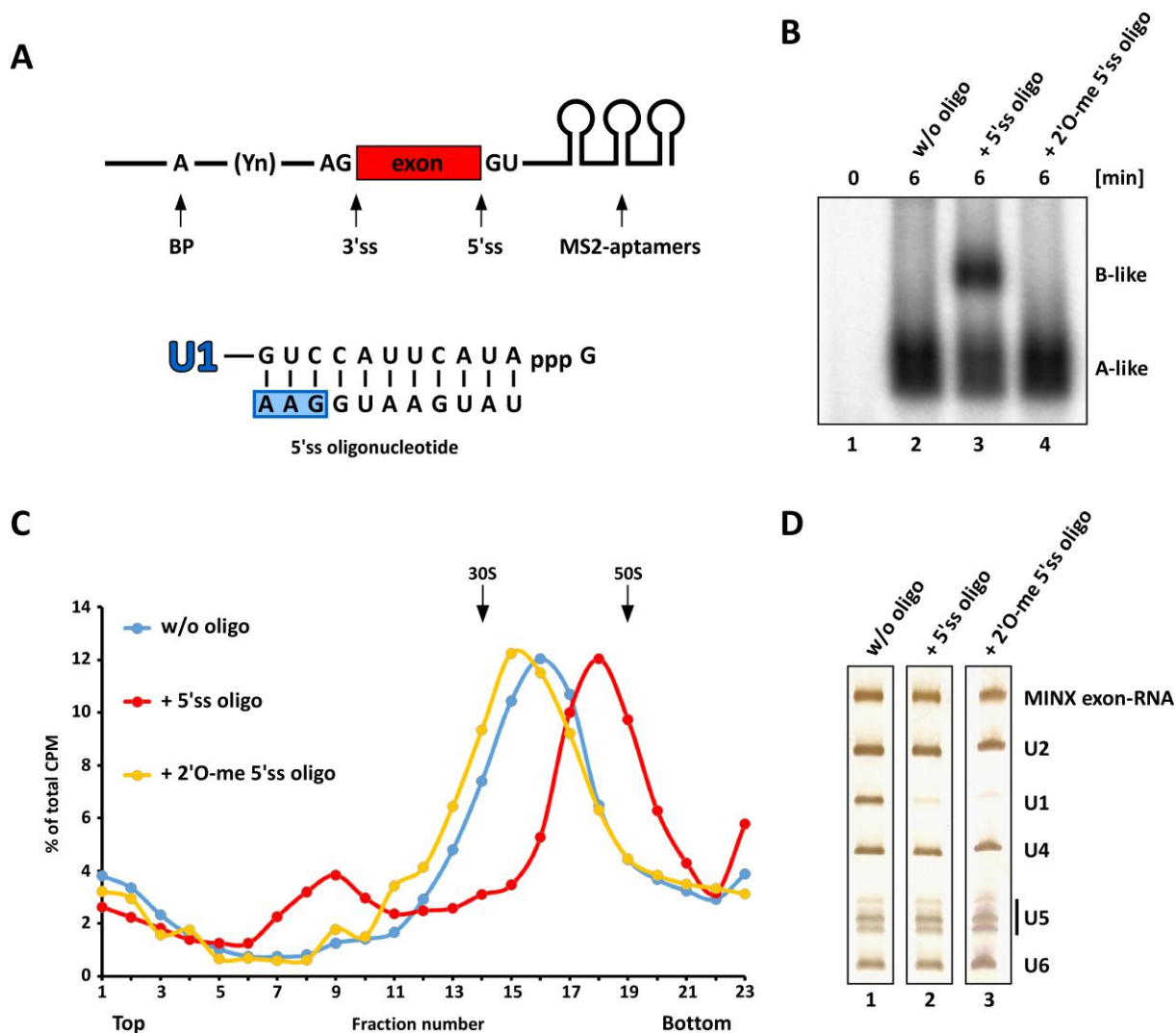


Figure 3.1: Addition of a 5'ss RNA oligonucleotide leads to the formation of a stable 45S B-like complex

(A) Schematic representation of the MINX exon-MS2 RNA [see Schneider *et al.* 2010a], which is used to assemble exon-defined spliceosomes and the sequence of the optimized 5'ss oligonucleotide that induces formation of the B-like complex. Exonic nucleotides are highlighted with a shaded box. (B) Exon-defined spliceosomes were assembled on uniformly 32 P-labeled MINX exon-MS2 RNA and analyzed via native agarose gel-electrophoresis in the presence of heparin. The stabilization of U4/U6.U5 tri-snRNP binding was tested upon addition of a 100-fold excess of a 5'ss RNA or 2'O-ribose methylated (2'O-me) 5'ss RNA oligonucleotide as indicated. The positions of A- and B-like complexes are indicated. (C) Glycerol gradient analysis of exon-defined spliceosome assembly. Splicing reactions were subjected to linear 10-30 % glycerol gradients containing 150 mM KCl. The percentage of total radioactivity in each gradient fraction is plotted. Sedimentation values were determined with prokaryotic ribosomal subunits. (D) Complexes in peak fractions of the gradients were purified by MS2 affinity-selection. RNA was recovered from the eluates, separated by denaturing PAGE and visualized by silver staining. RNA identities are indicated on the right.

Addition of 100-fold excess of a short RNA oligonucleotide containing an optimized 5'splice site sequence (Figure 3.1A) after 3 min of splicing, induces the formation of a B-like complex. During formation of this complex, the U4/U6.U5 tri-snRNP associates in a stable, heparin-resistant manner with the complex, allowing its detection in native gels (Figure 3.1B, lane 3). Further, glycerol gradient

centrifugation showed that stable U4/U6.U5 tri-snRNP integration is accompanied by a change in the sedimentation behavior of the complex from ~37S for the exon to ~45S for the B-like complex (Figure 3.1C). So, I set out to use this reductionist system to identify factors potentially contributing to the stabilization of U4/U6.U5 tri-snRNP binding.

3.1.1 Stabilization of U4/U6.U5 tri-snRNP integration is not induced by removing U1 snRNP from the downstream 5'ss

Due to the optimized complementarity of the 5'ss oligonucleotide with the 5'end of U1 snRNA, addition of the 100-fold excess of the 5'ss oligonucleotide should compete with the interaction between U1 snRNA and the downstream 5'ss of the MINX exon-RNA. Indeed, affinity-purified B-like complexes contain very little U1 snRNA, consistent with the 5'ss oligonucleotide outcompeting the bound U1 snRNP (Figure 3.1D, lane 2). Disrupting the U1:5'ss interaction could potentially allow the U6 snRNA to interact with the downstream 5'ss and lead thereby to stabilization of U4/U6.U5 tri-snRNP binding during B-like complex formation. To test if this is indeed the case, we modified the 5'ss RNA oligonucleotide by 2'O-ribose methylation (2'O-me), which still allows interaction with the U1 snRNP, but not other components of the 37S exon complex [Schneider *et al.*, 2010a]. Addition of this modified 5'ss oligonucleotide to the splicing reaction did not support stable B-like formation on native gels (Figure 3.1B, lane 4), nor the shift to a 45S complex on a glycerol gradient (Figure 3.1C), even though the complexes formed in its presence did not contain the U1 snRNA (Figure 3.1D, lane 3). Thus, displacement of U1 snRNP by the 5'ss oligonucleotide does not support stable U4/U6.U5 tri-snRNP binding during 45S B-like complex formation. This suggests an essential role for a previously shown interaction of the 5'ss oligonucleotide with the U4/U6.U5 tri-snRNP, as opposed to U1 snRNP, for inducing stable integration of the U4/U6.U5 tri-snRNP within the 45S B-like complex.

3.2 Formation of the 45S B-like complex is accompanied by the recruitment of B complex-specific proteins

To identify factors that potentially contribute to stable U4/U6.U5 tri-snRNP binding, we set out to determine which proteins are abundant components of 37S exon and 45S B-like complexes. We thus made use of a novel 2D gel-electrophoresis technique developed in our laboratory that is optimized for the investigation of spliceosomal complexes and allows a quantitative assessment of the relative amounts of a given protein within a complex mixture [Agafonov *et al.*, 2011]. However, due to the extremely large pore size of the gels used in this technique, visualization of proteins smaller than ~25 kDa was not possible.

Thus, I purified 37S exon and 45S B-like complexes by gradient centrifugation and subsequent MS2 affinity-selection under identical conditions to allow a direct comparison of the protein inventory of both complexes. In collaboration with Dr. Dmitry Agafonov, the proteins were separated via 2D gel electrophoresis, and visualized by staining with SyproRuby (Figure 3.2). The identity of each protein-spot was subsequently confirmed by mass spectrometry.

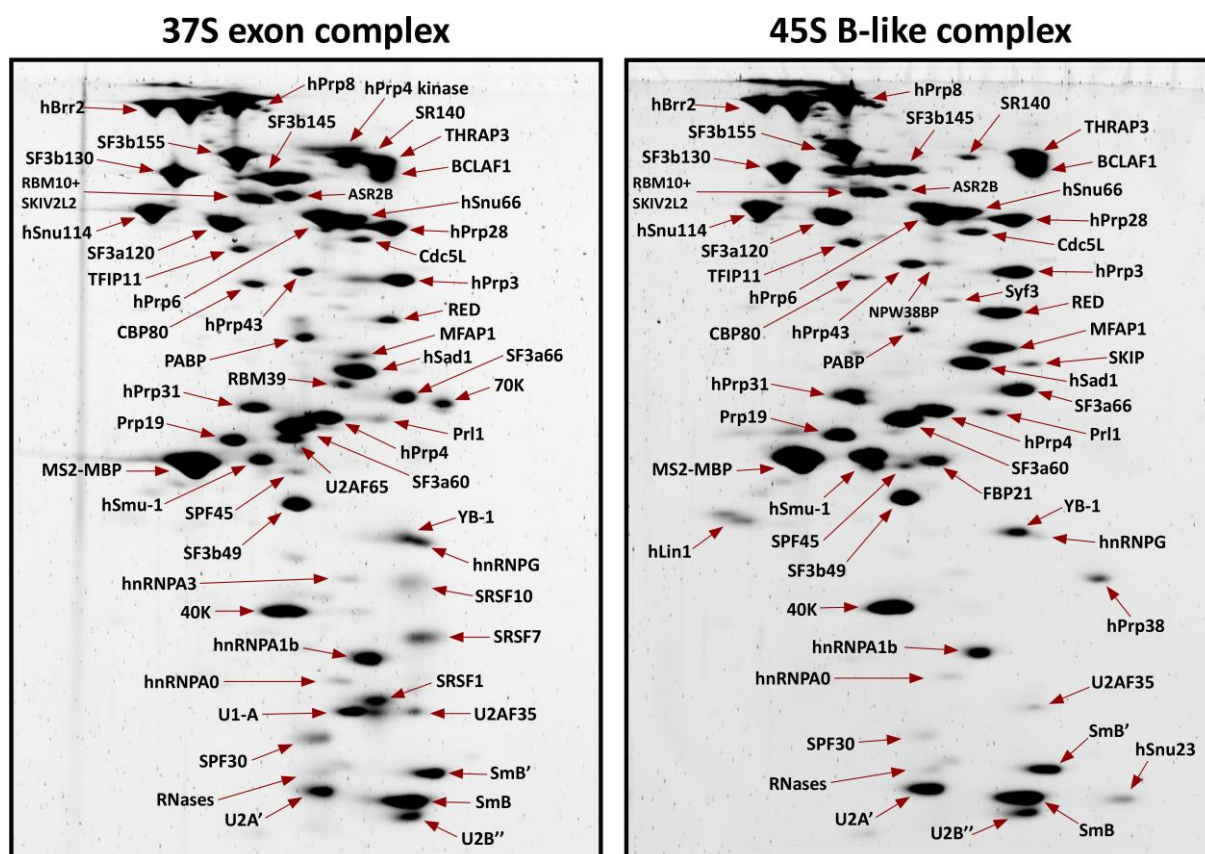


Figure 3.2: Identification of abundant proteins associated with 37S exon and 45S B-like complexes

Analysis of the protein composition of MS2 affinity-purified 37S exon and 45S B-like complexes by 2D gel electrophoresis according to Agafonov *et al.* [Agafonov *et al.*, 2011]. Proteins were stained with SyproRuby and the identities of protein-spots were determined by mass spectrometry.

The protein-spots varied considerably in their intensities and proteins were classified as abundant based on a visual evaluation of these intensities (Figure 3.2, see also Agafonov *et al.*, 2011). Proteins that were considered to be abundant in the 37S exon and 45S B-like complex are listed in Table 3.1.

The evaluation of the protein pattern identified all U1, U2 and U4/U6.U5 tri-snRNP proteins to be abundant in the 37S exon complex, which is consistent with its snRNA composition. Further, the proteins BCLAF1, THRAP3, hnRNPA1b, hPrp4 kinase and SRSF1 were also classified as abundant based on their staining intensities. Additionally, the SR proteins SRSF7 and SRSF10 were also included in the group of abundant factors, despite a less intensive staining as for example hnRNPA1b.

SR proteins migrate not as a distinct, single spot but rather diffuse in this 2D gel-electrophoresis and furthermore this group of proteins is known to be heavily phosphorylated, which in combination results in a poor intensity of staining ([Agafonov *et al.*, 2011], personal communication Dr. Agafonov).

Protein name	MW kDa	gi l number	37S exon complex	45S B-like complex	<i>S. cerevisiae</i> gene name
Sm proteins					
Smb/B'	24.6	gi 119631003			SMB1
U1 snRNP					
U1-70K	51.6	gi 36100			SNP1
U1-A	31.3	gi 189053747			MUD1
U2 snRNP					
U2A'	28.4	gi 50593002			LEA1
U2B''	25.4	gi 119630691			MSL1
SF3a120	88.9	gi 5032087			PRP21
SF3a66	49.3	gi 116283242			PRP11
SF3a60	58.5	gi 158255798			PRP9
SF3b155	145.8	gi 54112117			HSH155
SF3b145	100.2	gi 33875399			CUS1
SF3b130	135.5	gi 54112121			RSE1
SF3b49	44.4	gi 5032069			HSH49
U5 snRNP					
hPrp8	273.7	gi 91208426			PRP8
hBrr2	244.5	gi 40217847			BRR2
hSnu114	109.4	gi 12803113			SNU114
hPrp6	106.9	gi 189067252			PRP6
hPrp28	95.6	gi 193785886			PRP28
40K	39.3	gi 115298668			
U4/U6 snRNP					
hPrp3	77.6	gi 4758556			PRP3
hPrp31	55.4	gi 221136939			PRP31
hPrp4	58.4	gi 189053699			PRP4
U4/U6.U5 snRNP					
hSnu66	90.2	gi 10863889			SNU66
hSad1	65.4	gi 13926071			SAD1
B complex-specific					
RED	65.6	gi 125988409			
MFAP1	51.9	gi 50726968			
hSnu-1	57.5	gi 84370185			
FBP21	42.5	gi 189069453			
hPrp38	37.5	gi 24762236			PRP38
hSnu23	23.6	gi 13385046			SNU23
hPrp4 kinase	117.1	gi 158255924			
SR proteins					
SRSF1	27.8	gi 296202382			
SRSF7	27.4	gi 72534660			
SRSF10	31.3	gi 5730079			
hnRNPs					
hnRNP A1	38.7	gi 119617171			
Miscellaneous					
THRAP3	108.6	gi 167234419			
BCLAF1	106	gi 219520423			

Table 3.1: Abundant proteins detected in 37S exon and 45S B-like complexes

Overview of abundant proteins associated with 37S exon and 45S B-like complexes. Abundant proteins were identified by visual inspection and are indicated by a grey box. Proteins are grouped according to their association with snRNPs or stage of recruitment.

In contrast, hPrp19 was not considered to be abundant despite a similar staining intensity as e.g. 61K, as it was shown that hPrp19 is recruited in multiple copies to the spliceosome [Grote *et al.*, 2010]. Consistent with this finding other factors of the hPrp19 complex such as Cdc5L or Prl1 are also not abundant. For the same reason hSmu-1 was not classified as abundant within the 37S exon complex. Based on the increase in its staining intensity upon transition to the 45S B-like complex, we assume that additional copies of hSmu-1 are recruited to the complex upon interaction of the 5'ss oligonucleotide. The increase in staining intensity and previous investigations of Agafonov *et al.* suggest that hSmu-1 is present in multiple copies within the spliceosome ([Agafonov *et al.*, 2011], personal communication Dr. Agafonov). Upon formation of a 45S B-like complex a distinct change in the protein composition was observed. First we detected a loss of the U1-specific proteins, which is consistent with the displacement of U1 snRNP from the complex upon addition of the 5'ss oligonucleotide to the splicing reaction. Additionally, all SR proteins as well as the hPrp4 kinase were displaced from the complex. In contrast, we detected a recruitment of MFAP1, FBP21, RED and hSmu-1 during the transition from a 37S exon to the 45S B-like complex (Figure 3.2, table 3.1). These B complex-specific proteins are stage-specifically recruited during formation of a stable, intron-defined B complex and get already displaced during transition to a B^{act} complex [Agafonov *et al.*, 2011]. hPrp38 and hSnu23, which also belong to the group of B complex-specific proteins, were also classified as abundant in the 45S B-like complex despite showing a less intensive staining intensity. These two proteins migrate the longest distance in the first dimension of the two-dimensional gel, which results in the loss of material and therefore in a less intensive staining after separation in the second dimension ([Agafonov *et al.*, 2011], personal communication with Dr. Dmitry Agafonov). hPrp38 was shown to be phosphorylated, which results in a reduction in its staining efficiency [Agafonov *et al.*, 2011].

In general, the 45S B-like complex shows essentially the same composition of abundant proteins as an intron-defined B complex, which was assembled on the MINX pre-mRNA [Agafonov *et al.*, 2011] with the exception that the two proteins THRAP3 and BCLAF1 are not abundant in the intron-defined B complex. The presence of the B complex-specific proteins in spliceosomal complexes with a stably-integrated U4/U6.U5 tri-snRNP, namely 45S B-like and B complex, suggests that the latter proteins could potentially be required for the stabilization of U4/U6.U5 tri-snRNP binding upon its interaction with a 5'ssplice site. Despite the change in the protein composition during the transition from the 37S exon to 45S B-like complex, the difference in the theoretical mass of the 37S exon (loss of proteins: ~290 kDa) to a 45S B-like complex (recruitment of B complex-specific proteins: ~280 kDa) is negligible. Thus, the increased sedimentation value of the 45S B-like complex does not appear to be due to a higher mass of the complex, but rather suggests a structural rearrangement of the complex during stable binding of the U4/U6.U5 tri-snRNP that leads then to an increased sedimentation value.

3.3 EM reveals a major structural difference between the 37S exon and the 45S B-like complex

To determine whether addition of the 5' ss oligonucleotide changes the morphology of the 37S exon complex, its structure was investigated in comparison to the 45S B-like complex via negative-stain electron microscopy (EM). All electron microscopy analyses were performed in collaboration with Dr. Berthold Kastner and Dr. Norbert Rigo (Department of Cellular Biochemistry, MPI-BPC). For this purpose, I separated 37S exon and 45S B-like complexes on a glycerol gradient and subjected the respective peak fractions to MS2 affinity-selection. The eluates were then fractionated on a second glycerol gradient containing 75 mM KCl under GraFix conditions [Kastner *et al.*, 2008] and peak fractions were subsequently used for EM preparation. Figure 3.3 shows representative overviews of single particles of either the 37S exon or 45S B-like complex on the EM grid. To allow a structural comparison between 37S exon and 45S B-like complexes, we generated class averages from single particle images for both complexes. Therefore, we performed image processing of a dataset containing 12,000 and 10,400 individual raw images of the 37S exon and 45S B-like complex, respectively. Characteristic two-dimensional class averages of both complexes are shown in figure 3.3 and the relative percentages of the respective appearances of the 37S exon complex are indicated below. Due to the similar appearance of the 45S B-like complex in nearly all class averages percentages were omitted.

For the 37S exon and 45S B-like complexes clearly defined single particles are visible on the EM grid, showing that the increase in the sedimentation behavior during the transition is not due to an aggregation of the complexes (Figure 3.3, A & B). The 37S exon complex structures are characterized by an upper (head) and elongated lower (body) domain, which are connected via a slimmer neck domain (Figure 3.3D). The size and shape of the body domain are similar in most of the class averages, whereas the head domain displays more conformational heterogeneity. The head domain not only varies in its size, but it is also seen in different positions relative to the body domain (Figure 3.3D, black, blue, red). The majority of the classes exhibit a clearly-defined, triangular-shaped head domain, which is located close to the body domain (Figure 3.3A, galleries 1 & 2). In the less abundant classes, the head appears more blurred and is composed of globular domains with either horizontally (Figure 3.3A, galleries 3 & 4) or vertically (Figure 3.3A, gallery 5) arranged protrusions. Thus, the head domain appears to have similar structural elements, which are flexibly connected by the neck domain to the body.

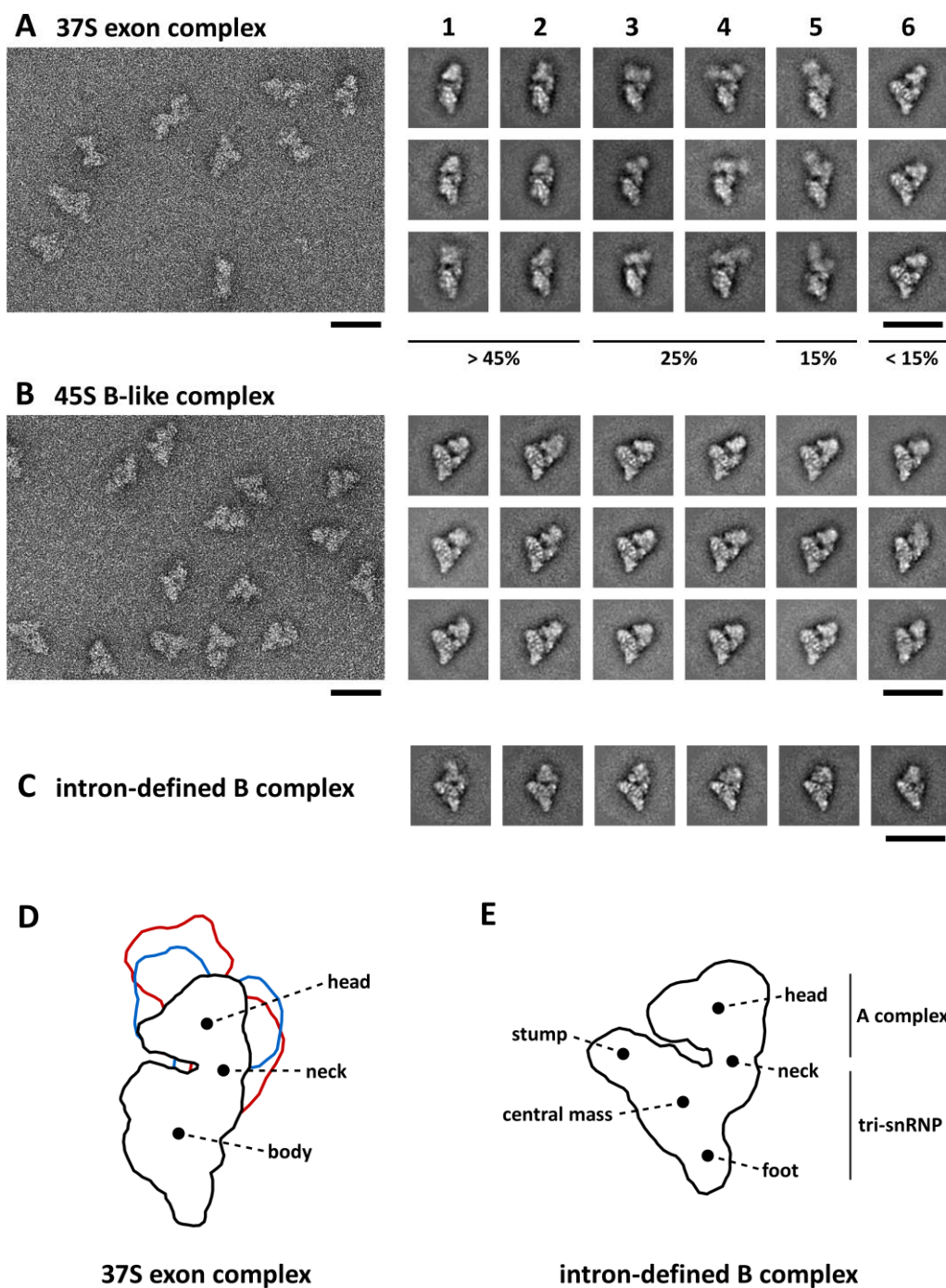


Figure 3.3: Structural comparison of 37S exon and 45S B-like complexes by negative-stain electron microscopy

An overview of negatively-stained 37S exon (A) and 45S B-like (B) complexes formed on MINX exon-RNA is shown on the left. Representative class averages of both complexes are shown in the galleries from most (1) to least (6) frequently observed classes on the right. The relative abundance of the different classes of the 37S exon complex is indicated. A small fraction (< 15 %) of images with a morphology typical for the 45S B-like complex was also detected in the preparation of the 37S exon complex (Gallery 6). The lower gallery (C) shows a selection of typical class averages of an intron-defined B complex formed on the MINX pre-mRNA. Scale bars correspond to 50 nm. (D) Schematic representation of the 37S exon complex including different orientations of the head domain characteristic for the galleries 1-2 (black), 3-4 (blue) and 5 (red). (E) Schematic representation of an intron-defined B complex. Main structural elements are labeled according to Boehringer *et al.* [Boehringer *et al.* 2004].

The class averages calculated from single particles of the 45S B-like complex appear structurally better defined and reveal more fine structural details in comparison to the 37S exon complex. The 45S B-like complex exhibits a predominant orientation for the majority of the calculated class averages, based on the appearance of almost identical views in all class averages. The 45S B-like complex consists of a triangular body and a globular head domain, which are connected by a neck-like structure. Interestingly, a small portion (< 15 %) of structures characteristic for the 45S B-like complex was also detectable in the preparation of the 37S exon complex (Figure 3.3, gallery 6). Overall the 45S B-like complex appears more compact and not as elongated as the 37S exon complex, which might explain the change in its sedimentation value. Surprisingly, the morphologies of the 45S B-like complex are highly similar to those of an intron-defined B complex with stably associated U4/U6.U5 tri-snRNP (Figure 3.3C), despite the fact that these complexes were assembled on different substrates, namely MINX exon-RNA or MINX pre-RNA, respectively. This suggests that the relative orientation of snRNPs within the 45S B-like and B complex are highly similar or even identical. Immunolabeling studies of the human B complex could show that the head domain contains the A complex and the body is composed of the U4/U6.U5 tri-snRNP (Figure 3.3E) [Wolf *et al.*, 2009]. Thus, the conformational change in the 37S exon complex triggered by its interaction with the 5' ss oligonucleotide, probably involves a rearrangement of the A complex domain with respect to the U4/U6.U5 tri-snRNP leading to more stable integration of the latter, which in turn may result in the stable integration of the U4/U6.U5 tri-snRNP within the complex.

The comparison of the class averages generated for the 37S exon and 45S B-like complexes provide evidence that the stable integration of the U4/U6.U5 tri-snRNP during 45S B-like formation is accompanied by a major structural rearrangement in the complex organization. As the assembly of the 45S B-like complex is characterized by the recruitment of stoichiometric amounts of the B complex-specific proteins, this suggests a potential role of these proteins in the structural change occurring during stable association of the U4/U6.U5 tri-snRNP with the complex.

3.4 Interaction of the 5' ss oligonucleotide with affinity-purified 37S exon complexes induces a structural change resulting in stable U4/U6.U5 tri-snRNP binding

To test whether the recruitment of the B complex-specific proteins is a prerequisite for the structural reorganization of the complex during stabilization of U4/U6.U5 tri-snRNP binding, I assayed if this structural change also occurs in the absence of nuclear extract. Thus, 37S exon complexes were assembled in splicing reactions and subsequently purified by glycerol gradient centrifugation followed by MS2 affinity-selection.

First, I monitored the stability of U4/U6.U5 tri-snRNP binding within the 37S exon complex upon addition of the 5' ss oligonucleotide via glycerol gradient centrifugation. Therefore, affinity-purified 37S exon complexes were mixed with either a 5' ss oligonucleotide or a 2'O-me version thereof and subjected to a second glycerol gradient centrifugation containing 150 mM KCl.

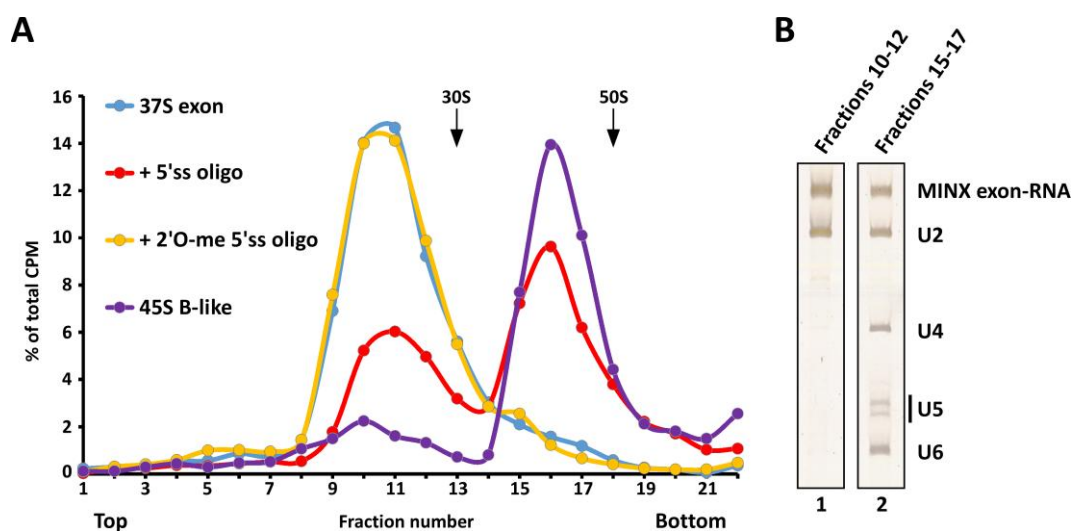


Figure 3.4: Addition of a 5' ss oligonucleotide to affinity-purified 37S exon complex stabilizes U4/U6.U5 tri-snRNP binding

(A) Analytical glycerol gradient centrifugation in the presence of 150 mM KCl of affinity-purified 37S exon complexes after addition of 5' ss oligonucleotide or 2'O-me 5' ss oligonucleotide. Purified 45S B-like complexes were run in parallel. (B) Peak fractions from the gradients were used for MS2 affinity-selection. RNA was recovered from the eluates, separated by denaturing PAGE and visualized by silver staining. Identities of snRNAs are indicated.

The 37S exon complex without any added oligonucleotide showed only a single peak with an S-value < 30S (Figure 3.4A), and thus subjecting the purified 37S exon complex to 150 mM KCl resulted in a significant reduction in its S-value on a second glycerol gradient. Fractions 10-12 containing the majority of the ³²P-labeled MINX exon-RNA were subsequently used for a second MS2 affinity-selection to characterize the RNA composition of this slower migrating complex. RNA was recovered from the eluates and analyzed by denaturing PAGE with subsequent silver staining. The RNA analysis identified only the MINX exon-RNA and U2 snRNA in fractions 10-12 of the second gradient (Figure 3.4B, lane 1), showing that under these conditions the U4/U6.U5 tri-snRNP as well as U1 snRNP dissociate from the 37S exon complex and only U2 snRNP stays bound at the MINX exon-RNA. Apparently, the 37S exon complex does not withstand salt concentrations of 150 mM KCl once it's in a purified state. Upon addition of the 5' ss oligonucleotide, but not the 2'O-ribose methylated version, the majority of the exon complex is converted into a faster migrating (~45S) complex that sediments in the same fractions as affinity-purified B-like complexes, which were initially assembled by adding the 5' ss oligonucleotide to the splicing reaction prior to the first gradient. I subjected this

second peak (fractions 15-17) also to MS2 affinity-selection. The RNA analysis of fractions 15-17 showed that the complex in these fractions contains the U4/U6.U5 tri-snRNP in addition to the U2 snRNP and the MINX exon-RNA (Figure 3.4B, lane 2), showing that the complex stays intact upon addition of the 5'ss oligonucleotide. Further, the change in the migration behavior is not due to the loss of U1 snRNP, as judged by the fact that the 2'O-me oligonucleotide also displaces U1 snRNP from the 5'ss of the MINX exon-RNA, but does not induce a change in the sedimentation value of the complex.

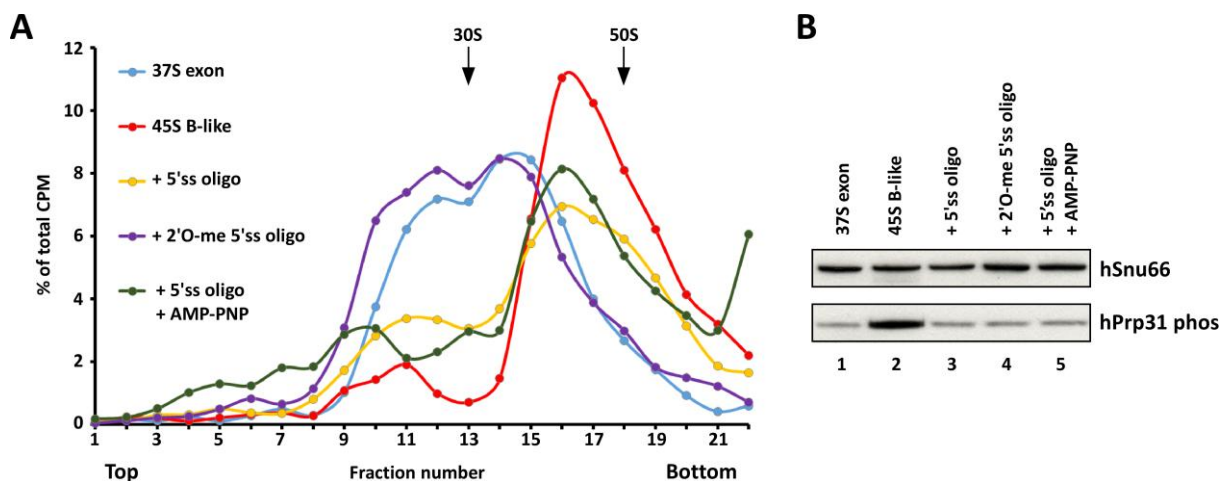


Figure 3.5: Addition of a 5'ss oligonucleotide to affinity-purified 37S exon complex induces the shift to a 45S complex

(A) Analytical centrifugation on glycerol gradients containing 75 mM KCl of affinity-purified 37S exon complexes after addition of 5'ss oligonucleotides or 2'O-me 5'ss oligonucleotide. Purified 45S B-like complexes were run in parallel. Additionally 2 mM of the non-hydrolysable ATP-analog AMP-PNP was added to the washing buffer to remove any residual ATP (+AMP-PNP). (B) Peak fractions from the second gradient were used for western blot analysis. Proteins were separated by 4-12 % SDS-PAGE, transferred onto a nitrocellulose membrane and immuno-stained with antibodies against the phosphorylated form of hPrp31 (hPrp31 phos). Antibodies against the U4/U6.U5 tri-snRNP-specific protein hSnu66 were used to ensure equal loading.

Thus, addition of solely the 5'ss oligonucleotide converts the exon complex into a complex exhibiting a higher S-value with stably-bound U4/U6.U5 tri-snRNP, consistent with it undergoing a structural rearrangement. Similar results were obtained when the second analytical centrifugation was performed with glycerol gradients containing only 75 mM KCl (Figure 3.5A). Under these conditions the 37S exon complex only partially dissociates, with ~50 % still migrating as a 37S complex. In presence of the 5'ss oligonucleotide, but not the 2'O-me form, nearly all of the exon complex was shifted to a complex with a higher S-value that co-migrated with a 45S B-like complex, which was initially generated by adding the 5'ss oligonucleotide to the splicing reaction. The addition of the 5'ss oligonucleotide to purified U4/U6.U5 tri-snRNP alone had no effect on its sedimentation behavior

(data not shown), suggesting that the change in the S-value only occurs upon interaction of the 5'ss oligonucleotide with a 37S exon complex.

Taken together, these data demonstrate that all of the factors required for the stable U4/U6.U5 tri-snRNP binding and the shift from a 37S to 45S complex upon addition of the 5'ss oligonucleotide are already present in the affinity-purified 37S exon complex. Thus, B complex-specific proteins do not appear to play a major role in this process.

3.4.1 ATP hydrolysis is not required for the shift in the S-value from 37S to 45S

Assembly of the multi-megadalton spliceosome involves a series of structural rearrangements that are mainly driven by ATPases and helicases upon their hydrolysis of NTPs/ATP. As no additional ATP was added to the purified 37S exon complexes and the incubation steps were performed on ice, ATP hydrolysis does not appear to be required for the shift in its sedimentation value. However, at this point of our investigations it could not be excluded that ATP is bound by the purified complexes.

The standard procedure to deplete splicing reactions from ATP is an incubation in the presence of glucose and hexokinase at 30 °C. But, in this case it was not possible to deplete ATP potentially retained by the 37S exon complexes by adding hexokinase and glucose due to the heat-sensitivity of the isolated complexes. Therefore, I set out to compete for ATP binding by supplementing the buffer that was used to wash the complexes while bound to the amylose beads with 2mM of the non-hydrolysable ATP-analog AMP-PNP. These AMP-PNP treated 37S complexes were eluted from the column and the eluate was afterwards incubated with the 5'ss oligonucleotide. The glycerol gradient analysis of this reaction showed that the AMP-PNP washed 37S exon complexes also exhibited a faster migration behavior upon addition of the 5'ss oligonucleotide. These results strongly suggest that the increased sedimentation value of the 37S exon complex is ATP-independent and relies only on the presence of a 5'ss oligonucleotide.

3.4.2 Phosphorylation of hPrp31 is not required for transforming the 37S exon complex into a 45S complex

Previous studies showed that stable B complex formation when performed with nuclear extract depends on the phosphorylation of the U4/U6.U5 tri-snRNP-associated proteins hPrp31 and hPrp6 by the hPrp4 kinase [Schneider *et al.*, 2010b]. Further, it was shown that these proteins can also be phosphorylated in purified 37S exon complexes upon addition of the 5'ss oligonucleotide and additional ATP and incubating at 30 °C [Schneider *et al.*, 2010a]. This suggested that the site-specific phosphorylation of these factors might be necessary for the stable integration of U4/U6.U5 tri-snRNP during 45S B-like complex formation. To test if this phosphorylation of hPrp31 might be a

prerequisite for the increased sedimentation value of the 37S exon complex upon addition of the 5'ss oligonucleotide, I monitored the phosphorylation-status of hPrp31 in peak fractions of the second gradient. Proteins from the peak fractions were precipitated and transferred to a nitrocellulose membrane. Then, the membrane was incubated with antibodies that specifically recognize the phosphorylated form of hPrp31 (Figure 3.5B). The phosphorylation of hPrp31 is strongly increased upon transition from the 37S exon to the 45S B-like complexes by addition of the 5'ss oligonucleotide to initial splicing reactions in nuclear extract (Figure 3.5B, lane 1 & 2). When 37S exon complexes were incubated with the 5'ss oligonucleotide after MS2 affinity-selection, no increase in hPrp31 phosphorylation was observed despite the increase in their sedimentation value. 37S exon complexes that were additionally treated with AMP-PNP also showed no increased phosphorylation. These results show that the shift to a 45S complex does not depend on the site-specific phosphorylation of hPrp31.

3.5 EM reveals a structural change in the purified 37S exon complex after addition of the 5'ss oligonucleotide

The shift in the migration behavior of purified 37S exon complexes after addition of the 5'ss oligonucleotide (stabilized exon complex) is likely due to a structural rearrangement in the complex. To identify potential structural changes, we subjected the stabilized exon complex to negative-stain EM. Therefore, affinity-purified 37S exon complexes were incubated with the 5'ss oligonucleotide and subsequently subjected to a second glycerol gradient under GraFix conditions. Complexes from the peak fractions of this fixating second gradient were then used for EM analysis with identical conditions as previously used for the 37S exon and 45S B-like complex (see figure 3.3). As judged by the appearance of single, clearly-defined particles on the EM grid (Figure 3.6A), we excluded an aggregation of the complex upon addition of the 5'ss oligonucleotide to be the reason for the increased sedimentation value. Subsequently, we generated class averages of the stabilized exon complex to allow a structural comparison with 37S exon and 45S B-like complexes, which were purified directly from splicing reactions. To generate representative class averages of the stabilized exon complex a total of 12000 raw images were subjected to image processing and characteristic class averages generated from these single particles are shown in the galleries 1-6 in figure 3.6A. The calculation of class averages resulted in similar structures in almost all classes, which might be explained by a predominant orientation of the complex on the EM grid, a feature also characteristic for the 45S B-like complex. The overall appearance of the stabilized exon complex was surprisingly similar to structures characteristic for the 45S B-like complex (Figure 3.6B).

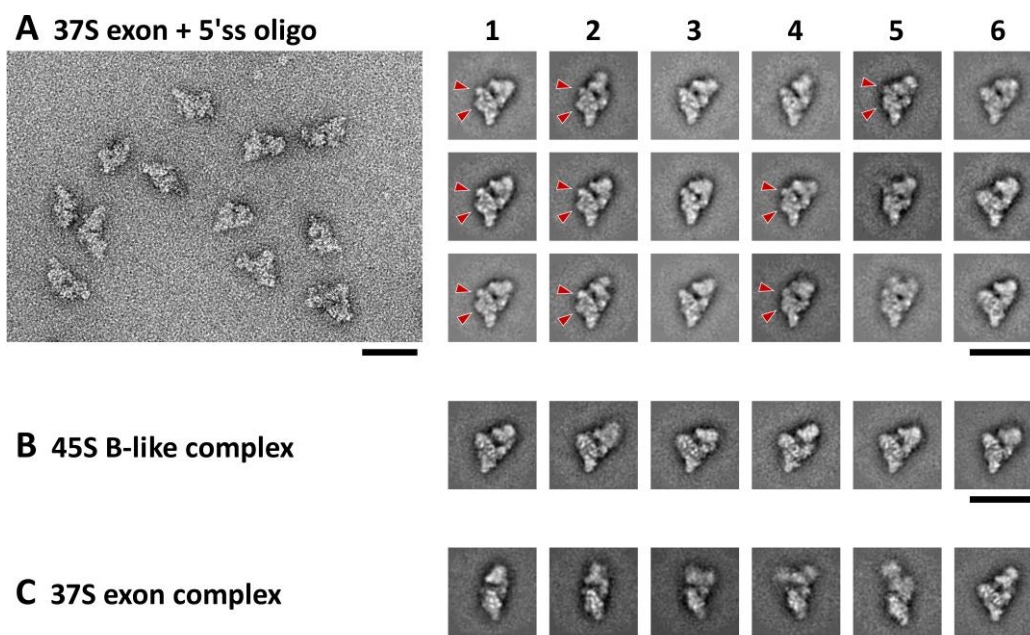


Figure 3.6: EM analysis of affinity-purified 37S exon complexes after addition of 5'ss oligonucleotide

(A) The overview on the left side shows negatively-stained particles of the stabilized exon complex on the EM grid. Representative class averages generated from single-particle images are shown in the galleries 1-6 on the right. Characteristic structural features within the body domain of the stabilized exon complex are indicated with red arrows. A selection of characteristic class averages of 45S B-like (B) and 37S exon (C) complexes is shown below. Scale bars correspond to 50 nm.

The dimensions of the complexes and the relative orientation of the head domain with respect to the body domain appear to be nearly identical in the stabilized exon complex and the 45S B-like complex, which was initially formed in nuclear extract. However, the structure of the U4/U6.U5 tri-snRNP containing body domain is slightly different in the stabilized exon complex in comparison to the 45S B-like complex. The majority of class averages calculated for the stabilized exon complex shows an additional belly-like protrusion in the center of the body domain, which is not present or significantly less pronounced in the structures of the 45S B-like complex. In contrast the stump of the body domain appears less pronounced in the class averages of the stabilized exon complex (Figure 3.6A, indicated with red arrows). These differences in the morphology of the body domain might indicate a slightly different orientation of the U4/U6.U5 tri-snRNP in the stabilized exon complex, eventually due to the absence of the B complex-specific proteins. In contrast, we detected no class averages with a morphology like the purified 37S exon complex (Figure 3.6C), which was prepared in absence of any oligonucleotide. The results shown here strongly suggest that solely the interaction of a free 5'ss oligonucleotide with the 37S exon complex induces a major remodeling of the complex organization. The rearrangement results in a complex morphology, which is very similar to the 45S B-like complex that was initially assembled in the splicing reaction. Apparently, the B complex-specific proteins are not essential for the structural rearrangement in the complex architecture since these

proteins are almost completely absent in the stabilized exon complex (see chapter 3.2). This provides strong evidence that the rearrangement of the complex is independent of protein factors not already found in the 37S exon complex or the activity of helicases or kinases since no ATP is required (see chapter 3.4.1).

3.6 Sequence requirements of the 5'ss oligonucleotide for U4/U6.U5 tri-snRNP stabilization during B-like complex formation

The results above show that solely the addition of a 5'ss oligonucleotide to the 37S exon complex is sufficient to stably integrate the U4/U6.U5 tri-snRNP and adopt a structural organization characteristic for a 45S B-like complex. Previous studies indicated that the 5'ss oligonucleotide contacts the U6 ACAGAG box of the U4/U6.U5 tri-snRNP in the 45S B-like complex [Schneider et al., 2010a]. But up to now it is not known, if the 5'ss/U6 base pairing and/or other interactions are essential to induce the structural rearrangement that is observed during formation of a 45S B-like complex. To assess the sequence requirements of the 5'ssplice site for transforming the 37S exon to a stable 45S B-like complex, we monitored the effects of different mutations within the oligonucleotide sequence on the formation of a stable B-like complex.

3.6.1 The exon-intron junction of the 5'ss oligonucleotide interacts with the U5 protein hPrp8 in stably-assembled 45S B-like complexes

Previous studies of the RNA-RNA network in pre-catalytic spliceosomes showed that exonic nucleotides of the 5'ssplice site base pair with loop I of U5 snRNA and intronic nucleotides with the ACAGAG box of U6 snRNA [Wassermann and Steitz, 1992]. Furthermore, it was shown in a trans-splicing assay using a radioactively-labeled 5'ss RNA oligonucleotide, that the conserved GU dinucleotide at the exon-intron junction is site-specifically crosslinked to the hPrp8 protein in stably-assembled B complexes [Reyes *et al.*, 1999] (Figure 3.7A). I first monitored whether hPrp8 also contacts this region of the 5'ss oligonucleotide in 45S B-like complexes, which were assembled on the MINX exon-RNA.

To allow the identification of a site-specific protein-RNA interaction, I designed a 5'ss oligonucleotide containing a 6-thio-G substitution at position +1. Thio-modified oligos can be covalently crosslinked to proteins at a wavelength of 365 nm, which prevents unspecific crosslinks between RNA and proteins. The modification of the 5'ss oligonucleotide at position +1 with a 6-thio-G nucleotide does not impair B-like complex formation, as evidenced by native gel-electrophoresis (Figure 3.7B, lane 2) or glycerol gradient centrifugation (data not shown).

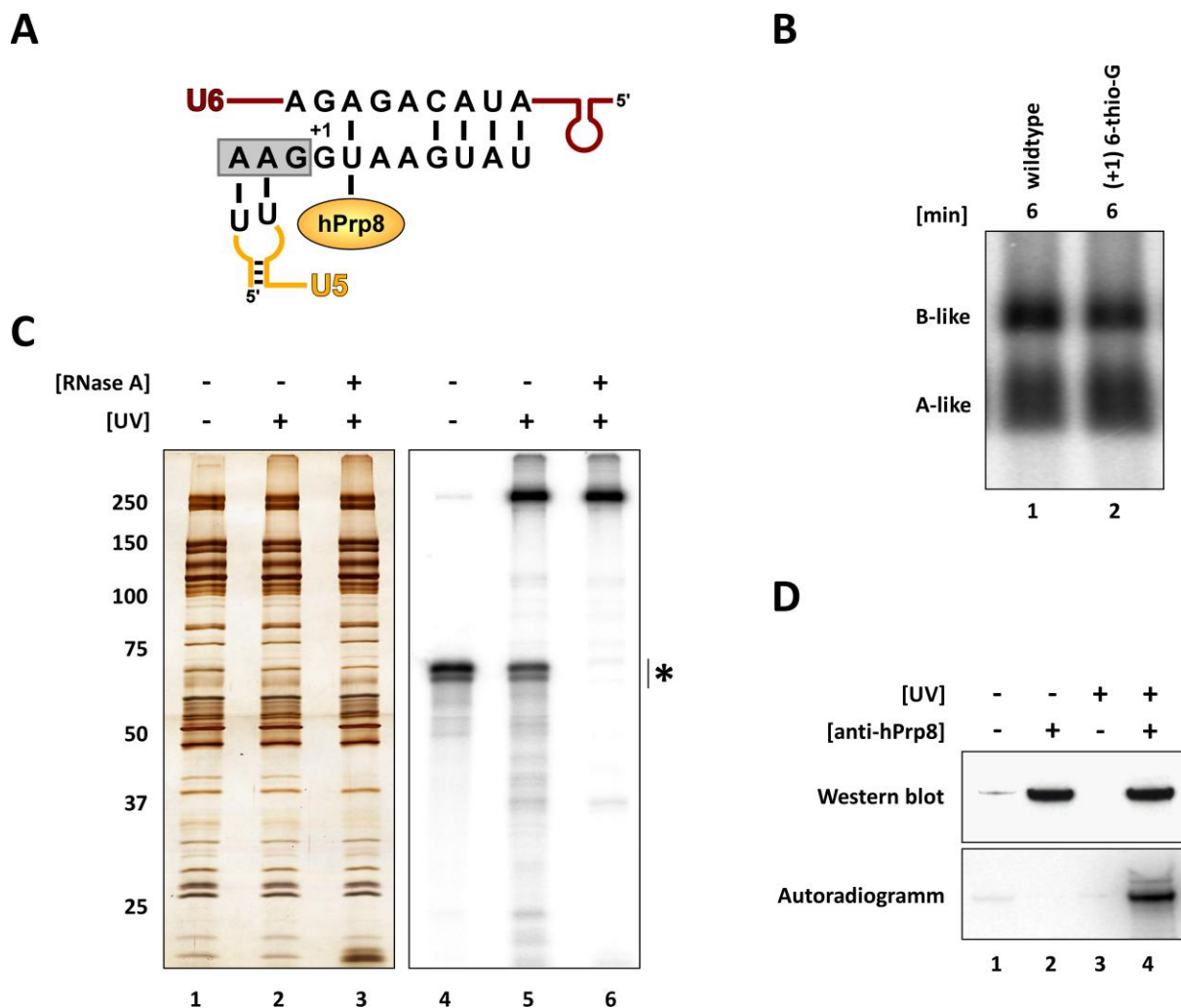


Figure 3.7: The exon-intron junction of the 5'ss oligonucleotide interacts with the U5 protein hPrp8 in stably-assembled 45S B-like complexes

(A) Scheme of the proposed interactions of a 5'splice site with the U5 snRNA, U6 snRNA and hPrp8 [adopted from Wassarmann and Steitz, 1992, Reyes et al., 1999]. The exonic part of the 5'splice site is represented by a shaded box. (B) B-like complex formation upon introduction of a (+1) 6-thio-G modification within the 5'ss oligonucleotide was tested by native gel analysis. (C) 45S B-like complexes were assembled in the presence of a 5'-32P-labeled (+1) 6-thio-G modified 5'ss oligonucleotide and subjected to glycerol gradient centrifugation. After MS2 affinity-selection of peak fractions, purified complexes were irradiated at 365 nm (lanes 2, 3, 5, 6) to induce protein-RNA crosslinks and subsequently treated with RNase A (lanes 3 & 6). Proteins were separated on a 10-13 % polyacrylamide gel and visualized by silver staining (lanes 1-3). Crosslinked proteins were detected by exposure to a phosphorimager screen (lanes 4-6). *: Position of MINX exon-RNA. (D) Immunoprecipitation of hPrp8 from denatured 45S B-like complexes after UV irradiation. Lanes 1 and 2 are controls without UV irradiation. Immunoprecipitation was performed using PAS-bound antibodies against hPrp8. The lanes 1 and 3 show negative controls, in which antibodies were omitted. The eluted proteins were separated by 4-12 % SDS-PAGE and blotted onto a nitrocellulose membrane. Western blotting was performed with hPrp8-specific antibodies (upper panel) and UV-induced crosslinks were detected by autoradiography (lower panel).

Irradiation of affinity-purified 45S B-like complexes assembled in the presence of a ^{32}P -labeled (+1) 6-thio-G oligonucleotide at 365 nm generated a highly-specific protein-RNA crosslink, which is resistant to RNase A treatment (Figure 3.7C, lane 6). The first cleavage site of RNase A, which cleaves after pyrimidines, is downstream of the exon-intron junction, so that the 5'- ^{32}P -label and the (+1) 6-thio-G crosslink are included within the same cleavage fragment. The crosslinked protein migrates in the range of ~250 kDa and co-migrates with the silver stained hPrp8 band (Figure 3.7C, lane 3). Immunoprecipitation with hPrp8-specific antibodies demonstrated that this crosslinked protein is indeed hPrp8 (Figure 3.7D). The same result was achieved using (-1) 6-thio-G or (+2) 4-thio-U modified 5'ss oligonucleotides (data not shown), showing that hPrp8 contacts nucleotides across the exon-intron boundary.

3.6.2 Base pairing interactions between 5'ss and U6 ACAGAG box are not absolutely required for stable B-like complex formation

To determine the sequence requirements for inducing stable integration of the U4/U6.U5 tri-snRNP during B-like formation, we introduced a variety of mutations into the 5'ss oligonucleotide sequence and analyzed their effects on B-like complex formation (Figure 3.8A). The stability of U4/U6.U5 tri-snRNP binding was assayed by native gel-electrophoresis in the presence of heparin.

First, I disrupted the Watson-Crick base pairing between loop I of U5 snRNA and the 5'ss oligonucleotide by mutating all three exonic nucleotides to uridines (U5:5'ss). This resulted in reduced formation of B-like complexes in comparison to the optimized wildtype sequence as assayed by native gel-electrophoresis (Figure 3.8B, lanes 3 & 4), but had little or no effect when assayed by the less stringent glycerol gradient centrifugation (Figure 3.8C). Next, I mutated intron nucleotides +5 to +8 of the 5'ss oligonucleotide to abolish Watson-Crick base pairing with the ACAGAG box of U6 snRNA (U6:5'ss). This mutation also impaired, but did not abolish formation of B-like complexes on native gels (Figure 3.8B, lane 5) and had no effect when assayed by glycerol gradient centrifugation (Figure 3.8C). Thus, neither the U5:5'ss nor the U6:5'ss interaction is absolutely necessary for stable B-like formation. But, when both mutations were introduced within the same oligonucleotide (U5:5'ss + U6:5'ss) B-like complex formation was completely abolished both on a native gel (Figure 3.8B, lane 6) and glycerol gradients (Figure 3.8C). These results show that individual disruption of either U5/5'ss or U6/5'ss base pairing has a moderate effect on B-like formation, but disruption of both interactions abolishes the stable integration of the U4/U6.U5 tri-snRNP.

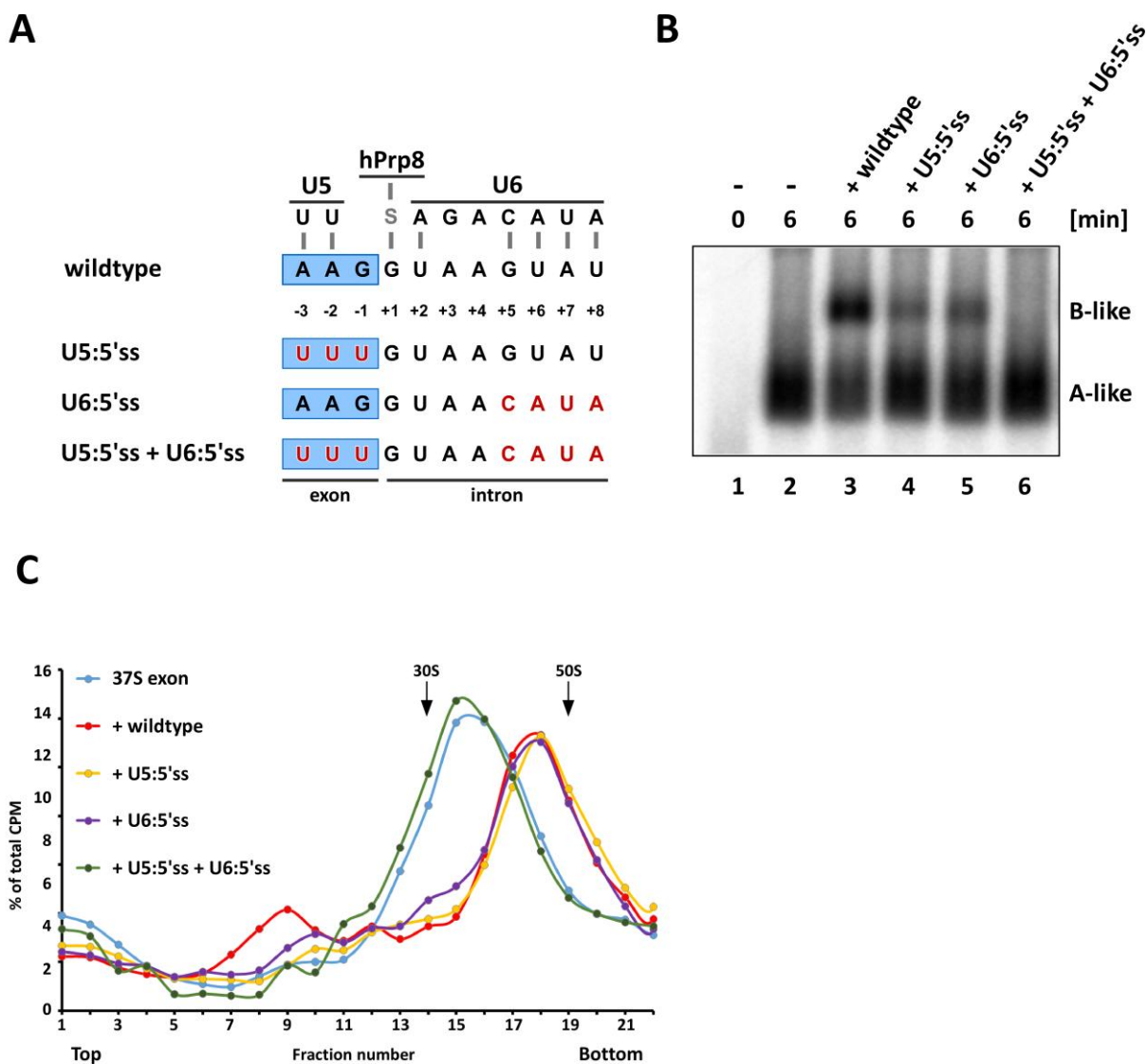


Figure 3.8: Effect of disruption of U5 and U6 interactions with the 5'ss oligonucleotide on B-like complex formation

(A) Overview of mutations introduced within the 5'ss oligonucleotide sequence to abolish Watson-Crick base pairing with U5 or/and U6 snRNA, respectively. Exonic nucleotides are highlighted by a blue box and mutations are labeled in red. (B) Native gel analysis of B-like complex assembly upon addition of mutated 5'ss oligonucleotides to the splicing reaction. Samples were analyzed on a 2 % (w/v) LMP agarose gel in the presence of heparin and visualized by autoradiography. The identities of the spliceosomal complexes are indicated. (C) Analytical glycerol gradient centrifugation of cross-exon complexes formed in splicing reactions after addition of the indicated 5'ss oligonucleotides. The percentage of total radioactivity is plotted for each gradient fraction.

3.6.3 Mutations of nucleotides at the exon-intron junction that contact hPrp8 abolish formation of a stable 45S B-like complex

Next, I investigated the role of the exon-intron junction of the 5'ss oligonucleotide, which is contacted by hPrp8, in formation of a stable B-like complex. Thus, I monitored the impact of mutations within the conserved G/GU nucleotides that define the exon-intron junction (Figure 3.9A).

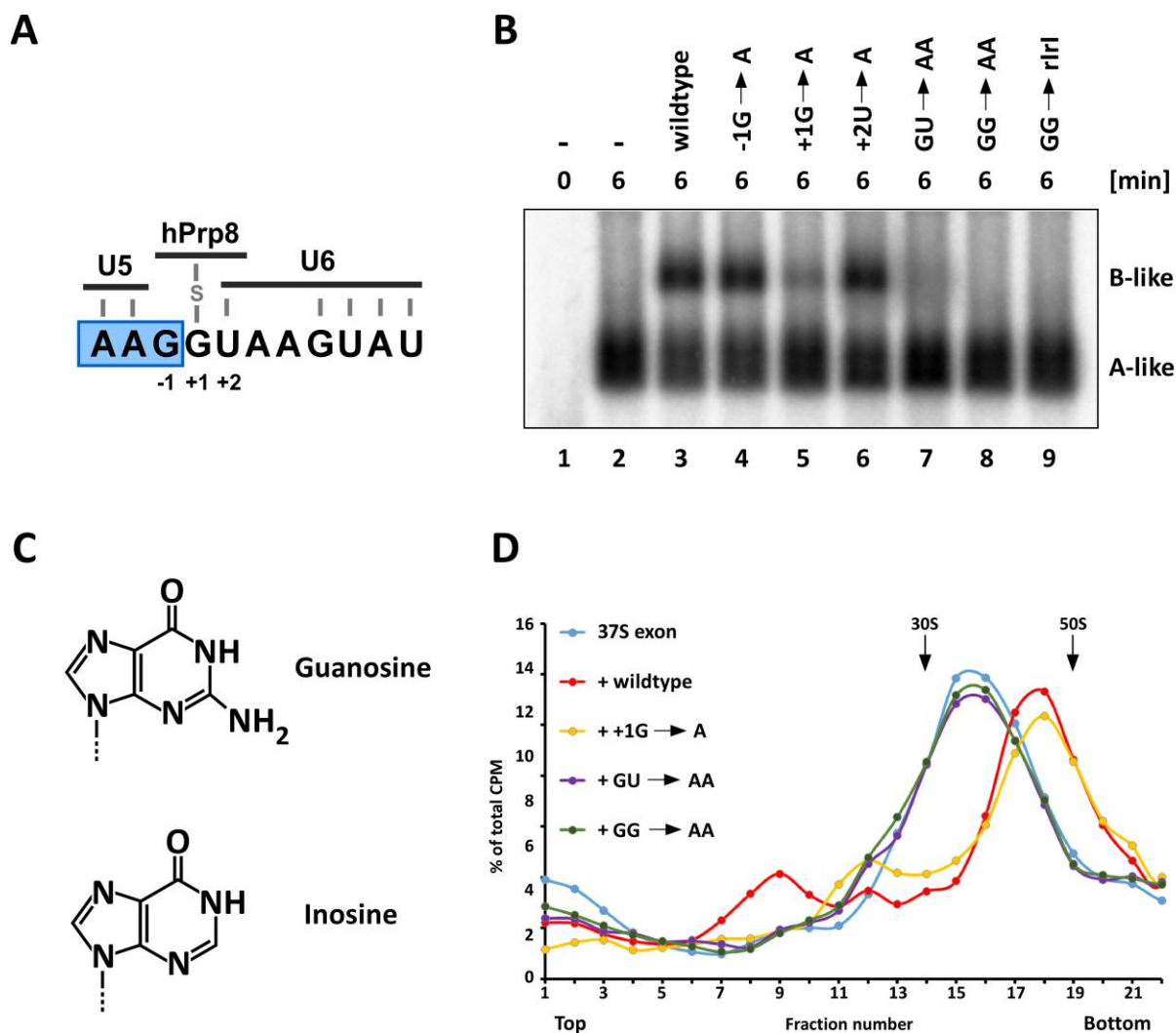


Figure 3.9: Mutations within the exon-intron junction of the 5'ss oligonucleotide abolish formation of a stable 45S B-like complex

(A) Schematic of interactions between the 5'ss oligonucleotide and U5 snRNA, U6 snRNA and hPrp8. (B) Native gel analysis of B-like formation with 5'ss oligonucleotides containing mutations within the G/GU triplet at the exon-intron junction. Mutations are indicated above the respective lane. Positions of the spliceosomal complexes are indicated. rI: ribo-inosine modification. (C) Schematic representation of guanosine and inosine base. (D) Analytical glycerol gradient centrifugation of complexes formed in extracts upon addition of the indicated 5'ss oligonucleotides.

Oligonucleotides containing single point mutations of $-1G \rightarrow A$ or $+2U \rightarrow A$ support B-like formation as efficiently as the wildtype sequence (Figure 3.9B, lanes 3, 4 & 6). The mutation of $+1G \rightarrow A$ strongly impaired the formation of a stable B-like complex in presence of heparin (Figure 3.9B, lane 5), but had only little effect when assayed by glycerol gradient centrifugation (Figure 3.9C). However, the mutation of two neighboring nucleotides within the exon-intron junction, either $GG \rightarrow AA$ or $GU \rightarrow AA$, resulted in a complete inhibition of B-like formation as judged by native gel analysis (Figure 3.9B, lanes 7 & 8) and glycerol gradient centrifugation (Figure 3.9C). Thus, a single point mutation at position $+1G$ strongly impairs B-like formation and mutation of a second neighboring nucleotide completely abolishes stable U4/U6.U5 tri-snRNP binding. Interestingly, the mutation of the GG dinucleotide to ribo-inosines also inhibited the stable integration of the U4/U6.U5 tri-snRNP (Figure 3.9B, lane 9) as well as the transition to a 45S complex (data not shown). As guanosine and ribo-inosine differ only by an amino group in the exocyclic group of the nucleotide (Figure 3.9D), this points to a very specific and functionally important recognition of guanosine-nucleotides at the exon-intron junction probably via interaction with hPrp8.

3.6.4 Double mutations at the intron-exon boundary abolish binding of 5'ss oligonucleotide to the exon complex

The mutations with the strongest impact on B-like formation are located in the region of the hPrp8:5'ss interaction and should have little or no effect on the RNA-RNA interactions between U5 or U6 snRNA and the 5'ss oligonucleotide. Since these 5'ss oligonucleotide mutants still have complementarity to the U5 snRNA and U6 snRNA, I tested if these RNA-RNA interactions are sufficient to stably bind the different oligonucleotides to the 37S exon complex.

Thus, 5'ss oligonucleotides containing mutations of a single nucleotide ($+1G \rightarrow A$) or two neighboring nucleotides ($GG \rightarrow AA$ and $GU \rightarrow AA$) were first 5'-³²P-labeled in order to detect them by denaturing PAGE after affinity-purification of the 37S exon or 45S B-like complexes, respectively. Then, spliceosomal complexes were assembled in presence of either labeled or unlabeled 5'ss oligonucleotides and subjected to glycerol gradient centrifugation. The peak fractions of these gradients, 45S peak for the wildtype and $+1G \rightarrow A$, and 37S peak for the $GG \rightarrow AA$ and $GU \rightarrow AA$ oligonucleotide (see figure 3.9D), were subjected to MS2 affinity-selection. RNA was recovered from the eluates, separated on a denaturing PAGE and ³²P-labeled RNA species were detected by autoradiography. After affinity-purification, I detected in all lanes similar amounts of ³²P-labeled MINX exon-RNA, which was used to assemble and purify the complexes (Figure 3.10). Additionally, I detected signals for the wildtype and $+1G \rightarrow A$ oligonucleotide upon 5'-³²P-labeling (Figure 3.10, lanes 2 & 4).

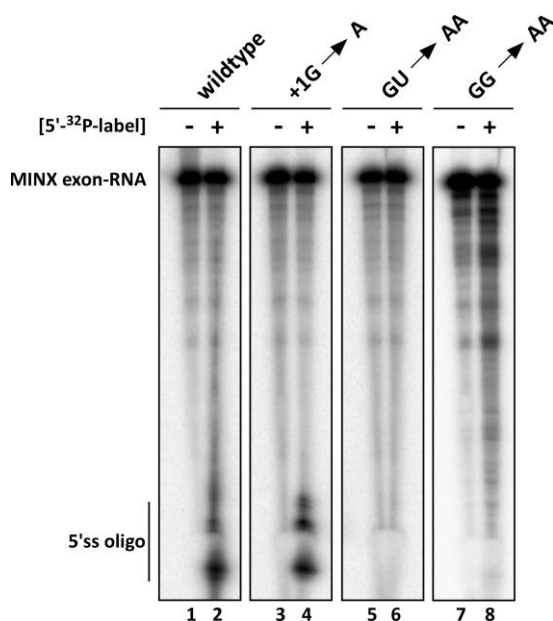


Figure 3.10: Double mutations within the exon-intron junction inhibit the integration of the 5'ss oligonucleotide

Spliceosomal complexes were assembled in the presence of the wildtype or mutated 5'-³²P-labeled 5'ss oligonucleotides, and subsequently subjected to glycerol gradient centrifugation. After MS2 affinity-selection of the respective peak fractions, RNA was recovered from the eluates, separated by denaturing PAGE and visualized by autoradiography. The positions of MINX exon-RNA and 5' labeled oligonucleotide are indicated.

This was not the case for the 5'-³²P-labeled oligonucleotides containing mutations GG → AA and GU → AA (Figure 3.10, lanes 6 & 8) showing that these oligonucleotides were not co-purified with the respective complex despite their complementarities to U5 and U6 snRNA. These results provide evidence that not only RNA-RNA interactions between the 5'ss oligonucleotide and the U5 snRNA and U6 snRNA are necessary for the physical association of the 5'ss with the complex, but also additional protein-RNA interactions are required for stable binding of the 5'ss oligonucleotide. This points to a crucial role for the hPrp8:5'ss interaction in binding of the 5'ss and further in mediating the structural change that leads then to stable integration of the U4/U6.U5 tri-snRNP.

I went on to test the co-purification of 5'-³²P-labeled 5'ss oligonucleotides mutants described in chapter 3.6.2 and 3.6.3 as well as the 2'O-me 5'ss oligonucleotide. A summary of the results is listed in Table 3.2. Interestingly, the 2'O-me 5'ss oligonucleotide was not co-purified with the complex, suggesting that the physical association of the 5'ss oligonucleotide with the 37S exon complex does not only depend on a specific interaction of hPrp8 with guanosine nucleotides at the exon-intron boundary, but also involves a recognition of the ribose-backbone of the RNA oligonucleotide. In addition, I could show that all 5'ss oligonucleotides that induce the transition to a 45S complex were also co-purified with the respective complex. By comparing the specific activity of the uniformly

³²P-labeled MINX exon-RNA and the 5'-labeled 5'ss oligonucleotides, we determined that approximately one 5'ss oligonucleotide interacts with a single 45S B-like complex.

5'ss oligonucleotide	sequence	B-like formation on native gel	S-value	co-purification
wildtype	A A G G U A A G U A U	+++	50S	+
2'O-me	A A G G U A A G U A U	-	37S	-
U5:5'ss	U U U G U A A G U A U	++	50S	+
U6:5'ss	A A G G U A A C A U A	++	50S	+
U5:5'ss + U6:5'ss	U U U G U A A C A U A	-	37S	-
-1G → A	A A A G U A A G U A U	+++	50S	+
+1G → A	A A G A U A A G U A U	+	50S	+
+2U → A	A A G G A A A G U A U	+++	50S	+
GU → AA	A A G A A A A G U A U	-	37S	-
GG → AA	A A A A U A A G U A U	-	37S	-
GU → rIrl	A A rI rI U A A G U A U	-	37S	-

-3 -2 -1 +1 +2 +3 +4 +5 +6 +7 +8

Table 3.2: Summary of the effects of the 5'ss oligonucleotide mutations on the 45S B-like complex formation

Overview of 5'ss oligonucleotide mutants and their effect on the formation of a 45S B-like complex. Exonic nucleotides are represented by a shaded box and mutations are labeled in red. The effect of mutations on B-like complex formation assayed by native gel analysis was classified in not reduced (+++), reduced (++) , strongly reduced (+) and complete inhibition (-). Sedimentation values of the spliceosomal complexes were determined by glycerol gradient centrifugation and co-purification of 5'-³²P-labeled 5'ss oligonucleotides was detected by MS2 affinity-selection followed by denaturing PAGE.

3.6.5 Recruitment of B complex-specific proteins is independent of complex stability in presence of heparin

In the presence of certain mutated 5'ss oligonucleotides, namely U5:5'ss, U6:5'ss and +1G → A, the formation of a B-like complex was reduced in the presence of heparin during native gel-electrophoresis, but not under the less stringent conditions used for glycerol gradient centrifugation. However, these 5'ss oligonucleotide mutants still bind to the cross-exon complex resulting in a quantitative shift to a 45S complex (Table 3.2), but the U4/U6.U5 tri-snRNP appears to be slightly less stably associated, i.e. sensitive to heparin. The formation of a stable 45S B-like complex in splicing reactions is not only characterized by an increased sedimentation value, but also by a site-specific phosphorylation of hPrp31 and strongly enriched amounts of the B complex-specific proteins. These characteristics of the B-like complex could potentially be involved in the stabilization of U4/U6.U5 tri-snRNP binding under harsh conditions, as e.g. in the presence of heparin during native gel analysis.

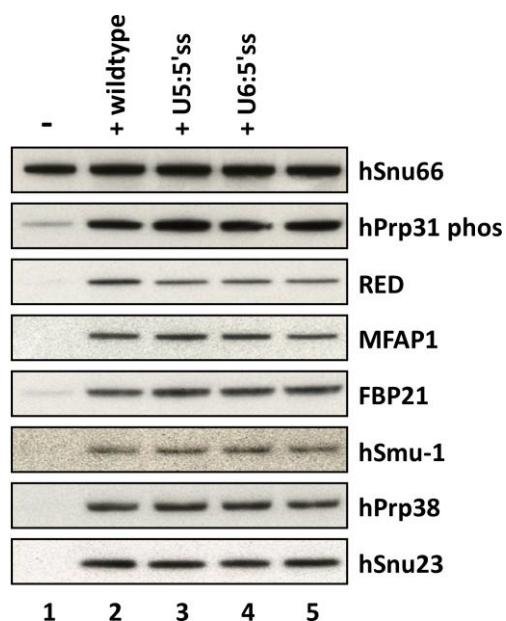


Figure 3.11: Western blot analysis of 45S B-like complexes assembled in presence of mutated 5'ss oligonucleotides

Affinity-purified 37S exon or 45S B-like complexes formed after addition of the indicated 5'ss oligonucleotide were separated on a 4-12 % SDS-PAGE, transferred to a nitrocellulose membrane and sequentially immunoblotted with the antibodies indicated on the right. Antibodies against the U4/U6.U5-specific protein hSnu66 were used to control for equal loading.

Therefore, I monitored the recruitment of B complex-specific proteins and the site-specific phosphorylation of hPrp31 in B-like complexes that were assembled by addition of the 5'ss oligonucleotide mutants U5:5'ss, U6:5'ss and +1G \rightarrow A to the splicing reaction. These splicing reactions were then subjected to glycerol gradient centrifugation and the 45S peak fractions (see figures 3.8C & 3.9D) were used for MS2 affinity-selection. Finally, the recruitment of B complex-specific proteins and the site-specific phosphorylation of hPrp31 within the purified complexes were investigated via immunoblotting with the respective antibodies. Western blot analysis showed the same amount of site-specific phosphorylation of hPrp31 in the B-like complexes that were assembled in presence of the U5:5'ss, U6:5'ss or +1G \rightarrow A oligonucleotide mutants as for the wildtype 5'ss oligonucleotide (Figure 3.11, lanes 2-5). Further, the amount of B complex-specific proteins was also nearly identical in all of the B-like complexes analyzed, despite their difference in heparin-resistance. These results show that the apparent difference in complex stability is independent of hPrp31 phosphorylation and the presence of B complex-specific proteins.

3.7 A dominant-negative mutant of the DEAD-box helicase hPrp28 stalls spliceosome assembly prior to stable B complex formation

Next I set out to investigate the requirements for the stable integration of the U4/U6.U5 tri-snRNP during formation of a pre-catalytic B complex that is assembled across an intron. A prerequisite for these studies was the isolation of an intron-defined splicing complex containing all five snRNPs, but in which the U4/U6.U5 tri-snRNP had not yet been stably-integrated.

During the initial steps of spliceosome assembly the 5' splice site of a pre-mRNA base pairs with the 5' end of the U1 snRNA. The DEAD-box helicase Prp28 disrupts this U1:5'ss interaction during formation of a stable pre-catalytic B complex and previous studies suggested that in yeast the U4/U6.U5 tri-snRNP initially associates with the spliceosome prior to the action of Prp28 [Staley and Guthrie, 1999, Chen *et al.*, 2001]. Therefore, we chose hPrp28 as a target to inhibit splicing prior to formation of an intron-defined B complex. The aim was to induce a retention of U1 snRNP at the 5' splice site of the pre-mRNA to impair its interaction with the U4/U6.U5 tri-snRNP. Thus, I used a His₆-tagged version of the human ortholog of Prp28 (hPrp28), in which the DEAD motif was mutated to AAAD, thereby abolishing its ATPase activity (kindly provided by Prof. Dr. Ralf Ficner, Department for Molecular Structural Biology, Georg-August-Universität Göttingen). This ATPase-deficient hPrp28 is further designated as hPrp28^{AAAD}. First, I tested if this ATPase-deficient protein is a suitable tool to stall spliceosome formation prior to B complex formation. Therefore, increasing amounts of recombinant hPrp28 wildtype or the hPrp28^{AAAD} protein were added to a splicing reaction containing a MINX pre-mRNA to investigate its effect on *in vitro* splicing. A pre-incubation in the absence of the pre-mRNA substrate was first carried out to allow an exchange of the endogenous hPrp28, which is an integral component of the U4/U6.U5 tri-snRNP, with the recombinant protein, and the splicing reaction was subsequently started by addition of the MINX pre-mRNA. The reaction was stopped after 30 min of incubation and the RNA was recovered and separated on a 14 % denaturing polyacrylamide gel. The formation of splicing intermediates and products was detected by autoradiography. The addition of recombinantly-expressed hPrp28 wildtype protein had little or no effect on splicing as judged by the amounts of splicing intermediates and products formed relative to the control without any recombinant protein (Figure 3.12, compare lane 2 with lanes 3-6). Addition of increasing concentrations of hPrp28^{AAAD} impaired pre-mRNA splicing (Figure 3.12, lane 7 & 8), and at a final concentration of 50 ng/ μ l hPrp28^{AAAD} a complete inhibition of *in vitro* splicing was observed (Figure 3.12, lane 9). *In vitro* splicing was blocked prior to the first catalytic step, as neither intermediates nor products of the splicing reaction were detected. These results show that pre-mRNA splicing is inhibited specifically by an excess of the hPrp28^{AAAD} mutant, but not of the wildtype

protein. Thus, the recombinant hPrp28^{AAAD} acts as a dominant-negative mutant during *in vitro* splicing.

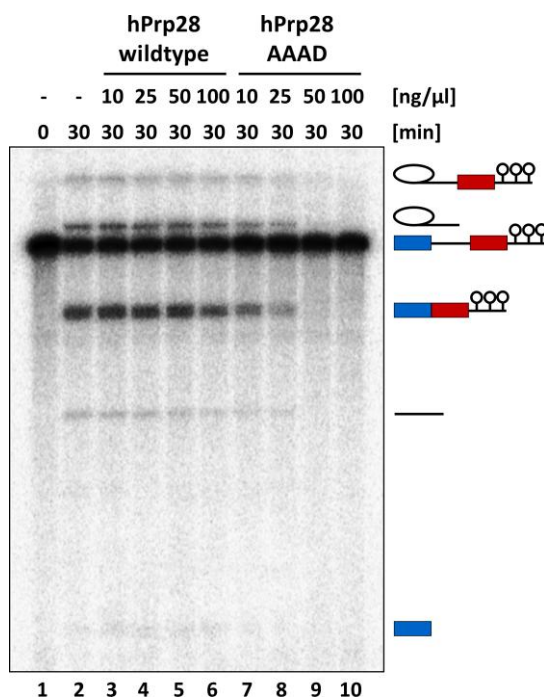


Figure 3.12: Recombinant hPrp28^{AAAD} protein inhibits splicing prior to the first catalytic step

In vitro splicing of uniformly ³²P-labeled MINX pre-mRNA was carried out in HeLa nuclear extract. Prior to addition of pre-mRNA, the splicing reaction was supplemented with recombinant wildtype hPrp28 or an AAAD mutant version of the protein to the final concentrations as indicated. RNA was analyzed on a 14 % polyacrylamide gel and visualized by autoradiography. The positions of the pre-mRNA, splicing intermediates and products are indicated on the right.

To identify which step of splicing is blocked by recombinant hPrp28^{AAAD}, I analyzed spliceosome assembly in the presence of the dominant-negative mutant by native gel-electrophoresis. Splicing reactions were performed in the presence of inhibitory concentrations of hPrp28^{AAAD} protein for the times indicated. Afterwards the samples were subjected to native gel-electrophoresis in the presence of heparin and complex formation was visualized by autoradiography.

The native gel analysis showed a sequential formation of A, B and B^{act}/C complexes in reactions without any recombinant protein (Figure 3.13, lanes 1-4) and in samples with the recombinant hPrp28 wildtype protein (Figure 3.13, lanes 5 & 6). In the presence of the hPrp28^{AAAD} mutant, B complex assembly was severely reduced and predominantly formation of A complex was observed (Figure 3.13, lane 7 & 8). These results show that the presence of hPrp28^{AAAD} blocks spliceosome assembly after A complex but prior to stable B complex formation. In summary, the use of the dominant-negative hPrp28^{AAAD} is an efficient and powerful tool to stall spliceosome assembly prior to stable B complex formation.

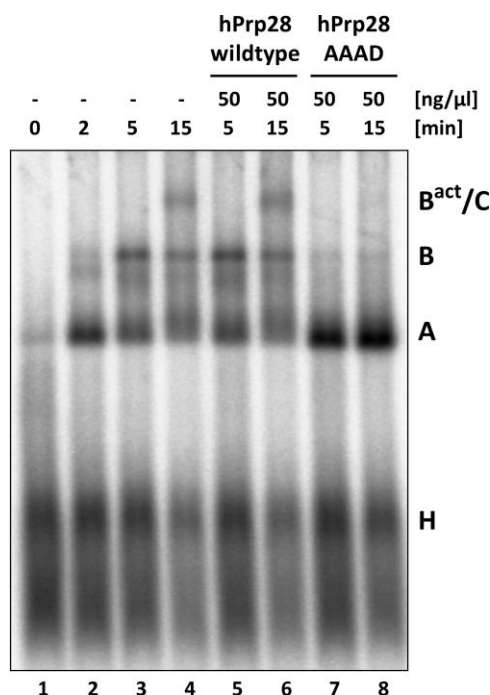


Figure 3.13: hPrp28^{AAAD} stalls spliceosome assembly prior to B complex formation

Spliceosome assembly was investigated in the presence of 50 ng/ μ l of recombinant hPrp28 wildtype or AAAD protein. Spliceosomal complexes were formed under splicing conditions in HeLa nuclear extract for the times indicated, subsequently analyzed on a 2 % (w/v) LMP agarose gel in the presence of heparin, and visualized by autoradiography. The positions of H, A, B and B^{act}/C complexes are indicated.

3.8 Isolation and characterization of a novel intron-defined spliceosome assembly intermediate

The presence of hPrp28^{AAAD} resulted in an inhibition of B complex formation and in native gel analyses mainly A complex assembly was detected. At this point it was not clear if the inhibition of spliceosome assembly occurs prior to recruitment of the U4/U6.U5 tri-snRNP or after association of the U4/U6.U5 tri-snRNP with the complex, but prior to its stable integration. Thus, I set out to characterize the effect of the hPrp28^{AAAD} on spliceosome assembly in greater detail. For this purpose I performed splicing reactions either in presence or absence of the hPrp28^{AAAD} mutant and separated the complexes by glycerol gradient ultracentrifugation. The gradient profile shows that spliceosomal complexes assembled in the presence of hPrp28^{AAAD} peaked in the region of ~37-40S (designated 37S cross-intron complex), while the kinetically-assembled B complex, which is formed after 6 min of *in vitro* splicing, peaked at ~45S (Figure 3.14A). To further characterize this 37S cross-intron complex I performed MS2 affinity-selection of the peak fractions. RNA was recovered from the eluates, separated on a denaturing polyacrylamide-gel and visualized by silver staining.

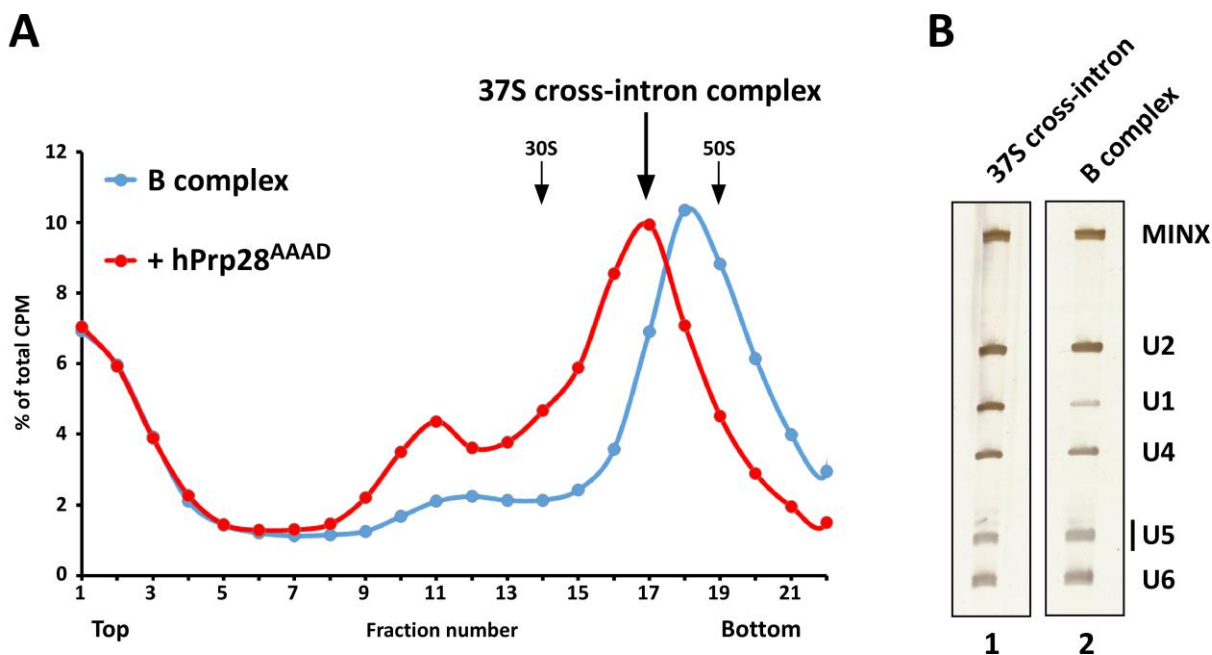


Figure 3.14: Addition of hPrp28^{AAAD} stalls spliceosome assembly after recruitment of the U4/U6.U5 tri-snRNP
 (A) Analysis of spliceosomal complexes assembled in the presence of inhibitory concentrations of the recombinant hPrp28^{AAAD} by centrifugation on glycerol gradients containing 150 mM KCl. Sedimentation values were determined with prokaryotic ribosomal subunits. (B) Peak fractions were subjected to MS2 affinity-selection. RNA was recovered from the eluted complexes, separated by denaturing PAGE and visualized with silver staining. snRNA identities are indicated on the right.

The RNA analysis showed that the hPrp28^{AAAD} stalled 37S cross-intron complex contains stoichiometric amounts of all five snRNAs (Figure 3.14B, lane 1). In contrast, U1 snRNA is significantly underrepresented in stably assembled B complexes (Figure 3.14B, lane 2). These results suggest that in presence of the hPrp28^{AAAD} a spliceosomal complex is formed, in which the U4/U6.U5 tri-snRNP is already recruited, but not yet stably bound such that it does not withstand the presence of heparin during native gel-electrophoresis. An intermediate with these characteristics has not yet been described for the human spliceosome assembly pathway. Thus, it represents a novel assembly intermediate that is formed prior to the action of hPrp28 and stable B complex formation. Consequently, I set out to identify the protein composition of this 37S cross-intron complex by mass spectrometry in order to characterize the change in the protein composition that occurs during formation of an intron-defined B complex. To identify proteins associated with the 37S cross-intron complex and compare them with the protein inventory of a kinetically-assembled B complex, affinity-purified complexes were separated on a 4-12 % SDS-PAGE and proteins were identified by LC-MS/MS. The identified proteins and their respective peptide counts are shown in Table 3.3. The MS analysis identified all proteins associated with the 17S U2 snRNP, as well as a number of 17S U2-related proteins in both complexes. Further, nearly all of the U5, U4/U6 and U4/U6.U5 tri-snRNP-

specific proteins including the Sm and LSm proteins were identified. This includes also the hPrp28 protein, which suggested that the recombinant hPrp28^{AAAD} is integrated in the 37S cross-intron complex. We subsequently confirmed the presence of the hPrp28^{AAAD} protein via western blot analysis with antibodies against the His₆-tag of the recombinant protein (data not shown). The 37S cross-intron complex contains also U1 snRNP-associated proteins, while in the B complex the U1 proteins are less abundant compared to the U2, U5 and U4/U6 associated proteins. This is consistent with the lower abundance of U1 snRNA in the B complex shown in figure 3.14B.

Moreover the B complex shows higher peptide counts for the B complex-specific proteins RED, MFAP1, FBP-21, hSmu-1, hPrp38 and hSnu23 in comparison to the 37S cross-intron complex. Proteins associated with the hPrp19 complex and hPrp19 complex-related proteins were identified in the B complex, while these proteins were nearly absent in the 37S cross-intron complex. Further, proteins of the RES complex are also underrepresented in the 37S cross-intron complex in comparison to the B complex. The MS analysis shows that the protein inventory of the 37S cross-intron complex consists mainly of U1, U2, U2-related and U4/U6.U5 tri-snRNP associated proteins, whereas the B complex additionally contains B complex-specific proteins and factors that are related to the hPrp19 and RES complex. Interestingly, the protein composition of the 37S cross-intron complex appears to be astonishingly similar to the 37S exon complex, which was previously investigated by mass spectrometry under comparable conditions [Schneider *et al.*, 2010a]. We thus set out to compare the protein composition of the 37S cross-intron and 37S exon complexes with a more quantitative approach using 2D gel-electrophoresis followed by MS identification, which also allows the identification of proteins that are abundant in both complexes.

preparation pmol	gi number	MW	28 ^{AAAD}			B complex			<i>S. cerevisiae</i> gene name
			#1 0.9	#2 0.9	#3 2.0	#1 0.9	#2 0.9	#3 2.0	
Sm									
Sm B/B'	gi 119631003	24 kDa	43	35	62	52	55	94	SMB1
Sm D1	gi 5902102	13 kDa	12	15	38	18	17	62	SMD1
SmD2	gi 4759158	14 kDa	22	39	51	26	42	72	SMD2
SmD3	gi 4759160	14 kDa	25	36	57	34	45	59	SMD3
Sm E	gi 4507129	11 kDa	18	25	65	17	31	70	SME1
Sm F	gi 4507131	10 kDa	11	-	10	7	-	12	SMX3
Sm G	gi 4507133	8 kDa	4	-	9	5	-	12	SMX2
U1									
U1-70K	gi 36100	52 kDa	23	19	38	7	11	13	SNP1
U1-A	gi 189053747	31 kDa	24	29	35	10	14	13	MUD1
U1-C	gi 119624201	20 kDa	4	-	7	3	-	3	YHC1
U2									
U2 A'	gi 50593002	28 kDa	65	47	66	65	59	82	LEA1
U2B''	gi 119630691	28 kDa	27	21	39	24	25	45	MSL1
SF3a120	gi 5032087	89 kDa	75	70	185	63	88	213	PRP21
SF3a66	gi 116283242	51 kDa	15	17	32	13	20	40	PRP11
SF3a60	gi 158255798	59 kDa	50	42	98	45	63	120	PRP9
SF3b155	gi 54112117	146 kDa	188	206	559	215	222	740	HSH155
SF3b145	gi 33875399	100 kDa	63	65	205	71	80	299	CUS1
SF3b130	gi 54112121	136 kDa	232	216	833	236	255	950	RSE1
SF3b49	gi 5032069	44 kDa	13	14	43	12	16	43	HSH49
SF3B14a / p14	gi 7706326	15 kDa	22	21	40	29	18	48	
SF3b14b	gi 14249398	12 kDa	10	6	12	13	11	21	RDS3
SF3b10	gi 13775200	10 kDa	5	-	16	4	-	21	YSF3
U2-related									
hPrp43	gi 68509926	91 kDa	52	44	130	60	46	142	Prp43
U2AF65	gi 228543	53 kDa	14	20	45	8	19	36	
U2AF35	gi 5803207	28 kDa	7	9	14	7	6	18	
SPF45	gi 14249678	45 kDa	15	14	18	11	10	20	
SPF30	gi 189054204	27 kDa	12	19	35	7	16	21	
CHERP	gi 119226260	104 kDa	20	16	23	12	10	20	
SR140	gi 122937227	118 kDa	25	21	67	20	19	67	
PUF60	gi 109087698	54 kDa	1	8	4	-	7	1	
U5									
hPrp8	gi 91208426	274 kDa	257	271	1048	392	450	1601	PRP8
hBrr2	gi 40217847	245 kDa	343	307	1316	519	521	1925	BRR2
hSnu114	gi 12803113	109 kDa	141	150	545	223	228	788	SNU114
hPrp6	gi 189067252	107 kDa	109	98	301	105	141	441	PRP6
hPrp28	gi 193785886	93 kDa	101	110	217	76	75	157	PRP28
40K	gi 115298668	39 kDa	46	63	141	70	75	237	
hDib1	gi 5729802	17 kDa	22	-	28	20	-	31	
hLin1	gi 5174409	38 kDa	8	5	4	10	18	28	Lin1
Lsm									
Lsm2	gi 10863977	11 kDa	13	11	23	13	14	25	LSM2
Lsm3	gi 189053316	12 kDa	4	4	1	2	6	2	LSM3
Lsm4	gi 6912486	15 kDa	5	10	14	5	13	22	LSM4
Lsm5	gi 195222722	7 kDa	3	-	4	1	-	5	LSM5
Lsm6	gi 5901998	9 kDa	3	3	6	1	6	10	LSM6
Lsm7	gi 119589795	15 kDa	5	-	6	7	-	7	LSM7
Lsm8	gi 7706425	10 kDa	12	11	13	10	7	23	LSM8
U4/U6									
hPrp3	gi 4758556	78 kDa	77	97	186	85	116	255	PRP3
hPrp31	gi 221136939	55 kDa	44	39	99	33	62	122	PRP31
hPrp4	gi 189053699	58 kDa	72	80	229	51	90	272	PRP4
Cyp-H	gi 119627556	17 kDa	17	26	57	23	27	68	CPRS / CPR3
S15.5K	gi 145580328	14 kDa	7	6	13	6	11	12	SNU13
U4/U6.U5									
hSnu66	gi 10863889	90 kDa	125	73	365	101	115	395	SNU66
hSad1	gi 13926071	65 kDa	42	37	82	31	45	66	SAD1
27K	gi 24307919	19 kDa	12	11	14	5	9	12	
A complex									
RBM10	gi 20127479	104 kDa	9	14	40	14	8	14	MSL5 / BBP1
RBM5 / LUCA15	gi 5032031	92 kDa	13	8	30	14	10	26	
S164 (fSAP94)	gi 118196855	100 kDa	1	11	6	1	9	3	
B complex-specific									
MFAP1	gi 50726968	52 kDa	7	5	7	15	18	62	
RED	gi 125988409	66 kDa	15	14	34	42	68	152	
hSmu-1	gi 84370185	58 kDa	18	24	58	53	75	234	
hPrp38	gi 24762236	37 kDa	11	9	10	32	40	83	PRP38
hSnu23	gi 13385046	24 kDa	1	1	-	10	11	-	SNU23
FBP21	gi 189069453	43 kDa	1	3	3	11	16	45	

preparation pmol	gi number	MW	28 ^{AAAD}			B complex			<i>S. cerevisiae</i> gene name
			#1 0.9	#2 0.9	#3 2.0	#1 0.9	#2 0.9	#3 2.0	
B complex									
TCERG1	gi 21327715	124 kDa	1	1	1	26	40	32	YPR152C / URN1
FBP11	gi 34222504	109 kDa	-	9	3	-	6	2	
DDX9	gi 100913206	141 kDa	16	44	150	15	27	89	
DDX17 / p72	gi 148613856	80 kDa	-	6	12	-	-	0	DBP2
CAPER / RNPC2	gi 194384132	58 kDa	12	22	35	10	23	25	
hsp27	gi 4504517	23 kDa	4	-	5	4	-	6	
UBL5	gi 13236510	9 kDa	1	-	2	2	-	8	HUB1
hPrp4 kinase	gi 158255924	117 kDa	65	66	185	40	28	86	YAK1
KIN17 / BTCDC	gi 13124883	45 kDa	2	1	2	21	25	59	RTS2
BCLAF1	gi 219520423	106 kDa	2	-	6	1	-	4	
SKIV2L2	gi 193211480	118 kDa	16	14	30	13	7	14	MTR4
THRAP3	gi 167234419	109 kDa	2	-	18	2	-	14	
TFIP11	gi 21619831	97 kDa	18	10	9	35	36	54	NTR1
hPrp19									
hPrp19	gi 7657381	55 kDa	12	13	36	46	50	196	PRP19
Cdc5L	gi 11067747	92 kDa	18	14	27	63	66	189	CEF1
SPF27	gi 5031653	26 kDa	2	4	6	20	31	37	SNT309
hPr11	gi 4505895	57 kDa	12	14	14	27	41	155	PRP46
CCAP1 (hsp73)	gi 5729877	71 kDa	13	17	-	9	27	-	Ssa/Ssb families
CCAP2 (AD002)	gi 116812573	27 kDa	1	1	-	6	6	-	CWC15
CTNBL1 (catenin, β -like 1)	gi 111306496	65 kDa	3	1	-	21	13	-	
NPW38BP	gi 194378864	67 kDa	2	5	-	36	36	-	
hPrp19-related									
RBM22	gi 119582116	47 kDa	-	2	1	-	16	41	CWC2 + ECM2
hSyf1	gi 10566459	100 kDa	9	1	1	47	36	151	SYF1
hSyf3	gi 119630613	99 kDa	8	9	18	55	38	107	CLF1
hlsy1	gi 20149304	33 kDa	2	4	5	16	9	29	ISV1
SKIP	gi 34783485	61 kDa	13	7	9	37	35	69	PRP45
Cyp-E	gi 2828149	33 kDa	3	-	5	18	-	42	
PPIL1	gi 258588180	22 kDa	1	-	3	10	-	24	
KIAA0560 / fsAP164	gi 38788372	171 kDa	25	14	9	91	66	307	SEN1
G10	gi 32171175	17 kDa	1	3	4	21	22	28	BUD31 / CWC14
B^{act}									
KIAA1604	gi 119631401	106 kDa	3	1	-	21	10	-	CWC22
hPrp17	gi 62897001	66 kDa	6	8	7	33	33	85	CDC40
RES complex									
MGC13125	gi 14249338	71 kDa	4	2	3	25	19	56	BUD13
CGI-79	gi 4929627	40 kDa	4	2	2	14	10	16	IST3 / SNU17
EIC/mRNP									
Pinin	gi 158258595	82 kDa	5	-	3	6	-	3	
RNPS1	gi 3253165	34 kDa	1	-	5	2	-	4	
ACINUS	gi 259906018	151 kDa	16	23	16	15	20	10	
SAP18	gi 6648547	18 kDa	2	-	3	2	-	6	
ALY / REF	gi 238776833	28 kDa	5	12	11	7	16	10	YRA1
UAP56 / Bat1	gi 114306812	51 kDa	6	16	21	8	11	15	
ELG / C17orf85	gi 166295179	71 kDa	4	7	6	6	5	5	
DDX3 / HLP2	gi 197692141	73 kDa	7	14	9	4	14	5	
cap binding complex									
CBP80	gi 4505343	92 kDa	62	76	149	78	74	209	STO1
CBP20	gi 1060899	18 kDa	3	8	12	4	7	16	CBC2
mRNA binding proteins									
PABP4	gi 119627667	71 kDa	15	21	31	5	20	12	
PABP1	gi 41386798	71 kDa	18	33	40	14	22	20	PAB1
YB-1	gi 181486	40 kDa	40	12	82	31	24	118	
ASR2, SRRT	gi 119596872	102 kDa	54	62	154	33	33	94	
DDX5	gi 197692465	69 kDa	9	14	17	8	15	12	DBP2
ELAV / HuR	gi 119589356	50 kDa	3	5	11	4	2	3	
NF45 / Ilf2	gi 13385872	43 kDa	11	19	46	14	17	38	
SR proteins									
SRSF1 / ASF/SF2	gi 296202382	32 kDa	21	24	27	28	15	29	
SRSF3	gi 119624305	15 kDa	6	-	14	7	-	8	
SRSF5	gi 119601416	24 kDa	11	17	15	10	16	12	
SRSF6	gi 1049086	38 kDa	8	-	11	7	-	9	
SRSF7	gi 119389969	11 kDa	13	14	28	17	9	20	
SRSF9	gi 4506903	26 kDa	7	9	16	10	15	12	
SRSF10	gi 16905517	31 kDa	12	6	13	9	6	10	
hTra2- α	gi 194385084	21 kDa	4	-	5	4	-	3	
hTra2- β	gi 119598613	34 kDa	8	9	16	9	7	17	
SR-related proteins									
SRm300	gi 118572613	300 kDa	32	69	66	71	91	162	CWC21
SRm160	gi 119615546	104 kDa	5	9	5	15	13	37	

preparation pmol	gi number	MW	28 ^{AAAD}			B complex			<i>S. cerevisiae</i> gene name
			#1 0.9	#2 0.9	#3 2.0	#1 0.9	#2 0.9	#3 2.0	
hnRNP									
hnRNP A0	gi 5803036	31 kDa	3	14	31	3	12	31	
hnRNP-A1	gi 119617171	34 kDa	8	34	43	23	50	77	
hnRNP-A2/B1	gi 14043072	37 kDa	21	33	28	30	36	31	
hnRNP-A3	gi 119631468	37 kDa	4	14	25	9	25	30	
hnRNP-C1/C2	gi 117190174	32 kDa	18	21	73	18	20	40	
hnRNP-D	gi 119626284	30 kDa	-	4	7	-	7	4	
hnRNP-E1	gi 460771	38 kDa	5	4	13	8	7	14	
hnRNP F	gi 16876910	46 kDa	3	-	4	4	-	6	
hnRNP-G	gi 3256007	42 kDa	4	7	13	5	7	19	
hnRNP-H1	gi 48145673	49 kDa	4	5	14	3	9	13	
hnRNP-H3	gi 14141157	37 kDa	2	5	-	3	6	-	
hnRNP K	gi 119583080	51 kDa	5	7	-	-	1	-	
hnRNP M	gi 187281	78 kDa	10	10	15	9	12	13	
hnRNP Q	gi 119569012	66 kDa	7	18	49	5	19	10	
hnRNP-R	gi 5031755	71 kDa	13	28	84	13	30	31	
hnRNP-U	gi 14141161	89 kDa	4	14	25	2	11	3	
hnRNP U-like1	gi 3319956	96 kDa	2	1	-	5	6	-	
RALY	gi 119596694	32 kDa	4	5	-	5	2	-	
TREX									
THOC1	gi 154448890	76 kDa	4	8	7	6	9	4	HPR1
THOC2	gi 125656165	183 kDa	11	9	20	6	7	9	RLR1
THOC6	gi 31543164	38 kDa	4	11	12	6	6	5	
THOC7	gi 34783006	23 kDa	3	-	4	4	-	8	
MISC									
hUBA3	gi 126031226	89 kDa	159	199	403	173	207	451	
TUBB	gi 18088719	50 kDa	29	47	97	27	60	99	
ZC3H18	gi 194390520	109 kDa	45	39	68	23	23	36	
PAXBP1 / GCFC	gi 22035565	105 kDa	15	15	11	39	37	71	
DSP	gi 58530840	332 kDa	7	8	26	6	25	49	
IGF2BP3 / KOC / IMP	gi 2105469	64 kDa	17	17	33	11	19	27	
eIF3A	gi 4503509	167 kDa	3	7	5	2	13	3	
GNB2L1 / RACK1	gi 5174447	35 kDa	13	17	28	11	12	10	
ZCCHC8	gi 14042579	78 kDa	9	14	28	17	15	24	
RBM42	gi 114676748	47 kDa	12	21	47	3	9	20	
SETD2	gi 197313748	288 kDa	6	14	-	-	5	-	
JUP	gi 15080189	82 kDa	5	5	20	4	14	31	
SON3	gi 119630222	270 kDa	18	12	17	26	9	18	
eEF1A1	gi 62896589	50 kDa	6	9	10	6	12	12	
RSRC1	gi 332818209	32 kDa	6	7	4	13	12	18	
MATR3	gi 21626466	95 kDa	6	4	17	5	8	12	
CPSF1	gi 1045574	161 kDa	2	7	-	-	6	-	
MSI2	gi 119614912	37 kDa	8	12	14	5	5	16	
IGF2BP1 / IMP1	gi 56237027	63 kDa	11	7	16	5	9	13	
RBM4 / LARK	gi 93277122	40 kDa	9	5	13	9	5	12	
CFAP20 / fSAP23	gi 8392875	23 kDa	1	4	1	5	9	4	
eIF3E	gi 17389740	52 kDa	2	8	6	2	5	6	
OTT-MAL	gi 14041646	206 kDa	1	3	3	1	3	-	
RBM7	gi 119587652	31 kDa	4	6	9	6	7	11	
eIF3L	gi 193786348	71 kDa	-	6	5	-	5	2	
eIF3F	gi 119589043	39 kDa	3	6	-	2	5	-	
MEPCE	gi 158256168	74 kDa	-	2	2	-	7	-	
KIAA1429 / fSAP121	gi 119612122	202 kDa	1	7	-	1	1	-	
TOE1	gi 10436256	57 kDa	-	5	5	-	4	6	
CPSF3	gi 62898706	77 kDa	3	5	-	-	1	-	
ZC3H13	gi 119629156	197 kDa	1	7	-	-	1	-	
WTAP	gi 10334526	43 kDa	2	4	-	-	1	-	
eIF3I	gi 4503513	37 kDa	2	3	-	-	2	-	
FLG2	gi 62122917	248 kDa	6	-	9	3	-	3	
RPSA	gi 34272	33 kDa	5	-	27	5	-	10	
GPANK1 / Bat4	gi 15042961	39 kDa	1	-	1	9	-	6	
DSG	gi 119703744	114 kDa	5	-	13	1	-	21	
TUBA1B	gi 193786502	46 kDa	19	-	76	23	-	89	
NKTR	gi 6631100	166 kDa	4	-	1	15	-	20	
RBBP6 / PACT	gi 33620769	202 kDa	1	-	8	6	-	2	
ZC3HAV1	gi 158259083	101 kDa	5	-	8	6	-	10	
ANXA2	gi 4757756	39 kDa	3	-	8	4	-	16	
EXOSC10	gi 50301240	101 kDa	6	-	11	3	-	5	
YBX3 / CSDA	gi 14250672	40 kDa	28	-	67	23	-	90	
S100A8	gi 21614544	11 kDa	5	-	8	5	-	7	
EXOSC7	gi 15215485	32 kDa	3	-	11	4	-	6	
AHNAK	gi 61743954	629 kDa	1	-	5	1	-	8	
ERH	gi 4758302	12 kDa	3	-	2	1	-	2	
EXOSC3	gi 122920913	31 kDa	2	-	2	3	-	4	
EXOSC9	gi 119625657	47 kDa	6	-	13	4	-	11	
GPATCH8	gi 119571978	155 kDa	2	-	4	-	-	-	
HBB	gi 229752	16 kDa	1	-	8	11	-	-	
TUBB4B	gi 23958133	50 kDa	26	-	87	26	-	83	
Mtr3 / EXOSC6	gi 17402904	28 kDa	3	-	6	3	-	5	
EXOSC5	gi 122920910	25 kDa	3	-	6	3	-	6	

Table 3.3: Protein compositions of the 37S cross-intron and B complex were identified by mass spectrometry
Proteins of the indicated affinity-purified complexes were identified by LC-MS/MS after separation by 4-12 % SDS-PAGE. Proteins that were identified in at least two out of three independent preparations (#1-#3) are shown. Proteins not reproducibly detected or proteins generally considered to be common contaminants, such as ribosomal proteins, are omitted. Shown are the total spectral counts for each protein. Proteins are grouped according to function or stage of recruitment.

3.9 The 37S cross-intron and 37S exon complexes have nearly identical protein compositions

To directly compare the protein composition of the 37S cross-intron and 37S exon complexes, affinity-purified complexes were separated via 2D gel-electrophoresis and all visible protein-spots were subsequently identified by mass spectrometry.

The direct comparison of affinity-purified 37S cross-intron and 37S exon complexes by 2D gel-electrophoresis showed an almost identical protein pattern for both complexes, despite the fact that these complexes were assembled on different RNA substrates, namely MINX pre-mRNA and MINX exon-RNA. Like the 37S exon complex, nearly all U1, U2 and U4/U6.U5 tri-snRNP proteins were abundant in the 37S cross-intron complex (Figure 3.15). The B complex-specific proteins were absent or underrepresented in both complexes.

The comparison of both complexes side by side allowed not only a qualitative but also a semi-quantitative comparison of abundant proteins associated with the 37S cross-intron and 37S exon complex, respectively. The evaluation of the staining intensities showed lower amounts of hnRNPA1b and BCLAF1 (red dots) in the 37S cross-intron complex so that these proteins were not considered to be abundant in the 37S cross-intron complex. Additionally, the two proteins THRAP3 and SRSF10 (blue dots) are abundant in the 37S exon complex, while they are completely absent in the 37S cross-intron complex. The cap binding protein CBP80 is the only factor that was abundant in the 37S cross-intron complex, while not being abundant in the 37S exon complex (green dot). This is likely due to the fact that the MINX pre-mRNA, which was used to assemble the 37S cross-intron complex, contains a 5'-cap, while the MINX exon-RNA is synthesized in the absence of a 5'-cap. The very similar protein compositions of both 37S complexes suggest that these complexes are similar assembly intermediates of the spliceosome.

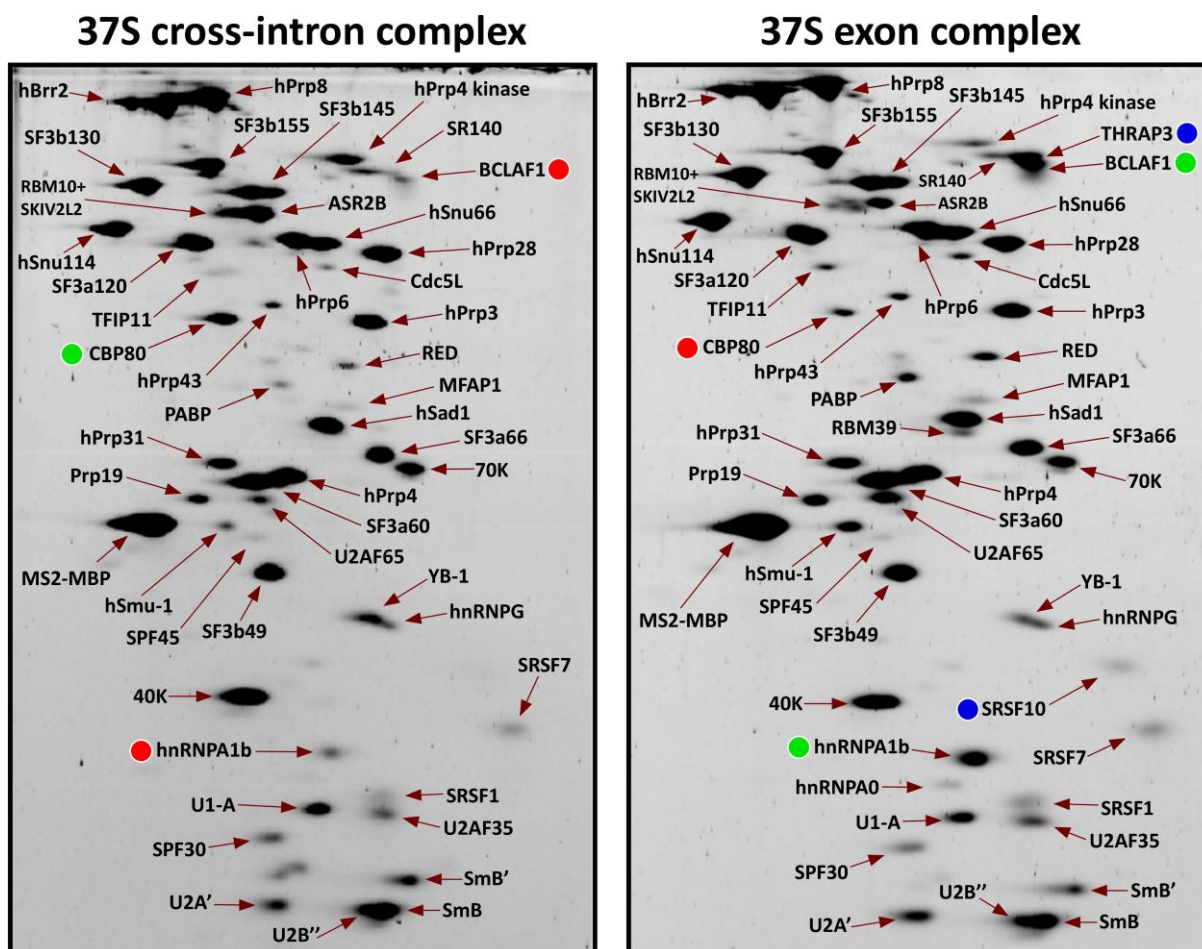


Figure 3.15: 2D gel-electrophoresis of affinity-purified 37S exon and 37S cross-intron complexes

Affinity-purified complexes were analyzed by 2D gel-electrophoresis and individual protein-spots were identified by mass spectrometry. The abundance of individual proteins was determined by visual inspections and differences in the relative abundance of single proteins between both complexes are indicated by green (abundant) or red (not abundant) dots, respectively. Proteins that are exclusively abundant within a particular complex are marked with blue dots.

Interestingly, the proteins THRAP3 and BCLAF1 are abundant in the 37S exon complex not in the 37S cross-intron complex. This is consistent with the results shown in chapter 3.2 and data from Agafonov *et al.* [Agafonov *et al.*, 2011], which indicate that the protein compositions of the 45S B-like and the intron-defined B complex differ only in abundance of these two proteins. This suggests that THRAP3 and BCLAF1 might be involved in the formation of exon-defined spliceosomes or the process of exon definition.

3.10 Analysis of the RNA-RNA network in the 37S cross-intron complex

Next I performed psoralen-mediated RNA-RNA crosslinking to investigate RNA-RNA interactions within the 37S cross-intron, as well as in the B complex. Thus, affinity-purified complexes were UV-irradiated at 365 nm in presence of psoralen (AMT) to induce RNA-RNA crosslinks. The crosslinked RNAs were separated on a denaturing 5 % polyacrylamide-gel and transferred to a nitrocellulose membrane, which was then sequentially incubated with ³²P-labeled probes against the pre-mRNA, U1, U2, U4, U5 and U6 snRNAs. The identities of crosslinked RNAs can be deduced by comparison of the migration behavior of various bands in the denaturing PAGE. Radioactive signals by two or more probes at the same position indicate the formation of a crosslink of the respective RNAs.

No signals of cross-linked RNAs were detected with any of the probes in the absence of psoralen (Figure 3.16A, lanes 1, 3, 5, 7, 9, 11, 13, 15, 17 & 19). After incubation with a probe specific for the MINX pre-mRNA, we detected signals of slower migrating bands upon addition of AMT (Figure 3.16A, lanes 2 & 4). Next, we incubated the membrane with an U1-specific probe and detected a signal at the same position as the pre-mRNA in the lane of the 37S cross-intron complex (Figure 3.16A, lanes 2 & 6). This crosslinking product was almost absent in the B complex (Figure 3.16A, lanes 4 & 8) consistent with lower amounts of U1 snRNA in affinity-purified B complexes as seen in figure 3.14B. This indicates that the U1 snRNA is still base paired with the pre-mRNA in the 37S cross-intron complex, but not anymore or at least to a significantly reduced extend in the B complex (U1/5'ss). Then, we sequentially incubated the membrane with probes specific for the U2, U4 and U6 snRNA. During these investigations, we identified a signal at the same position using probes against U2 and U6 snRNA (Figure 3.16A, lanes 10 & 18, 12 & 20). Based on the migration behavior of this crosslinking product, we conclude that it represents a crosslink in U2/U6 helix II (U2/U6) suggesting that the U4/U6.U5 tri-snRNP is associated via U2/U6 helix II to the 37S cross-intron and B complex, respectively (Figure 3.16B). The incubation with a U4-specific probe identified a crosslink between U4 and U6 at the same position within both complexes (Figure 3.16A, lanes 14 & 18, 16 & 20), showing that U4 and U6 snRNA are still base paired (U4/U6), even after stable integration of the U4/U6.U5 tri-snRNP within the B complex (Figure 3.16B). These results show clearly that stable integration of the U4/U6.U5 tri-snRNP and B complex formation occur prior to disruption of the U4/U6 base pairing. Additionally, several crosslinks between U2, U4 and U6 were identified in the B complex (Figure 3.16A, lanes 12, 16 & 20), which are significantly weaker or absent in the 37S exon complex (Figure 3.16A, lanes 10, 14 & 18).

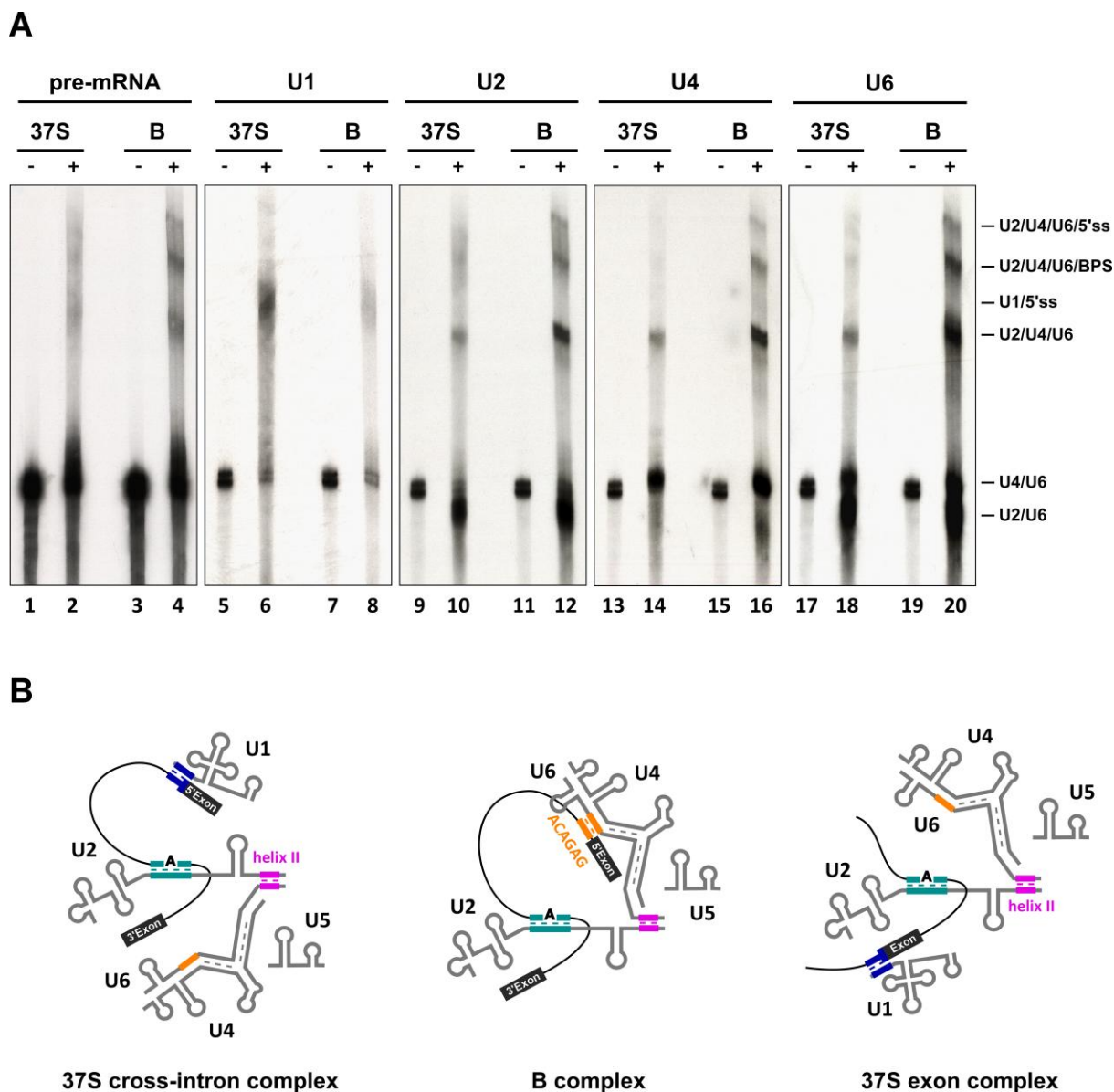


Figure 3.16: Investigation of RNA-RNA base pairing interactions in the 37S cross-intron complex

(A) Affinity-purified 37S cross-intron and B complexes were UV-irradiated in presence of psoralen (AMT) to induce RNA-RNA crosslinks (even-numbered lanes). As a negative control, AMT was omitted (odd-numbered lanes). RNA was recovered, separated on a denaturing 5 % polyacrylamide gel and transferred to a nitrocellulose membrane. The membrane was sequentially incubated with 32 P-labeled probes against the pre-mRNA, U1, U2, U4 and U6 snRNAs. The positions of crosslinked products are indicated on the right side. (B) Schematic representation of the RNA-RNA networks in the 37S cross-intron, B and 37S exon complexes. The U1 snRNP is still base paired with the 5'ss of the pre-mRNA, whereas the U4/U6.U5 tri-snRNP is bound to the U2 snRNP via U2/U6 helix II.

The fastest migrating species of this U2/U4/U6 triple-crosslink shows a dominant signal within in the B complex and is significantly weaker in the 37S cross-intron complex. Since the pre-mRNA-specific probe showed no or only weak signals at this position, we concluded that this crosslinking product resembles a triple crosslink between the U2 snRNA and the base paired U4/U6 di-snRNA (U2/U4/U6) (Figure 3.16B). The lower crosslinking efficiency of this RNA species in the 37S cross-intron complex

might indicate that the association between the U2 snRNP and the U4/U6.U5 tri-snRNP is somehow weaker or less optimal to generate RNA-RNA crosslinks. The second slowest migrating crosslinking product showed nearly the same signal intensities for the pre-mRNA, U2, U4 and U6 snRNA, suggesting that the U2-associated U4/U6 di-snRNA was additionally crosslinked to the pre-mRNA (U2/U4/U6/BPS). Since we detected faint signals of this crosslink also in the 37S cross-intron complex, we conclude that the pre-mRNA crosslink occurred at the BPS sequence of the pre-mRNA via interaction with the U2 snRNA. The slowest migrating crosslinking product between the pre-mRNA and the U2, U4 and U6 snRNA was only detected in the B complex (Figure 3.16, lanes 4, 12, 16 & 24) suggesting that in this RNA species the U6 snRNA was crosslinked to the pre-mRNA at the 5'splice site (U2/U4/U6/5'ss). Hybridization of the membrane with a U5-specific probe showed no signals for both complexes (data not shown).

In summary, the analyses of the RNA-RNA interactions within the 37S cross-intron showed that U1 snRNP is still base paired with the 5'ss of the pre-mRNA, while the U4/U6.U5 tri-snRNP associates via the U2/U6 helix II to the pre-mRNA bound U2 snRNA (Figure 3.16B). Previous investigations of the RNA-RNA network of the 37S exon complex showed a similar pattern of RNA-RNA interactions [Schneider *et al.*, 2010a], with the difference that the U1 snRNP base pairs with the downstream 5'ss of the MINX exon-RNA. Notably, the interaction between the U4/U6.U5 tri-snRNP and the pre-mRNA bound U2 snRNA appears to be stronger or more suitable for RNA-RNA crosslinking in the B complex in comparison to the 37S cross-intron complex. Additionally, we detected a crosslinking product exclusively in the B complex, in which the U6 snRNA potentially contact the pre-mRNA at its 5'splice site.

3.11 Electron microscopy investigation of the 37S cross-intron complex

Next we set out to determine structural features of the 37S cross-intron complex via negative-stain EM. Additionally, we also investigated a kinetically-assembled B complex via electron-microscopy under exactly the same conditions. The direct comparison of the 37S cross-intron to an intron-defined B complex should give insights into potential structural rearrangements during stable U4/U6.U5 tri-snRNP integration in the intron-defined spliceosome assembly pathway.

To characterize the novel intermediate structurewise, we subjected purified 37S cross-intron complexes to a second glycerol gradient under GraFix conditions and investigated the peak fractions by negative-stain EM. A gallery of individual class averages of the 37S cross-intron complex obtained by averaging approximately 10300 individual raw images is shown in figure 3.17. In parallel, a total of 9300 raw images of the kinetically-assembled B complex were subjected to image processing to allow a structural comparison under the same conditions.

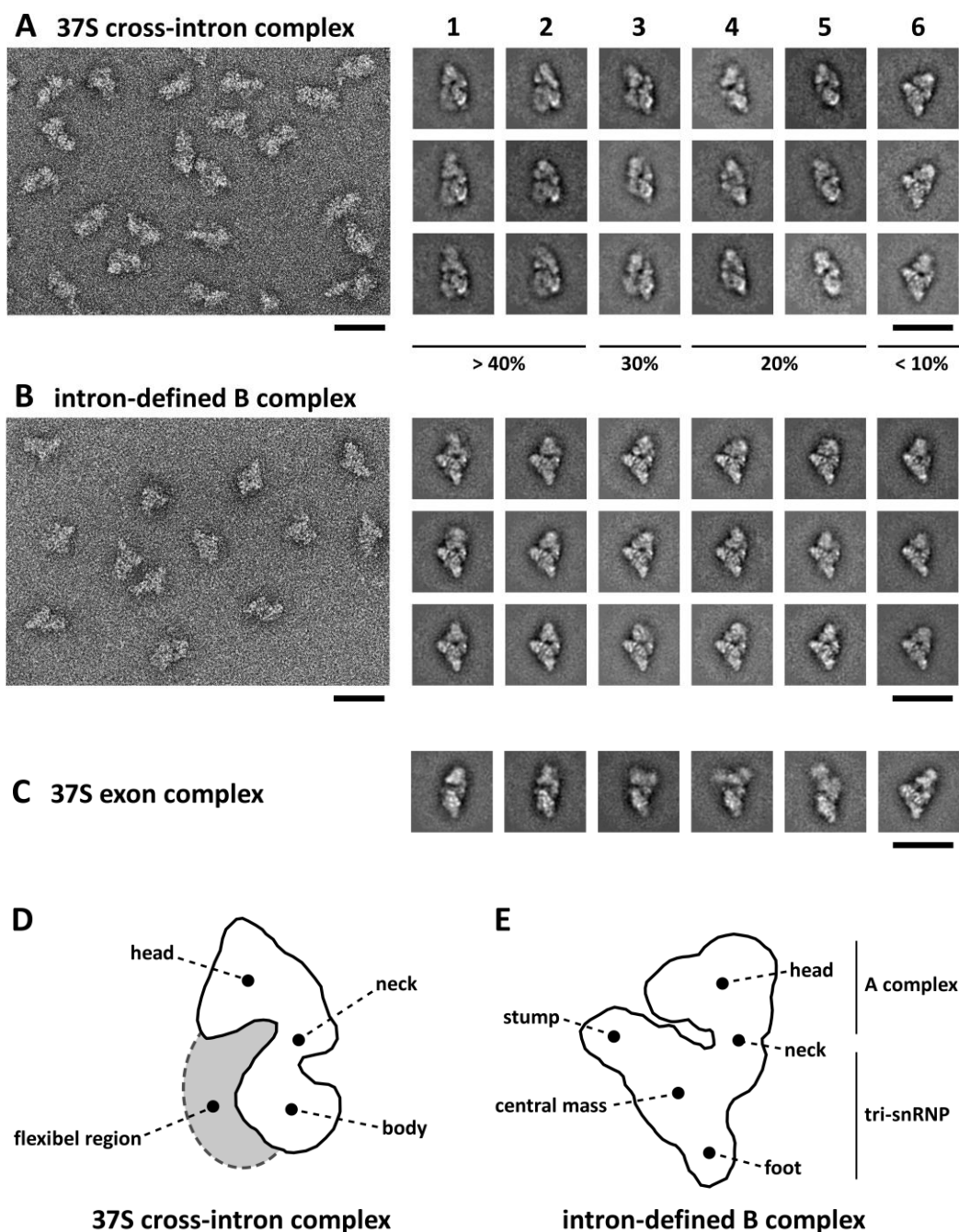


Figure 3.17: Negative-stain electron microscopy of the 37S cross-intron complex

Overviews of negatively-stained 37S cross-intron (A) and kinetically-assembled B complexes (B), i.e. 6 min incubation of splicing, are shown on the left. On the right representative class averages of the complexes are shown in the galleries 1-6 starting with the most frequently observed class. A small fraction (< 10 %) of images typical for the B complex was also detected in the preparation of the 37S cross-intron complex. Scale bars correspond to 50 nm. (C) Typical class averages of the 37S exon complex are shown in the gallery. (D) Schematic representation of the 37S cross-intron complex. The flexible and structurally heterogeneous region of the complex is shown as a grey circle. The circle indicates the maximal dimension of this domain, while the actual size of this domain may vary in the respective class averages. (E) Schematic representation of an intron-defined B complex. Main structural elements are labeled according to Boehringer *et al.* [Boehringer *et al.*2004].

The class averages of the 37S cross-intron complex are shown in figure 3.17A and the relative abundance of the respective structures is shown below. The upper domain of the particle, designated head, exhibits a triangular structure and appears similar in all classes, while the lower body domain shows significant differences in its structure. The lower left domain of the body appears diffuse or blurred without many structural details. Further, this domain varies in size and form in almost all class averages suggesting that this region of the complex is flexible or structurally heterogeneous (Figure 3.17A & D). In the majority of the classes the flexible region accounts for a substantial part of the body domain (Galleries 1 & 2), but in the less frequently observed classes this domain appears smaller (Gallery 3) or is not visible at all (Galleries 4 & 5). The head and body domains are connected by a hook-like neck domain. At this point, we can't determine if the structural diversity of the 37S cross-intron complex is based on a conformational heterogeneity potentially by movements of the domains relative to each other or if the different structures reflect different orientations of the complex on the EM grid.

In contrast, the kinetically-assembled B complex appears structurally homogenous with a characteristic orientation in almost all class averages. Further, the B complex reveals more structural details in the class averages in comparison with the 37S cross-intron complex, what supports the assumption that the spliceosome adopts a structurally homogenous appearance upon formation of a stable B complex (Figure 3.17B). A small fraction (< 10 %) of B complex structures is also present in the 37S preparation. The appearance of the B complex generated in this preparation is consistent with previous structural investigations of the intron-defined B complexes [Deckert *et al.*, 2006, Wolf *et al.*, 2009]. These results show that the transition from a 37S cross-intron to a B complex, and consequently stable integration of the U4/U6.U5 tri-snRNP, is accompanied by a dramatic change in the structure of the complex. Potentially, the relative orientation of the U4/U6.U tri-snRNP with respect to the U2 snRNP rearranges to a more favorable orientation during the stabilization of the U4/U6.U5 tri-snRNP binding (see chapter 3.3). However, at this level of the structural investigations it is not possible to conclude, how these domains are rearranged.

Interestingly, no structures similar to that of the 37S exon complex were identified in the class averages of the 37S cross-intron complex (Figure 3.17A & C). Actually, the structural investigation of the 37S cross-intron and 37S exon complex identified significantly different structures for these complexes, despite their nearly identical protein composition. The different appearance of these two complexes might reflect the difference in the location of U1 snRNP, which is base paired with the upstream 5'ss in the 37S cross-intron and with the downstream 5'ss in the 37S exon complex, respectively. Additionally, the presence of 5'-cap bound by CBP80 may influence the appearance of the 37S cross-intron complex or its absorption behavior. It was shown that the cap-binding complex,

formed of CBP80 and CBP20 interact with various proteins associated with the U4/U6.U5 tri-snRNP [Pabis *et al.*, 2013] and these additional protein-protein interactions may alter the structure or organization of the complex.

3.12 The 37S cross-intron complex is converted into a stable B complex in presence of a 5'ss oligonucleotide

The characterization of the RNA-RNA network of the 37S cross-intron complex suggests that this assembly intermediate is formed upon association of the U4/U6.U5 tri-snRNP with the U2 snRNA via U2/U6 helix II. But, native gel analysis showed that the U4/U6.U5 tri-snRNP is not yet stably-integrated within the complex. In the exon-defined system, the interaction of a 5'ss oligonucleotide with the exon complex bound U4/U6.U5 tri-snRNP results in its stable integration and changes the morphology of the complex so that it looks very similar to a B complex. But, despite the nearly identical protein composition and a similar RNA-RNA network of the 37S exon and 37S cross-intron complex, the structure of both complexes differs quite significantly as judged by a comparison of their appearance via negative-stain EM.

Thus, I tested if the addition of a 5'ss oligonucleotide also induces the stable integration of the U4/U6.U5 tri-snRNP within the 37S cross-intron complex, which should finally result in B complex formation. Therefore, I assembled spliceosomes in the presence of inhibitory concentrations of hPrp28^{AAAD} and added either the 5'ss oligonucleotide or the 2'O-me oligonucleotide after 3 min of incubation to the splicing reaction. The formation of a stable B complex was then monitored by native gel-electrophoresis in the presence of heparin.

As described above, the addition of 50 ng/ μ l hPrp28^{AAAD} protein to the splicing reaction results in assembly of a complex with loosely-bound U4/U6.U5 tri-snRNP. Upon treatment with heparin the U4/U6.U5 tri-snRNP dissociates and only an A complex signal is visible in the native gel (Figure 3.18, lane 3). The addition of 100-fold excess of the 5'ss oligonucleotide, but not a 2'O-me form, to the splicing reaction, induced the stable integration of the U4/U6.U5 tri-snRNP as judged by the appearance of a B complex signal in the native gel (Figure 3.18, lane 4 & 5). These results show that the 37S cross-intron complex is competent for B complex formation, despite the absence of hPrp28 action. As the 2'O-ribose methylated oligonucleotide competes for U1 snRNP binding and releases U1 snRNP from the 5'ss of the MINX pre-mRNA, a free 5'ss is apparently not sufficient to induce stable U4/U6.U5 tri-snRNP association.

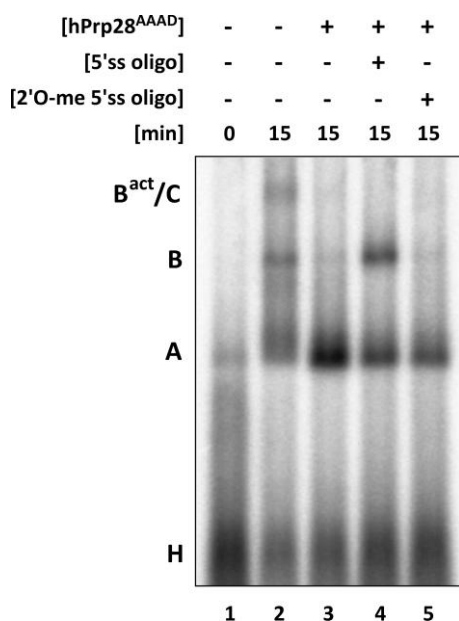


Figure 3.18: A stable B complex is formed upon addition of a 5'ss oligonucleotide to the splicing reaction containing inhibitory concentrations of hPrp28^{AAAD}

Uniformly ³²P-labeled MINX pre-mRNA was incubated under splicing conditions in the absence (lanes 1 & 2) or presence (lanes 3-5) of inhibitory concentrations of recombinant hPrp28^{AAAD} protein for the times indicated. Either the 5'ss oligonucleotide or 2'O-me 5'ss oligonucleotide was added in a 100-fold excess after three minutes of incubation. Spliceosome assembly was analyzed on a 2 % (w/v) LMP agarose gel in presence of heparin and visualized by autoradiography. The positions of H, A, B and B^{act}/C complexes are indicated.

The stabilization of U4/U6.U5 tri-snRNP binding within the hPrp28^{AAAD} stalled 37S cross-intron complex was tested in splicing reactions, which contain all proteins required for splicing. To exclude any secondary or passive effects of the 5'ss oligonucleotide in inducing the stable U4/U6.U5 tri-snRNP binding, I set out to investigate the requirements of stabilization under more defined conditions. Subsequently, I tested if the stable association of the U4/U6.U5 tri-snRNP also occurs upon addition of the 5'ss oligonucleotide to affinity-purified 37S cross-intron complexes. Thus, affinity-purified 37S cross-intron complexes were mixed with either the 5'ss oligonucleotide or the 2'O-me form and the U4/U6.U5 tri-snRNP binding was then analyzed by centrifugation on a second glycerol gradient containing 150 mM KCl, at which a loosely-associated U4/U6.U5 tri-snRNP dissociates from the complex. In absence of any added oligonucleotide the majority of the 37S cross-intron complexes localize in fractions with an S-value < 30S, which is consistent with the dissociation of the U4/U6.U5 tri-snRNP from the complex (Figure 3.19A). Addition of the 5'ss oligonucleotide, but not the 2'O-methylated form led to the formation of a complex that co-migrated with purified B complexes. I pooled fractions 15-17 from this gradient and subjected them to MS2 affinity-selection in order to determine the RNA composition of this complex.

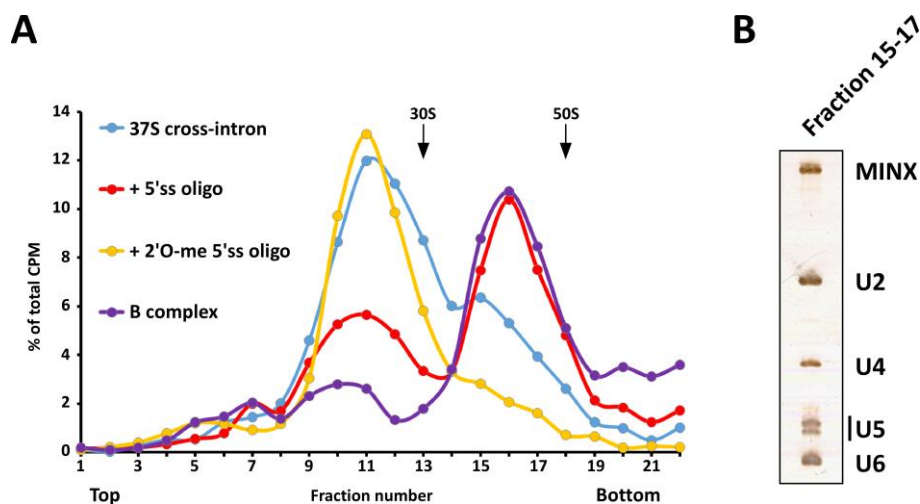


Figure 3.19: Addition of a 5'ss RNA oligonucleotide to affinity-purified 37S cross-intron complex induces stabilization of U4/U6.U5 tri-snRNP binding

(A) Affinity-purified 37S cross-intron complexes were incubated with either 5'ss oligonucleotide or 2'O-me 5'ss oligonucleotide and subsequently subjected to a second analytical centrifugation on a glycerol gradient containing 150 mM KCl. A kinetically-assembled B complex was run in parallel. (B) Peak fractions from the gradients were used for MS2 affinity-selection. RNA was recovered from the eluates, separated by denaturing PAGE and visualized by silver staining. Identities of snRNAs are indicated.

The RNA analysis showed that the complex, which peaks in fraction 15-17, contains the U2 snRNP and U4/U6.U5 snRNP as well as the MINX pre-mRNA (Figure 3.19B). This demonstrates that in the presence of a 5'ss oligonucleotide the U4/U6.U5 tri-snRNP gets stably-integrated within the 37S cross-intron complex without the requirement of any proteins, which are not associated with this complex. Interestingly, the presence of the 2'O-me 5'ss oligonucleotide does not induce the stabilization, despite it displaces U1 snRNP from the 5'ss of the pre-mRNA (data not shown). This supports the results of the native gel analyses, in which a free 5'ss of the pre-mRNA was not sufficient for stable U4/U6.U5 tri-snRNP binding in absence of hPrp28 function (Figure 3.18).

Taken together, these results are consistent with the idea that the 37S complexes with loosely-associated U4/U6.U5 tri-snRNP represent a very similar intermediate in both cross-exon and cross-intron spliceosome assembly pathways and that stable integration of the U4/U6.U5 tri-snRNP is triggered solely by its interaction with the 5'ss oligonucleotide. Further, these results also support the idea that the B complex-specific proteins are not required for stable cross-intron B complex formation.

3.13 EM reveals that the purified 37S cross-intron complexes adopt a B complex appearance after incubation with the 5'ss oligonucleotide

Finally, we set out to structurally investigate the 5'ss oligonucleotide induced shift of the 37S intron complex by negative-stain EM. Therefore, I performed MS2 affinity-selection of 37S cross-intron complexes assembled in the presence of inhibitory concentrations of hPrp28^{AAAD}. Subsequently, the purified complexes were supplemented with the 5'ss oligonucleotide and the reaction was separated on a second glycerol gradient under GraFix conditions. Particles in the peak fractions were stained with uranyl formate and subsequently analyzed by negative-stain EM. The overview shows clearly defined, single particles on the EM grid (Figure 3.20A), which were used to calculate class averages.

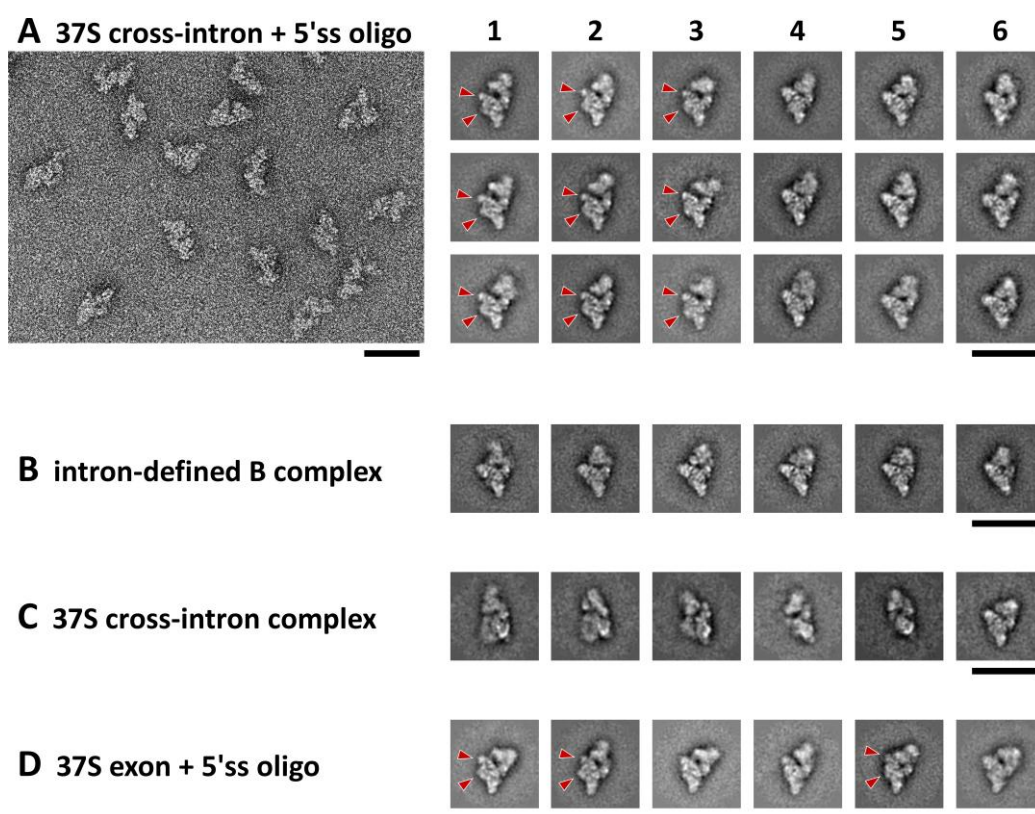


Figure 3.20: EM analysis after addition of the 5'ss oligonucleotide to purified 37S cross-intron complexes

Affinity-purified 37S cross-intron complexes were mixed with 5'ss oligonucleotide and subjected to a second glycerol gradient under GraFix conditions. Complexes from the peak fraction were used for negative-stain EM. (A) Raw images of affinity-purified 37S cross-intron complex after addition of 5'ss oligonucleotide are shown on the left. The galleries on the right side show representative class averages generated from single particle images. Typical class averages of the intron-defined B (B), the 37S cross-intron (C) and the stabilized exon (D) complex are shown below. Characteristic structural features within the body domain of the stabilized cross-intron an exon complex are indicated with red arrows. Scale bars correspond to 50 nm.

Based on the appearance of single particles on the EM grid, we excluded an aggregation to be the reason for the increased S-value of the 37S cross-intron complex after addition of the 5'ss oligonucleotide. To generate representative class averages of the stabilized cross-intron complex a total of 11000 raw images were subjected to image processing. The most frequently observed classes (Figure 3.20A, galleries 1-6) of the stabilized cross-intron complex are very similar and show only a low degree of structural heterogeneity, which is highlighted by the fact that in each class average complexes in structurally nearly identical states were obtained. The evaluation of the generated class averages showed that the stabilized cross-intron complex adopts a structure almost identical to class averages of a kinetically-assembled intron-defined B complex (Figure 3.20B), but shows nearly no similarities to the structure of the 37S cross-intron in the absence of any added oligonucleotide (Figure 3.20C). Strikingly, no classes characteristic for the 37S cross-intron complex are detectable in this preparation. These results show that the addition of a 5'ss oligonucleotide induces a significant change in the structure of the 37S cross-intron complex and rearranges the structure of the complex in such a way that it adopts an organization characteristic for a stably-assembled B complex. Astonishingly, the stabilized cross-intron complex shows an appearance that is also very similar to the 37S exon complex after addition of the 5'ss oligonucleotide (Figure 3.20D). Especially, the body domain of the stabilized cross-intron complex exhibit similar features, which are also characteristic for the stabilized exon complex, namely the belly-like protrusion in the center of the body as well as slimmer stump (Figure 3.20A & D, indicated by red arrows). This supports the idea that these complexes might resemble similar assembly intermediates of the spliceosome.

4. Discussion

In eukaryotes, most protein-coding genes contain coding exons and non-coding sequences known as introns. The splicing of pre-mRNA introns is catalyzed by the spliceosome, which assembles by the interaction of five snRNPs and numerous splicing factors with the pre-mRNA across an intron sequence (intron definition). An alternative assembly pathway exists, in which the spliceosome first forms across an exon (exon definition). As the chemical steps of splicing can only occur across an intron, a rearrangement from the exon-defined to an intron-defined organization must occur to allow generation of mature mRNAs. Previously it was shown that exon-defined spliceosomes not only contain U1 and U2 snRNPs, but also the U4/U6.U5 tri-snRNP (37S exon complex), providing evidence that it is possible for an exon-defined complex to be converted directly into a intron-defined B complex via interaction with an upstream 5'ss. During my studies I have investigated the requirements for stable B complex formation and factors contributing to this process, as this is a crucial step in which these two spliceosome assembly pathways converge. My data reveal that interaction of the 37S exon complex with solely a 5'ss oligonucleotide triggers a major conformational change that is visible by EM and accompanies stable integration of the U4/U6.U5 tri-snRNP within the spliceosome. This conformational change is triggered by the interaction of U4/U6.U5 tri-snRNP components with the 5'ss sequence, most importantly hPrp8, but does not require the B complex-specific proteins RED, MFAP1, FBP21, hSmu-1, hPrp38 and hSnu23, which are recruited during this stabilization process. Using an ATPase-deficient mutant of the DEAD-box helicase hPrp28, I was able to identify and characterize a novel intermediate of the intron-defined spliceosome assembly pathway (37S cross-intron complex) that is formed prior to stable B complex formation. This 37S cross-intron complex contains all of the snRNPs, but the U4/U6.U5 tri-snRNP is only loosely-associated. Characterization of its protein composition by mass spectrometry showed distinct differences in the composition of this novel intermediate in comparison to an intron-defined B complex, which helps to extend our understanding of how the protein inventory of the spliceosome changes during formation of a stable, pre-catalytic B complex. Interestingly, the intron- and exon-defined 37S assembly intermediates show a nearly identical RNA and protein composition, but their structures differ significantly. However, upon stable integration of the U4/U6.U5 tri-snRNP within the complexes induced by its interaction with a 5'ss sequence, their appearances become almost identical. Thus, the data presented here suggest that the exon- and intron-defined spliceosome assembly pathways converge at the stage, when the U4/U6.U5 tri-snRNP interacts with an upstream 5'ss.

4.1 Addition of a 5'ss-containing RNA oligonucleotide transforms the 37S exon complex into a 45S B-like complex with stably-integrated U4/U6.U5 tri-snRNP

To investigate the requirements for stable integration of the U4/U6.U5 tri-snRNP within the spliceosome, I used an established system to assemble exon-defined spliceosomes on a single exon pre-mRNA substrate in HeLa nuclear extract [Schneider *et al.*, 2010a]. Although this 37S exon complex contains all five snRNAs, the U4/U6.U5 tri-snRNP is only loosely-associated and sensitive to the presence of heparin. The addition of an RNA oligonucleotide containing an optimized 5'ss sequence induces the formation of a 45S B-like complex, in which the U4/U6.U5 tri-snRNP is now stably-integrated. During this stabilization process, the sedimentation value increases from 37S for the exon complex to 45S for the B-like complex and the U4/U6.U5 tri-snRNP binding becomes resistant against heparin (Figure 3.1). As the optimized 5'ss oligonucleotide is added in excess to the splicing reaction, it competes with the downstream 5'ss of the MINX exon-RNA for U1 snRNP binding, and consistent with this, the RNA composition of affinity-purified 45S B-like complexes shows a loss of U1 snRNP. Upon 2'O-ribose methylation of the 5'ss oligonucleotide, it no longer interacts with the U4/U6.U5 tri-snRNP but still binds to U1 snRNA. Addition of this modified 5'ss oligonucleotide did not support stable B-like formation on native gels, nor the shift to a 45S complex on a glycerol gradient, even though the complexes formed in its presence did not contain U1 snRNP. These data rule out that the loss of U1 snRNP alone induces stable U4/U6.U5 tri-snRNP binding and suggest an essential role for a previously shown interaction of the 5'ss oligonucleotide with the ACAGAG motif of U6 snRNA [Schneider *et al.*, 2010a], as opposed to U1 snRNP, for inducing stable integration of the U4/U6.U5 tri-snRNP within the 45S B-like complex.

4.2 B complex-specific proteins are recruited upon formation of the 45S B-like complex, but are not required for stable integration of the U4/U6.U5 tri-snRNP

To identify factors that potentially contribute to stable U4/U6.U5 tri-snRNP binding, we characterized abundant factors associated with affinity-purified 37S exon and 45S B-like complexes by 2D gel electrophoresis. These analyses allowed a direct comparison of their protein compositions with each other, as well as with previously characterized spliceosomal complexes of the intron-defined assembly pathway [Agafonov *et al.*, 2011]. The comparison of abundant factors in the 37S exon and 45S B-like complex revealed that proteins associated with the U1 snRNP and SR proteins are lost during the stabilization of U4/U6.U5 tri-snRNP binding and formation of a B-like complex. Further,

the formation of a 45S B-like complex was accompanied by the recruitment of the B complex-specific proteins RED, MFAP1, FBP21, hSmu-1, hPrp38 and hSnu23 to the complex. These proteins are also recruited first during formation of an intron-defined B complex [Agafonov *et al.*, 2011]. In general, the 45S B-like complex shows the same composition of abundant proteins as an intron-defined B complex, which was assembled on the MINX pre-mRNA [Agafonov *et al.*, 2011]. The 45S B-like complex contains additionally abundant amounts of the two proteins THRAP3 and BCLAF1.

The presence of the B complex-specific proteins in spliceosomal complexes with a stably-integrated U4/U6.U5 tri-snRNP, namely the 45S B-like and intron-defined B complex, suggested that these proteins could potentially be required for the stabilization of U4/U6.U5 tri-snRNP binding upon its interaction with a 5' splice site. To test whether the recruitment of the B complex-specific proteins is required for the increased stability of the complex, I subsequently assayed if the addition of the 5' ss oligonucleotide to the 37S exon complex in the absence of nuclear extract also results in stronger U4/U6.U5 tri-snRNP binding. Surprisingly, addition of the 5' ss oligonucleotide alone to affinity-purified 37S exon complexes induced the formation of a 45S complex with stably-integrated U4/U6.U5 tri-snRNP (Figure 3.4 & 3.5). Thus, all factors required for stable U4/U6.U5 tri-snRNP binding upon interaction with the 5' ss oligonucleotide are already present in the 37S exon complex. As the B complex-specific proteins are for the most part absent from the 37S exon complex, these results show that the B complex-specific proteins are not essential for stable binding of the U4/U6.U5 tri-snRNP *in vitro*.

The B complex-specific proteins were shown to be abundant in the intron-defined B complex, but are already displaced during the transition to a B^{act} complex [Agafonov *et al.*, 2011]. As it was shown that these proteins are not essential for transition to a 45S complex, this suggests a role for these proteins after B complex and prior to or during B^{act} complex formation. Consistent with this result, the Prp38 protein was shown not to be required for assembly of a B complex in yeast and has a proposed function in promoting U4/U6 unwinding [Xie *et al.*, 1998]. Yeast-2-hybrid experiments showed that certain B complex-specific proteins interact with factors of the U4/U6.U5 tri-snRNP, as well as with proteins of the hPrp19 complex [Hegele *et al.*, 2012]. Therefore, the B complex-specific proteins might be involved in the recruitment of factors that are necessary for B^{act} formation, e.g. as binding partners for the hPrp19 complex. But, while the B complex-specific proteins are conserved in *C. elegans* and *D. melanogaster*, only hSnu23 and hPrp38 have homologues in *S. cerevisiae*, which suggests a role of these proteins in spliceosome function restricted to higher eukaryotes, e. g. in alternative splicing. However, Prp38 and Snu23 are components of the U4/U6.U5 tri-snRNP in *S. cerevisiae* but not in human, and may therefore play a different role in yeast [Gottschalk *et al.*, 1999, Xie *et al.*, 1998].

4.3 Stable binding of the U4/U6.U5 tri-snRNP likely depends on the interactions with U2 snRNP proteins

The characterization of abundant factors in the 45S B-like complex showed that the complex is mainly composed of proteins associated with the U2 snRNP and U4/U6.U5 tri-snRNP and just a small number of additional factors. As we showed that the B complex-specific proteins are not essential to stabilize the interaction of the U4/U6.U5 tri-snRNP, its stable binding within the complex must depend on interactions with other factors that are also abundant in the 45S B-like complex. The 2D analysis of the protein inventory of the 45S B-like complex suggests that the stable association of the U4/U6.U5 tri-snRNP likely relies on proteins associated with the U2 snRNP, since these proteins are the only abundant ones present. Yeast-2-hybrid experiments identified interactions between U2-associated SF3b proteins and U5-specific proteins, especially hPrp8, hBrr2 and hSnu114, in the intron-defined B complex [Hegele *et al.*, 2012]. Therefore, interactions between these proteins likely play a role in stable binding of the U4/U6.U5 tri-snRNP. The interaction of the 5' splice site oligonucleotide with the U4/U6.U5 tri-snRNP, in particular hPrp8, may trigger the formation of new interactions, e.g. between U2 and U5 proteins, or stabilize existing ones.

The factor SPF30 was shown to be important for association of the U4/U6.U5 tri-snRNP with the A complex [Rappsilber *et al.*, 2001, Meister *et al.*, 2001], but neither the 37S exon nor the 45S B-like complex contain abundant amounts of this protein, showing that the stable integration of the U4/U6.U5 tri-snRNP does not depend on the presence of this factor. SPF30 could play a transient role in U4/U6.U5 tri-snRNP stabilization, but nevertheless its presence apparently is not required to maintain the stable binding of the U4/U6.U5 tri-snRNP. Further, previous studies suggested SR proteins to be important for integration of the U4/U6.U5 tri-snRNP and stable B complex formation [Rosigno and Garcia-Blanco, 1995]. However, the SR proteins SRSF1, SRSF7 and SRSF10, which are abundant in the 37S exon complex, are displaced upon formation of the 45S B-like complex and therefore do not contribute to the increased stability of U4/U6.U5 tri-snRNP binding in the 45S B-like complex. SR proteins have an important role in exon recognition and establish protein-protein interactions with the general splicing machinery, which is supported by the presence of SR proteins in the 37S exon complex. But upon commitment of the spliceosome to a 5' splice site, these interactions might be disrupted in order to establish new ones.

4.4 The hPrp4 kinase is abundant solely in the 37S exon complex

Interestingly, the hPrp4 kinase was shown to be abundant in the 37S exon but not in the 45S B-like complex. Previous studies showed that this protein is neither abundant in the intron-defined A complex nor in the B complex [Agafonov *et al.*, 2011]. This suggests that the hPrp4 kinase is stage-

specifically recruited upon association of the U4/U6.U5 tri-snRNP with the A-like complex during formation of the 37S exon complex. It was shown that the hPrp4 kinase phosphorylates the U4/U6.U5 tri-snRNP-associated factors hPrp31 and hPrp6 during formation of a stable, intron-defined B and 45S B-like complex [Schneider *et al.*, 2010a, b]. Although the hPrp4 kinase is present in the 37S complex, it does not phosphorylate its target proteins as seen by the very low phosphorylation levels of hPrp31 in the 37S exon complex (Figure 3.5). The addition of the 5' ss oligonucleotide to purified 37S exon complexes induces stable binding of the U4/U6.U5 tri-snRNP, but the phosphorylation of hPrp31 does not increase as compared to the level of its phosphorylation within the 37S exon complex. The fact that no additional ATP was required for stable U4/U6.U5 tri-snRNP integration and that the incubation with the 5' ss oligonucleotide was performed at 4 °C supports the idea that no enzymatic activity is required or involved in the stabilization process. These results show that the transition to a 45S complex is not dependent on the site-specific phosphorylation of hPrp31 and presumably also hPrp6. The phosphorylation of hPrp31 and hPrp6 observed in nuclear extract occurs after interaction of the 5' ss oligonucleotide with the 37S exon complex and consequently after transition to a 45S complex. Thus, the activation of hPrp4 kinase might even rely on the structural change accompanying 45S complex formation, i.e. a B complex structure, e.g. by inducing the accessibility of the phosphorylation sites or establishing new protein-protein interactions. However, this conformational rearrangement appears to induce changes in protein-protein interactions that result in the release of hPrp4 kinase upon transition to a 45S B-like complex.

4.5 The proteins THRAP3 and BCLAF1 are abundant in exon-defined spliceosomes

Notably, the proteins THRAP3 and BCLAF1 are abundant in the exon-defined 37S exon and 45S B-like complexes, but not in the intron-defined B complex, which was assembled on the MINX pre-mRNA. The MINX exon-RNA construct was derived from the MINX pre-mRNA and contains very few nucleotides not found in the MINX pre-mRNA sequence. Therefore, a sequence-specific recruitment of BCLAF1 and THRAP3 appears unlikely and the recruitment of these factors would favor a model in which both proteins are associated in the exon-defined complexes due to the presence of a downstream located 5' ss or the formation of an exon-defined spliceosomal complex. THRAP3 and BCLAF1 have a function in the subcellular distribution and stability of mRNAs in human cells and interact with components of the EJC [Varia *et al.*, 2013]. Further, THRAP3 was shown to activate pre-mRNA splicing *in vivo* and an interaction with ongoing transcription and early stages of splicing was proposed [Lee *et al.*, 2010]. Thus, these proteins might play a role in formation of exon-defined spliceosomes on nascent pre-mRNAs, but their function remains unclear.

4.6 The 37S exon complex undergoes a major structural change upon interaction with the 5'ss oligonucleotide and adopts the appearance of a cross-intron B complex

To determine whether addition of the 5'ss oligonucleotide changes the morphology of the 37S exon complex as suggested by the increase in its S-value, we investigated the structures of the 37S exon and 45S B-like complexes via electron microscopy. Class averages generated from single-particle images revealed that the 37S exon complex exhibits an elongated structure, in which the body domain appears similar in all classes, whereas the head domain shows a high degree of flexibility (Figure 4.1A). In contrast, the 45S B-like complex appears more compact, consistent with a change in its sedimentation behavior. Moreover the 45S B-like complex exhibits a predominant structure in the vast majority of all classes, in which the head and body domain of the complex are almost in the same orientation with respect to each other. The comparison of the class averages generated for the 37S exon and 45S B-like complexes provides evidence that the stable integration of the U4/U6.U5 tri-snRNP during 45S B-like formation is accompanied by a major rearrangement in the structure of the complex. Strikingly, the 45S B-like complex has an almost identical morphology as the intron-defined B complex, indicating that in B and B-like complexes similar interactions may occur. This assumption is supported by the fact that these two complexes share almost the same set of abundant factors as judged by mass spectrometry and 2D gel-electrophoresis. Previous studies used immunolabeling in combination with negative-stain EM to determine the localization of the pre-mRNA and the U2 snRNP-associated protein SF3b155. In this way, the U2 snRNP could be mapped to the head domain of an intron-defined B complex [Wolf *et al.*, 2009] (Figure 4.1B). A similar approach with B complexes of *S. cerevisiae* indicated that U5-associated proteins are located in the body domain, while the neck domain is mainly composed of U4/U6 di-snRNP-specific proteins (personal communication Dr. Norbert Rigo and Dr. Berthold Kastner). A comparison of the EM structures of the 37S exon complex with the 45S B-like complex suggests that the position of the head domain relative to the body is the main structural difference between these complexes. Thus, the conformational change triggered by the interaction with the 5'ss oligonucleotide, probably involves a rearrangement of the U4/U6.U5 tri-snRNP (body) with respect to the pre-mRNA bound U2 snRNP (head), leading then to the stable integration of the U4/U6.U5 tri-snRNP within the complex.

Structure probing of 37S exon and 45S B-like complexes showed no significant changes in the snRNA structures aside from the accessibility of the ACAGAG box of U6 snRNA [Schneider *et al.*, 2010a], which is apparently necessary to induce the structural change upon interaction of the 5'ss oligonucleotide with the 37S exon complex. Importantly, in the 37S exon complex the U4/U6.U5 tri-snRNP establishes base pairing interaction only with the U2 snRNA, via U2/U6 helix II, and does not

directly interact with the pre-mRNA, at least not by RNA-RNA interactions [Schneider *et al.*, 2010a]. Thus, the interaction of the 5'ss oligonucleotide probably enables the transition to a more favorable orientation between U2 snRNP and the U4/U6.U5 tri-snRNP based on changes in protein-protein interactions. Previous studies showed that the addition of a 5'ss oligonucleotide to HeLa extract results in formation of a U2/U4/U6/U5 tetra-snRNP [Konforti and Konarska, 1994] suggesting that the interaction of a 5'ss oligonucleotide with the U4/U6.U5 tri-snRNP induces or stabilizes interactions between U2 snRNP and the U4/U6.U5 tri-snRNP already in the absence of a pre-mRNA. Since the formation of the 45S B-like complex is accompanied by the recruitment of stoichiometric amounts of the B complex-specific proteins, we also tested if these proteins have a potential role in the structural change occurring during stable association of the U4/U6.U5 tri-snRNP with the complex.

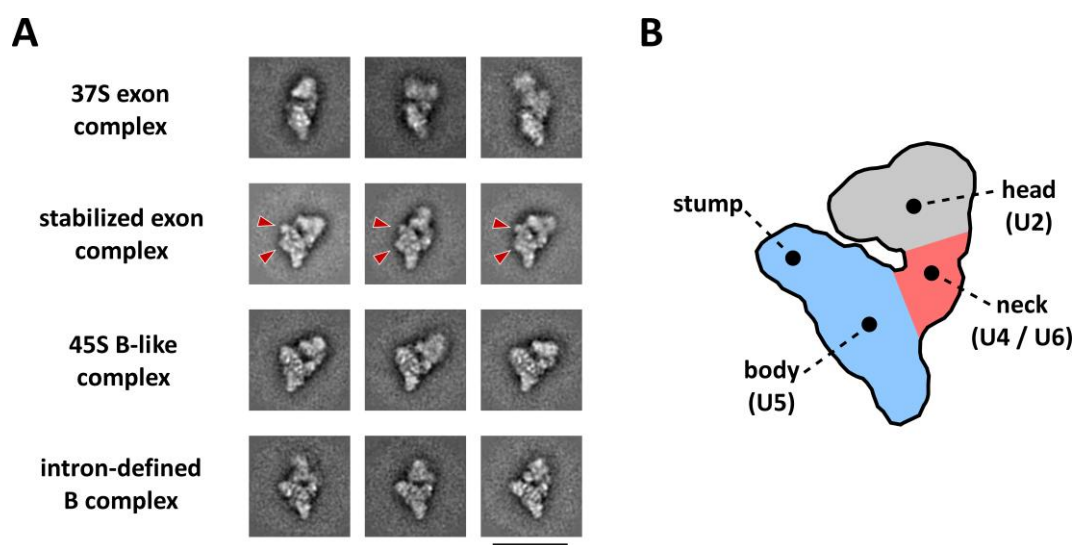


Figure 4.1: Comparison of class averages generated from exon-defined spliceosomes

(A) The most abundant structures of the indicated complex are shown. Characteristic structural features within the body domain of the stabilized exon complex are indicated with red arrows. Scale bars correspond to 50 nm. (B) Schematic representation of an intron-defined B complex and localization of snRNPs within the structure as determined by immunolabeling with subsequent negative-stain EM.

We could show that solely the addition of the 5'ss oligonucleotide to affinity-purified 37S exon complexes not only induced the stable integration of the U4/U6.U5 tri-snRNP, but also resulted in an increase in its S-value (Figure 3.4 and 3.5). The increased S-value indicates a remodeling in the complex during the stabilization process, similar to what was seen with the 45S B-like complex in the presence of nuclear extract. EM analyses of this stabilized exon complex revealed structural features highly similar to those observed with the 45S B-like complex formed in nuclear extract (Figure 4.1A). Further, the stabilized exon complex shows a predominant structure in the majority of all classes, which is also a characteristic feature of the 45S B-like complex, but not the 37S exon complex.

These results demonstrate that binding of the 5'ss oligonucleotide alone triggers a conformational change in the structural organization of the exon complex, which potentially leads to stable integration of the U4/U6.U5 tri-snRNP. This provides strong evidence that the significant conformational rearrangement of the complex is independent of protein factors not already found in the 37S exon complex and occurs even in the absence of additional ATP (see chapter 3.4). The data presented here indicate that the conformational changes observed upon binding of the 5'ss oligonucleotide occur prior to the recruitment of the B complex-specific proteins and might even be a prerequisite for their interaction with the spliceosomal complexes. This suggests that these proteins are recruited to the spliceosome after it adopts a structure characteristic for a B complex.

But despite the structural similarities of the stabilized exon complex and the 45S B-like complex formed in nuclear extract, we identified differences in the morphologies of their body domains. The body domain of the stabilized exon complex contains an additional belly-like protrusion and exhibits a slimmer stump (Figure 4.1A, indicated with red arrows), whereas the body of the 45S B-like complex appears broader and lacks this additional protrusion. Since the differential appearance of the body domain is observed in the majority of all classes, we assume that the U4/U6.U5 tri-snRNP containing part of the complex might have a slightly different orientation with respect to the head domain, which appears similar to the 45S B-like complex formed in nuclear extract. Alternatively, this difference might be due to the absence of the B complex-specific proteins in the stabilized exon complex. However, whether these proteins contribute directly to the mass of the body domain or alternatively whether the lack of these proteins alters the orientation of the body domain is presently unclear.

4.7 Sequence requirements for the 5'splice site to induce stable U4/U6.U5 tri-snRNP binding

The drastic changes in composition, structure and stability, which occur during formation of a 45S B-like complex, are solely induced by addition of the 5'ss oligonucleotide to the splicing reaction. To better understand the mechanism underlying this transition, I assessed the 5'ss oligonucleotide sequence requirements for transforming the 37S exon complex into a stable 45S B-like complex, by monitoring the effect of different mutations within the 5'ss oligonucleotide on the stabilization of U4/U6.U5 tri-snRNP binding and formation of a 45S complex. Nucleotides in the exonic part of the 5'ss oligonucleotide can base pair with loop I of U5 snRNA and intronic nucleotides with the ACAGAG box of U6 as evidenced by psoralen crosslinking [Sontheimer and Steitz, 1993]. Additionally, a highly-specific crosslink of the 5'ss at position +2 to the RNase H domain of hPrp8 was identified, which coincides with B complex formation [Reyes *et al.*, 1996, Reyes *et al.*, 1999]. Further, there is evidence

that hPrp8 not only contacts intronic nucleotides of a 5'ss, but also makes contacts with nucleotides in the 5'exon [Sha *et al.*, 1998]. Consistent with this result, site-specific protein-RNA crosslinking in stably-assembled 45S B-like complexes showed that the 5'ss oligonucleotide is directly contacted by hPrp8, at the G/GU nucleotides defining the exon-intron junction (see chapter 3.6). Consequently, I introduced mutations in the 5'ss oligonucleotide sequence to potentially disrupt its interaction with the U5 or U6 snRNAs, or with hPrp8.

When the potential for Watson-Crick base pairing between loop I of U5 snRNA and the 5'ss oligonucleotide was disrupted, the formation of B-like complexes in the presence of heparin was reduced. Similar results were achieved when mutations were introduced that disrupt base pairing with the ACAGAG box of U6 snRNA. However, no inhibitory effect of these mutations was detected when the transition to a 45S complex was assayed by glycerol gradient centrifugation. As no effect on the formation of a 45S complex was observed, we conclude that the interaction of the 5'ss oligonucleotide with either loop I of U5 snRNA or the ACAGAG box of U6 is not required to induce the structural change in the complex. Apparently, introduction of mutations within the 5'ss oligonucleotide influences the U4/U6.U5 tri-snRNP interaction such that it is sensitive to the presence of heparin, but the structural change as indicated by the increased S-value still occurs as assayed by the less stringent glycerol gradient analysis. Thus, the conformational change of the complex to a 45S complex does not necessarily translate into an increased heparin resistance. Further, western blot analysis showed that the apparent difference in complex stability is independent of hPrp31 phosphorylation and recruitment of the B complex-specific proteins (Figure 3.11). I could show that all 5'ss oligonucleotides that induce the transition to a 45S complex were also co-purified with the respective complex suggesting that the interaction between the 5'ss oligonucleotide and the U4/U6.U5 tri-snRNP must be maintained in order to stabilize the complex and also to support the conformational change to a 45S complex.

However, if both base pairing interactions between the 5'ss oligonucleotide and the U5 and U6 snRNAs were disrupted simultaneously, B-like formation was abolished in the presence (native gels) and absence (glycerol gradient) of heparin. These results show that individual disruption of either U5/5'ss or U6/5'ss base pairing has a moderate effect on B-like formation, but the disruption of both interactions abolishes the stable integration of the U4/U6.U5 tri-snRNP. The former result is consistent with previous results showing that the loop I of U5 snRNA is not essential for efficient pre-mRNA splicing in HeLa nuclear extract [Segault *et al.*, 1999]. The base pairing interactions between the U5 and U6 snRNA, and the 5'ss oligonucleotide, thus appear to be redundant and might functionally substitute for each other during formation of a stable B-like complex.

Next, I assayed the effect of single point mutations in the G/GU triplet, which defines the exon-intron junction and is directly contacted by hPrp8. While mutations of -1G → A and +2U → A had no effect on B-like formation, the G → A transition at position +1 reduced stable U4/U6.U5 tri-snRNP binding in the presence of heparin significantly. Nevertheless, glycerol gradient and western blot analysis showed an efficient transition to a 45S complex and the recruitment of the B complex-specific proteins as well as phosphorylation of hPrp31. This underlines that the structural change and recruitment of B complex-specific proteins does not always translate into resistance against heparin. Thus, suboptimal 5' splice site sequences are also competent for the formation of a B-like complex, but the interaction with hPrp8 might be less stable and therefore lead to destabilization of the complex in the presence of heparin. However, in all cases tested here, a structural rearrangement, i.e. 45S complex formation, appears to be a prerequisite for heparin stability and also the resistance against increased salt concentrations during glycerol gradient centrifugation.

The mutation of two neighboring nucleotides within the exon-intron junction abolished the potential for formation of a B-like complex completely. Copurification studies showed that upon mutation of GU → AA, as well as GG → AA (or rlrI), the 5' splice site oligonucleotide not only loses the potential to induce 45S B-like complex formation, but also its physical interaction with the 37S exon complex is abolished. The fact that the most severe impairment of B-like formation was observed upon mutations within the exon-intron junction, which should not contribute to base pairing with U5 or U6 snRNA, provides evidence that not only RNA-RNA interactions between the 5' splice site oligonucleotide and the snRNAs are necessary for the physical association of the 5' splice site with the complex, but also additional protein-RNA interactions are required for stable binding of the 5' splice site oligonucleotide. This points to a crucial role for the hPrp8:5' splice site interaction in stable binding of the 5' splice site and further in discrimination between suitable and aberrant 5' splice site sequences. The data presented here suggest that recognition of a suitable 5' splice site sequence by hPrp8 triggers the structural rearrangement that leads then to stable integration of the U4/U6.U5 tri-snRNP and consequently to B-like complex formation.

Apparently, the recognition of a suitable 5' splice site substrate by hPrp8 involves also the exocyclic part of the GG dinucleotide at the exon-intron junction, because mutation to ribo-inosine nucleotides inhibit B-like complex formation (Table 3.2). This points to a very specific and functionally important recognition of guanosine nucleotides at the exon-intron junction. Additionally, binding of the 5' splice site oligonucleotide within in the complex and consequently the transition to a 45S complex also involves the recognition of the ribose backbone, as judged by the fact that 2'-O-ribose methylation of the RNA oligonucleotide abolishes the formation of a B-like complex. This is in line with previous results, which showed that especially modifications of the ribose backbone at position -2 to +3 of a 5' splice site oligonucleotide have a strong impact on spliceosome formation [Sha *et al.*, 1998]. Therefore, the

physical association of the 5'ss oligonucleotide with the 37S exon complex does not only depend on a specific interaction of hPrp8 with guanosine nucleotides at the exon-intron boundary, but also involves the recognition of the ribose-backbone of the RNA strand. In summary, base pairing with the U6 ACAGAG box is not required to trigger the observed structural rearrangement during transition to a 45S B-like complex, but instead the latter likely requires a highly specific interaction of the U5 snRNP protein hPrp8 with the exon-intron junction. These results were observed during exon-defined formation of a 45S B-like complex. But given the compositional, structural and functional similarities between the B-like and the intron-defined B complex, they likely also hold true for the formation of an intron-defined B complex. Although the 5'ss oligonucleotide represents a 5'splice site *in trans*, one can extrapolate to the situation with a 5'splice site *in cis*, i.e. the 5'ss present in the MINX pre-mRNA. Thus, the observed sequence requirements for the 5'ss sequence probably also hold true for the stable formation of an intron-defined B complex.

4.8 Structural implications for the stabilizing effect of a 5'ss sequence on stable U4/U6.U5 tri-snRNP binding

Structural investigations of the RNase H domain of Prp8 showed that it adopts an RNase H fold even in absence of a substrate [Pena *et al.*, 2008, Ritchie *et al.*, 2008, Schellenberg *et al.*, 2013]. In previous studies it was shown that residues 1894-1898 of the RNase H domain of hPrp8 crosslink with the +2 position of a 5'ss in stably-assembled B complexes [Reyes *et al.*, 1996, Reyes *et al.*, 1999]. By superimposing the hPrp8 crystal structure with an RNA oligonucleotide mimicking a 5'ss sequence, it was shown that the 5'ss fits in a positively-charged cleft of the hPrp8 structure, which would favor interaction with the negatively-charged sugar-phosphate backbone of the RNA [Pena *et al.*, 2008]. During this superimposition the conserved GU dinucleotide at position +1 and +2 of the 5'ss is located directly next to the five amino acid peptide, which was cross-linked in stably-assembled B complexes [Reyes *et al.*, 1999]. We detected crosslinks between the nucleotides -1 to +2 of the 5'ss oligonucleotide and hPrp8 in stably-assembled 45S B-like complex and it is likely that the crosslink is also located in the RNase H domain of hPrp8 (Figure 3.7).

Recently it was shown that the RNase H domain of Prp8 can adopt alternatively an open and a closed conformation [Schellenberg *et al.*, 2013]. In the closed conformation a two-stranded antiparallel β -hairpin (thumb) is formed, whereas in the open conformation this hairpin is disrupted. This thumb is in direct proximity of the positively-charged cleft, which is proposed to interact with the ribose backbone of the 5'ss RNA strand, and in the closed state the thumb is ideally positioned to interact with bound RNA [Pena *et al.*, 2008]. Structural investigation of a C-terminal part of Prp8 comprising not only the RNase H domain but also the reverse transcriptase (RT) and endonuclease (En) domain

of Prp8 revealed considerable interdomain movements of the RNase H domain with respect to the RT and En domains [Galej *et al.*, 2013]. It was proposed that the alternative positions of the RNase H domain may transmit conformational changes of the RNA network after each transesterification reaction. These studies show that the RNase H domain can adopt alternative conformations and that these changes may also influence the interactions with other domains of hPrp8.

During the structural investigation of the 37S exon complex by negative-stain EM we could show that solely the presence of a 5' ss oligonucleotide induces a significant change in the organization of the complex (Figure 3.6). Further, we provided evidence that the stable binding of the 5' ss oligonucleotide within the spliceosome likely requires interactions with hPrp8 (see chapter 3.6). The binding of the 5' ss oligonucleotide by hPrp8 might induce a conformational change in the RNase H domain of hPrp8 and also in other domains of this protein. These rearrangements in the hPrp8 protein might subsequently induce changes in protein-protein interactions between proteins of the U4/U6.U5 tri-snRNP and the U2 snRNP, and as a consequence, result in the structural transition to a complex with stably bound U4/U6.U5 tri-snRNP. This mode of action could also explain the difference in complex stability regarding heparin and glycerol gradients. It is known that in the presence of heparin less stable protein-RNA interactions are disrupted. Thus, heparin might interfere with the interaction between the 5' ss oligonucleotide and the RNase H domain of hPrp8 when the former is mutated to a less optimal sequence. As soon as the hPrp8:5' ss interaction is disrupted, the stabilizing effect on the U4/U6.U5 tri-snRNP binding is reversed or abolished.

4.9 A dominant-negative mutant of the DEAD-box helicase hPrp28 inhibits stable B complex formation

Next I investigated the requirements for stable B complex formation in the intron-defined assembly pathway. To learn more about factors contributing to stable B complex formation, I set out to isolate splicing complexes formed after the A complex but prior to a stable B complex. In *S. cerevisiae* the DEAD-box helicase Prp28 is necessary for B complex formation, and it was shown to destabilize the U1:5' ss interaction [Staley and Guthrie, 1999]. The ATP-dependent activity of Prp28 is required for dissociation of U1 snRNP from the 5' ss of the pre-mRNA, but there are indications that the U4/U6.U5 tri-snRNP can associate with the spliceosome prior to the action of Prp28 [Staley and Guthrie, 1999]. The U5-specific protein hPrp28 is the human homolog of Prp28 and is an integral component of the U5 snRNP and U4/U6.U5 tri-snRNP [Teigelkamp *et al.*, 1997]. The integration of hPrp28 within the U4/U6.U5 tri-snRNP depends on its phosphorylation by SRPK2 and only a U4/U6.U5 tri-snRNP containing hPrp28 is competent for productive B complex formation [Mathew *et al.*, 2008]. Based on these previous observations in *S. cerevisiae* and human, I chose hPrp28 as a target for my

investigations. As it was shown that Prp28 and ATP are required for B complex formation, I used an ATPase-deficient version of hPrp28, in which the DEAD motif was mutated to AAAD (hPrp28^{AAAD}). *In vitro* splicing assays and native gel analysis showed that hPrp28^{AAAD} is a dominant-negative inhibitor of splicing that stalls intron-defined spliceosome assembly after A but prior to stable B complex formation.

4.10 Identification of a novel cross-intron assembly intermediate that is formed prior to hPrp28 action

Analysis of spliceosome assembly on glycerol gradients revealed that in the presence of the dominant-negative mutant hPrp28^{AAAD}, a 37S cross-intron complex is formed that contains stoichiometric amounts of all five snRNAs (Figure 3.14). These results show that association of the U4/U6.U5 tri-snRNP occurs prior to the action of hPrp28, but it is not yet stably-integrated in the complex as judged by native gel-electrophoresis in the presence of heparin (Figure 3.13). This complex thus represents a novel intermediate stage of spliceosome assembly, which is formed after U4/U6.U5 tri-snRNP recruitment, but prior to its stable integration within the spliceosome. Thus, initial association of the U4/U6.U5 tri-snRNP does not require the removal of the U1 snRNA from the 5'ss. Further, the presence of stoichiometric amounts of U1 snRNA in the 37S cross-intron complex is consistent with a function of hPrp28 in destabilizing the interaction between U1 snRNP and the 5'splice site of the pre-mRNA, since the U1 snRNA is significantly underrepresented in stably-assembled B complexes. These results are consistent with the known function of Prp28 in *S. cerevisiae*. In summary, these data indicate that in the absence of hPrp28 action, U1 snRNP remains base paired to the 5'ss, which was additionally supported by the detection of a prominent crosslink between U1 snRNA and the pre-mRNA in the 37S cross-intron complex (Figure 3.16). In the B complex the U1 snRNA is no longer base paired with the pre-mRNA and we detected additional RNA-RNA interactions between the U4/U6.U5 tri-snRNP and the pre-mRNA. Thus, in the 37S cross-intron complex the 5'ss sequence is not available for interaction with the U4/U6.U5 tri-snRNP and consequently the transition to a pre-catalytic B complex is inhibited.

Characterization of the protein composition of the 37S cross-intron complex revealed the presence of all U1, U2 and U4/U6.U5 tri-snRNP proteins. However, unlike the cross-intron B complex, the 37S cross-intron complex contains only very low levels of the B complex-specific proteins RED, MFAP1, FBP21, hSmu-1, hPrp38 and hSnu23. Further, proteins associated or related to the hPrp19 complex, as well as factors of the RES complex were also significantly underrepresented in the 37S cross-intron complex, consistent with the idea that these subcomplexes are recruited first upon/after stable B complex formation. The mass spectrometric analysis confirmed that hPrp28 is still

incorporated in the 37S cross-intron complex, i.e. the defect in splicing is not due to absence of hPrp28, but lack of its activity. Interestingly, the protein composition of the 37S cross-intron complex is astonishingly similar to that of the 37S exon complex, which was previously investigated by mass spectrometry under comparable conditions [Schneider *et al.*, 2010a]. Based on the same snRNA composition and the very similar protein compositions of these 37S complexes, they appear to resemble similar spliceosome assembly intermediates. Consequently, we determined abundant factors associated with the 37S cross-intron complex via 2D gel-electrophoresis and compared them directly with the protein composition of the 37S exon complex. The comparison of their compositions on a semi-quantitative level showed also a very similar inventory of abundant proteins. Interestingly, the hPrp4 kinase is also abundant in the 37S cross-intron complex, which supports the idea that this kinase is stage-specifically recruited to the spliceosome after/upon association of the U4/U6.U5 tri-snRNP, but prior to its stable integration (see chapter 4.4). Only the THRAP3 protein was absent, and BCLAF1 significantly underrepresented, in the 37S cross-intron complex, while being abundant in the 37S exon complex. These factors are also abundant in the exon-defined 45S B-like complex, but they are absent or underrepresented in B complexes assembled across an intron (see 4.5), supporting the idea that THRAP3 and BCLAF1 might have a role solely in the assembly of exon-defined spliceosomes. In contrast, the 37S cross-intron complex contains abundant amounts of the cap-binding protein CBP80, whereas the 37S exon complex shows only low amounts of this protein. This is likely due to the fact that the MINX pre-mRNA, which was used to assemble intron-defined spliceosomes, contains a 5'cap, while the MINX exon-RNA does not contain a 5'cap.

4.11 The 37S cross-intron complex can be converted into a stable B complex via addition of a 5'ss oligonucleotide

The 37S cross-intron complex represents an intermediate stage of spliceosomal assembly, which is formed after initial A complex assembly and prior to stable pre-catalytic B complex formation. Our data suggest that due to the retention of U1 snRNP at the 5'ss of the pre-mRNA, this sequence is not available for interaction with the U4/U6.U5 tri-snRNP and thus the transition to a pre-catalytic B complex is inhibited. At this point, it was not clear whether the 37S cross-intron complex resembles a functional intermediate of intron-defined spliceosome assembly or whether it is a dead-end product that is not competent to proceed to subsequent steps of splicing. Therefore, I tested whether the 37S cross-intron complex could be chased into a stable B complex via addition of an accessible 5'splice site *in trans*, in form of an oligonucleotide. Indeed, the addition of a 5'ss oligonucleotide to a splicing reaction containing inhibitory concentrations of hPrp28^{AAAD} resulted in formation of a heparin-resistant B complex as assayed by native gel analysis (Figure 3.18). This shows that the 37S cross-intron complex can be chased to the next functional intermediate of spliceosome

assembly. However, as the stabilization was tested in total nuclear extract, I next tested whether the stabilization of the complex also occurs under more defined conditions, namely if an affinity-purified 37S cross-intron complex is also competent for stable U4/U6.U5 tri-snRNP binding, as shown for the 37S exon complex (Figure 3.4). The addition of the 5'ss oligonucleotide to affinity-purified 37S cross-intron complexes led to the formation of a complex with stably associated U4/U6.U5 tri-snRNP, as evidenced by the shift in its migration behavior on glycerol gradients containing 150 mM KCl, which are restrictive conditions for loosely-associated U4/U6.U5 tri-snRNPs (Figure 3.19). A second affinity-selection followed by analysis of the RNA composition verified that this stabilized cross-intron complex contains stoichiometric amounts of the U4, U5 and U6 snRNA, and thus the U4/U6.U5 tri-snRNP. Therefore, addition of solely a 5'ss oligonucleotide to the 37S cross-intron complex increases dramatically the stability of the complex, in particular the binding of the U4/U6.U5 tri-snRNP, even in the absence of hPrp28 action. These results show that the 37S cross-intron complex is competent for B complex formation, despite the absence of hPrp28 activity, and contains all factors required for stable U4/U6.U5 tri-snRNP binding. This is consistent with the idea that the 37S complexes with loosely-associated U4/U6.U5 tri-snRNP represent a very similar intermediate in both exon-defined and intron-defined spliceosome assembly pathways and that stable integration of the U4/U6.U5 tri-snRNP is triggered solely by its interaction with the 5'ss. In summary, hPrp28 ATPase activity is not required for initial binding of the U4/U6.U5 tri-snRNP, but action of hPrp28 destabilizes the U1:5'ss interaction, which makes the 5'ss accessible for interaction with the U4/U6.U5 tri-snRNP. Further, we conclude that the B complex-specific proteins are not essential for the stable integration of the U4/U6.U5 tri-snRNP within the 37S exon complex (3.4) or formation of an intron-defined B complex (Figure 3.19).

4.12 The 37S cross-intron and 37S exon complex adopt an almost identical appearance upon interaction with a 5'ss oligonucleotide

Based on the identical snRNA and a very similar protein composition of the 37S cross-intron and 37S exon complex, we investigated the EM structure of the 37S cross-intron complex to see if the almost identical compositions of the complexes also result in a similar appearance. Surprisingly, EM analysis of the 37S cross-intron complex revealed that despite the similarities in their compositions, the structures of the 37S cross-intron and 37S exon complex differ quite significantly (Figure 4.2B). The 37S cross-intron complex exhibit areas of structural heterogeneity in its body domain, whereas the 37S exon complex showed the most structural heterogeneity in its head domain. The differences in the appearance of these complexes might be due to the different localization of the 5'ss-bound U1 snRNP, which is upstream of the BPS in the 37S cross-intron and downstream of the BPS in the 37S exon complex (Figure 4.2A), with respect to the U2-associated U4/U6.U5 tri-snRNP. Additionally,

the presence of the cap binding complex, i.e. CBP80 and CBP20, might influence the structure of the 37S cross-intron complex, since it was shown that the cap binding complex interacts with proteins of the U4/U6.U5 tri-snRNP [Pabis *et al.*, 2013]. These additional protein-protein interactions may alter the relative orientation of the U4/U6.U5 tri-snRNP within the complex or its absorption behavior on the EM grid and result thereby in a different appearance in comparison to the 37S exon complex, which lacks this 5' cap.

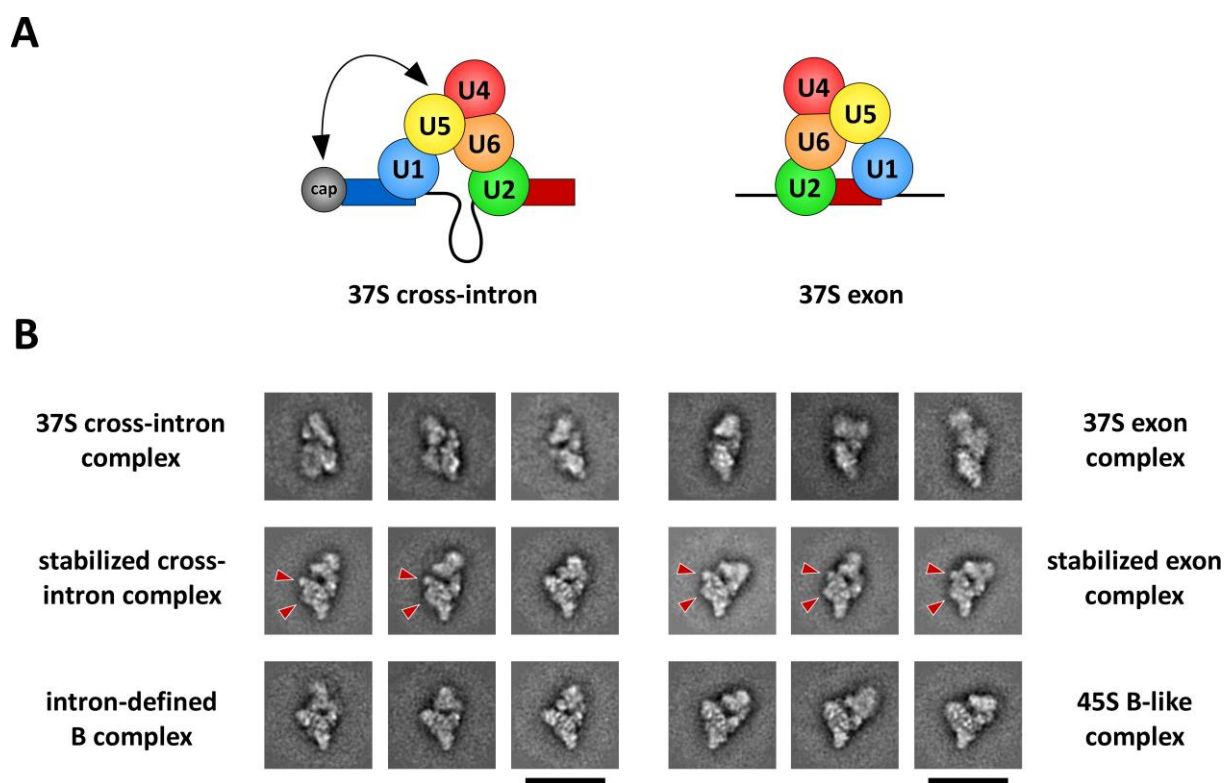


Figure 4.2: Comparison of class averages generated from exon- and intron-defined spliceosomes

(A) Schematic representation of the relative orientation of snRNPs in the 37S cross-intron and 37S exon complex. The arrow indicates interaction between the cap binding complex bound to the 5' cap and the U4/U6.U5 tri-snRNP. (B) The most abundant structures of the indicated complex are shown. Characteristic structural features within the body domain of the stabilized cross-intron and exon complex are indicated with red arrows. Scale bars correspond to 50 nm.

Finally, we investigated the structure of the affinity-purified 37S cross-intron complex after addition of the 5' ss oligonucleotide, since this stabilized cross-intron complex showed an increased S-value presumably due to a change in its structure. The EM analysis revealed that the addition of a 5' ss oligonucleotide induces a significant change in the structure of the 37S cross-intron complex and rearranges its organization in such a way that it adopts an organization more characteristic for a stably-assembled B complex. Astonishingly, the stabilized cross-intron complex appears very similar to the 37S exon complex after addition of the 5' ss oligonucleotide (see Figure 4.2B). Especially the

body domain of both 37S complexes share structural features, namely the belly-like protrusion in the center of the body and the slimmer stump (Figure 4.2B, indicated with red arrows), after addition of the 5'ss oligonucleotide to the purified complexes. Based on the comparison of RNA and protein compositions, we suggest that the 37S cross-intron and 37S exon complex might resemble similar assembly intermediates of spliceosome formation. Upon interaction with the 5'ss oligonucleotide also their structure and presumably the organization of U2 snRNP with respect to the U4/U6.U5 tri-snRNP is rearranged in such a way that these complexes adopt a very similar appearance. Taken together, these results are consistent with the idea that the 37S complexes with loosely-associated U4/U6.U5 tri-snRNP represent a very similar intermediate in both exon- and intron-defined spliceosome assembly pathways. Further, our data suggest that these alternative assembly pathways converge at the stage where the spliceosome is committed to using a particular 5'ss sequence via its interaction with the U4/U6.U5 tri-snRNP.

4.13 Changes in the RNA-RNA network during spliceosome assembly prior to the first catalytic step

The characterization of the RNA-RNA interactions within the 37S cross-intron complex extend our understanding of rearrangements within the RNA network during formation of a catalytically activated spliceosome and how helicases are involved in this process (Figure 4.3). In the A complex U1 snRNP is base paired with the 5'ss of the pre-mRNA (blue), whereas the U2 snRNP interacts with the branch point sequence (turquoise). Then the pre-assembled U4/U6.U5 tri-snRNP associates via U2/U6 helix II (purple) to the A complex resulting in formation of the 37S cross-intron complex. At this stage the U4/U6.U5 tri-snRNP is only loosely-associated with the complex and U1 snRNP is still occupying the 5'ss sequence. The results provided in this study suggest that the action of hPrp28 leads then to a destabilization of the U1 snRNP:5'ss interaction resulting finally in the displacement of U1 snRNP from the complex, which is consistent with the function of its ortholog in yeast [Staley and Guthrie, 1999]. This enables an interaction of the U4/U6.U5 tri-snRNP with the now accessible 5'ss, probably via a highly-specific recognition by hPrp8, resulting in the stronger binding of the U4/U6.U5 tri-snRNP and formation of a stable B complex. Base pairing interactions between the 5'ss and the ACAGAG box of U6 snRNAs (orange) might be necessary to stabilize the transition during exchange of U1:5'ss to hPrp8:5'ss interaction (see chapter 4.7). Thus, in a stably-assembled B complex U1 snRNA is not base paired with the pre-mRNA anymore, while new RNA-RNA interactions between the 5'ss and the U6 snRNA are established. Importantly, the U4 and U6 snRNAs are still base paired within in the pre-catalytic B complex to keep the U6 snRNA in an inactive state [Brow and Guthrie, 1998]. These results show that the displacement of U1 and U4 snRNA occur sequentially with distinct intermediates, and not in a coordinated fashion. Upon catalytic activation

of the spliceosome the action of the U5-protein hBrr2 leads to disruption of the U4/U6 base pairing and extensive interactions between U2 and U6 snRNA are established resulting in formation of U2/U6 helix Ia and Ib (red) as well as the U6 internal-stem loop (green) [Yean *et al.*, 2000, Anokhina *et al.*, 2013].

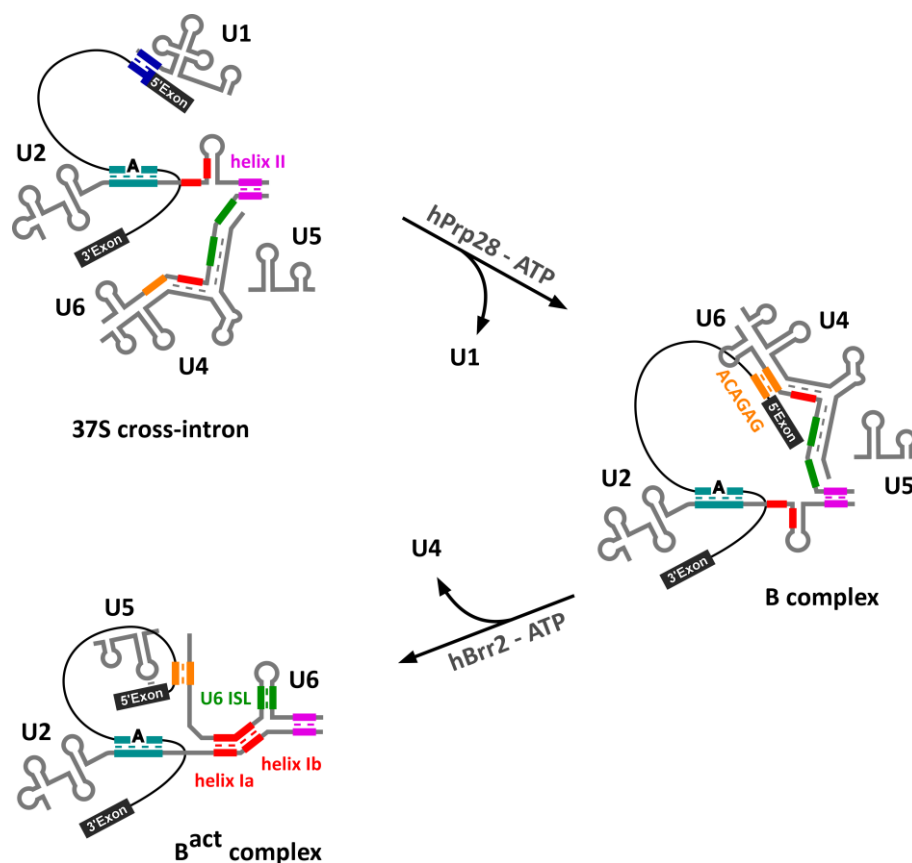


Figure 4.3: Changes in the RNA-RNA network during stable integration of the U4/U6.U5 tri-snRNP within the spliceosome and its activation.

4.14 The role of hPrp28 in formation of a stable B complex

The results of my studies show that the 37S cross-intron complex already contains all factors that are required for stable binding of the U4/U6.U5 tri-snRNP even in absence of the ATPase-activity of hPrp28 and only depend on an interaction with a 5'ss sequence (Figure 3.19). This points to a role of hPrp28 in generating an accessible 5'ss, rather than stable U4/U6.U5 tri-snRNP binding per se. Interestingly, the addition of the 2'O-ribose methylated 5'ss oligonucleotide to the splicing reaction, which contains inhibitory amounts of hPrp28^{AAAD}, does not support B complex formation (Figure 3.18), even though it displaces U1 snRNP from the 5'ss of the pre-mRNA (Figure 3.1, 3.19 and data not shown). We could show that this oligonucleotide only interacts with the U1 snRNP, but does not support the stabilization of U4/U6.U5 tri-snRNP binding nor interacts with the ACAGAG box of

U6 snRNA (Table 3.2). Thus, addition of the 2'-O-ribose methylated 5'ss oligonucleotide displaces U1 snRNP from the 5'ss of the MINX pre-mRNA and thus creates an accessible 5'ss, which is competent to induce stable integration of the U4/U6.U5 tri-snRNP. But apparently, additional interactions are necessary to facilitate an interaction between the U4/U6.U5 tri-snRNP and the accessible 5'ss that is present *in cis*, i.e. in the pre-mRNA, since the 37S cross-intron complex is not stabilized. In contrast, the stabilization of the 37S cross-intron complex upon addition of an unmodified 5'ss oligonucleotide *in trans* is likely due to the fact that a 100-fold excess of the 5'ss oligonucleotide is added to the purified complexes. Previous studies provide evidence that hPrp28 might not only displaces U1 snRNP from the 5'ss but also have a role in mediating the interaction between the 5'ss and the U4/U6.U5 tri-snRNP during stable B complex formation. Site-specific crosslinking studies showed that upon B complex formation the ATP-binding site of hPrp28 is in close proximity to the 5'ss, just a few nucleotides downstream of the exon-intron junction [Ismaili *et al.*, 2001], which is contacted by hPrp8. Further, it was shown that not only the presence of ATP is required for hPrp28 interaction with the 5'ss, but rather its hydrolysis, as no crosslink was detected in presence of a non-hydrolysable ATP-analog [Ismaili *et al.*, 2001]. The hPrp28:5'ss crosslink correlates with an interaction of the 5'ss with the U6 snRNA at the same intron position, which suggest that interaction between the 5'ss and hPrp28, as well as U6 snRNA, are established in the same complex upon hydrolysis of ATP [Ismaili *et al.*, 2001]. This suggests that the hPrp28 driven displacement of U1 snRNP from the 5'ss of a pre-mRNA generates a close proximity of the U6 snRNA and hPrp8 to the 5'ss. It is likely that at this stage, RNA-RNA interactions between the U6 snRNA and the 5'ss are established. However, we showed that the Watson-Crick base pairing between U6 and the 5'ss is not essential for stable B-like complex formation, as long as sequence complementarities between U5 loop I and the 5'ss exist (Figure 3.8). Either of these base pairing interactions might keep the 5'ss in close proximity to the U4/U6.U5 tri-snRNP until hPrp8 can engage interactions with the exon-intron junction. Such a coordinated handover of the 5'ss to hPrp8 might also explain how the spliceosome achieves the high accuracy of splice site recognition and identify *bona fide* 5'ss from the numerous pseudo sites found in any pre-mRNA. Consequently, a 5'ss has first to be recognized by the U1 snRNP to avoid that a wrong 5'ss interacts with the U4/U6.U5 tri-snRNP. The recently identified crystal structure of hPrp28 showed that the RecA domains of the DEAD box-helicase are not competent for ATP binding [Möhlmann *et al.*, 2014] and that conformational changes within the protein have to occur in order for it to bind and hydrolyze ATP. Further, it was shown that hPrp28 is only able to bind ATP in the presence of a pre-mRNA under splicing conditions and not within the U4/U6.U5 tri-snRNP, suggesting that ATP binding by hPrp28 requires the formation of a spliceosomal complex [Möhlmann *et al.*, 2014, Lagerbauer *et al.*, 1996]. The results of this study suggest that in the human spliceosome the ATPase-activity of hPrp28 is required to destabilize the interaction

between U1 snRNP and the 5'ss of the pre-mRNA in order to allow B complex formation (Figure 3.13), which is consistent with its function in yeast [Staley and Guthrie, 1999]. We would propose that hPrp28 action takes place only upon assembly of the spliceosome and does not occur in the context of a U4/U6.U5 tri-snRNP. After hPrp28-mediated displacement of U1 snRNP, the 5'ss sequence is integrated within the U4/U6.U5 tri-snRNP and a reorganization in the complex occurs, which finally results in stable U4/U6.U5 tri-snRNP binding and B complex formation.

4.15 Perspectives

The aim of this thesis was to elucidate the requirements for B complex formation and in particular the prerequisites for stable integration of the U4/U6.U5 tri-snRNP during this process. Strikingly, the results of my studies show that solely the interaction of a 5'ss sequence with a 37S complex is sufficient to stably integrate the U4/U6.U5 tri-snRNP within the complex. Here I have presented biochemical and biophysical data that shed light on the nature of the conformational change that occurs upon interaction of the U4/U6.U5 tri-snRNP with a 5'ss sequence and accompanies its stable integration within the spliceosome. Remarkably, the functional interaction of the 5'ss with the spliceosome, in particular with hPrp8, depends on a highly-specific recognition of conserved nucleotides at the exon-intron junction. These extensive changes in stability and morphology of the spliceosome occur without requirement for additional factors or ATP suggesting that changes in protein-protein interactions between factors already present in the complex, presumably U2 and U4/U6.U5 tri-snRNP proteins, account for the dramatic rearrangement of the complex. However, it is still unclear which protein-protein interactions are changed or established during B complex stabilization. Thus, further studies are needed to identify these interactions and how they are established or changed in order to support stable U4/U6.U5 tri-snRNP binding. A promising approach towards a comprehensive identification of protein-protein interactions in complex and protein-rich samples is the implementation of a technique in which protein-protein crosslinks are identified via mass spectrometry. This method is currently established in the Lührmann laboratory, together with Prof. Dr. Henning Urlaub's group, to detect interactions between spliceosomal proteins in purified and subsequently crosslinked spliceosomes. Recent progress in the sensitivity and reproducibility of the detection of protein-protein crosslinks are auspicious, such that by using this approach it is now possible to detect also the dynamics of interactions by comparing distinct assembly intermediates. Therefore, we will apply this technique to identify protein-protein interactions within spliceosomes before and after stable integration of the U4/U6.U5 tri-snRNP to determine how the spatial organization of the U4/U6.U5 tri-snRNP with respect to the U2 snRNP is changed and which factors contribute to the stabilizing effect. In this way, several additional questions could be addressed in the near future, allowing us not only to characterize in more detail the interactions between proteins

associated with U2 and the U4/U6.U5 tri-snRNP, but also to elucidate other important protein-protein interactions, such as binding partners of the B complex-specific proteins, which are recruited after stable U4/U6.U5 tri-snRNP binding, or interaction partners of the hPrp4 kinase, which might be important for its activation and release during B complex formation.

During my studies I was able to show how catalytically inactive forms of spliceosomal ATPases/helicases can potentially be used to stall spliceosome assembly at novel stages. We have identified and characterized a novel assembly intermediate that is formed prior to stable B complex formation and identification of its protein composition provided us with a comprehensive picture of changes in the protein inventory of the spliceosome during formation of a B complex. This approach may allow new insights into the assembly of the spliceosome by identification of novel intermediates and could potentially improve its structural determination. Upon stalling of the splicing cycle at a functionally distinct step, it should be possible to obtain more homogenous populations of spliceosomes in contrast to the situation when a kinetic termination of the splicing process is carried out. Structural analysis of spliceosomes in general would greatly profit from purification of more homogenous preparations of isolated spliceosomes.

5. References

- Agafonov D.E., Deckert J., Wolf E., Odenwalder P., Bessonov S., Will C.L., Urlaub H., Luhrmann R. (2011). Semiquantitative proteomic analysis of the human spliceosome via a novel two-dimensional gel electrophoresis method. *Mol Cell Biol* (13):2667-82.
- Anokhina M., Bessonov S., Miao Z., Westhof E., Hartmuth K., Luhrmann R. (2013). RNA structure analysis of human spliceosomes reveals a compact 3D arrangement of snRNAs at the catalytic core. *EMBO J* (21):2804-18.
- Ast G. (2004). How did alternative splicing evolve? *Nat Rev Genet* (5):773-782.
- Bach M., Winkelmann G., Luhrmann R. (1989). 20S small nuclear ribonucleoprotein U5 shows a surprisingly complex protein composition. *Proceedings of the National Academy of Sciences of the United States of America* (86):6038-6042.
- Barrass J.D. and Beggs J.D. (2003). Splicing goes global. *Trends Genet* (19):295-298.
- Behrens S.E. and Luhrmann R. (1991). Immunoaffinity purification of a [U4/U6.U5] tri-snRNP from human cells. *Genes & development* (5):1439-1452.
- Behzadnia N., Golas M.M., Hartmuth K., Sander B., Kastner B., Deckert J., Dube P., Will C.L., Urlaub H., Stark H., Luhrmann R. (2007). Composition and three-dimensional EM structure of double affinity-purified, human prespliceosomal A complexes. *EMBO J* (26):1737-1748.
- Berget S.M. (1995). Exon recognition in vertebrate splicing. *J Biol Chem* (270):2411-2414.
- Berglund J.A., Chua K., Abovich N., Reed R., Rosbash M. (1997). The splicing factor BBP interacts specifically with the pre-mRNA branchpoint sequence UACUAAC. *Cell* (89):781-787.
- Bessonov S., Anokhina M., Krasauskas A., Golas M.M., Sander B., Will C.L., Urlaub H., Stark H., Luhrmann R. (2010). Characterization of purified human B^{act} spliceosomal complexes reveals compositional and morphological changes during spliceosome activation and first step catalysis. *RNA* (12):2384-403.
- Black D.L. (2003). Mechanisms of alternative pre-messenger RNA splicing. *Annu Rev Biochem* (72):291-336.
- Blum H., Beier H., Gross H.J. (1987). Improved silver staining of plant proteins, RNA and DNA polyacrylamide gels. *Electrophoresis* (8):93-99.
- Boehringer D., Makarov E.M., Sander B., Makarova O.V., Kastner B., Luhrmann R., Stark H. (2004). Three-dimensional structure of a pre-catalytic human spliceosomal complex B. *Nat Struct Mol Biol* 11(5): 463-468.
- Bonnal S., Martınez C., Forch P., Bachi A., Wilm M., Valcarcel J. (2008). RBM5/Luca-15/H37 regulates Fas alternative splice site pairing after exon definition. *Mol Cell* (32):81-95.
- Brow D.A. and Guthrie C. (1988). Spliceosomal RNA U6 is remarkably conserved from yeast to mammals. *Nature* (334):213-8.
- Busch A. and Hertel K.J. (2012). Evolution of SR protein and hnRNP splicing regulatory factors. *Wiley Interdiscip Rev RNA* (3):1-12.
- Chen J.Y., Stands L., Staley J.P., Jackups R.R. Jr., Latus L.J., Chang T.H. (2001). Specific alterations of U1-C protein or U1 small nuclear RNA can eliminate the requirement of Prp28p, an essential DEAD box splicing factor. *Mol Cell* (7):227-32.

- Dalbadie-McFarland G. and Abelson J. (1990). PRP5: a helicase-like protein required for mRNA splicing in yeast. *Proceedings of the National Academy of Sciences of the United States of America* (87):4236-4240.
- Das R., Zhou Z., Reed R. (2000). Functional association of U2 snRNP with the ATP-independent spliceosomal complex E. *Mol Cell* (5):779-787.
- Deckert J., Hartmuth K., Boehringer D., Behzadnia N., Will C.L., Kastner B., Stark H., Urlaub H., Lührmann R. (2006). Protein composition and electron microscopy structure of affinity-purified human spliceosomal B complexes isolated under physiological conditions. *Mol Cell Biol* (26):5528-5543.
- Deutsch M. and Long M. (1999). Intron-exon structures of eukaryotic model organisms. *Nucleic Acids Res* (27):3219-28.
- Dignam, J.D., Lebovitz, R.M., and Roeder, R.G. 1983. Accurate transcription initiation by RNA polymerase II in a soluble extract from isolated mammalian nuclei. *Nucleic Acids Res* 11(5):1475-1489.
- Dube P., Tavares P., Lurz R., van Heel M. (1993). The portal protein of bacteriophage SPP1: a DNA pump with 13-fold symmetry. *The EMBO journal* (12):1303-1309.
- Dziembowski A., Ventura A.P., Rutz B., Caspary F., Faux C., Halgand F., Laprevote O., Seraphin B. (2004). Proteomic analysis identifies a new complex required for nuclear pre-mRNA retention and splicing. *EMBO J* (23):4847-4856.
- Fabrizio P., Dannenberg J., Dube P., Kastner B., Stark H., Urlaub H., Lührmann R. (2009). The evolutionarily conserved core design of the catalytic activation step of the yeast spliceosome. *Mol Cell* (36):593-608.
- Fica S.M., Tuttle N., Novak T., Li N.S., Lu J., Koodathingal P., Dai Q., Staley J.P., Piccirilli J.A. (2013). RNA catalyses nuclear pre-mRNA splicing. *Nature* (503):229-34.
- Fleckner J., Zhang M., Valcarcel J., Green M.R. (1997). U2AF65 recruits a novel human DEAD box protein required for the U2 snRNP-branchpoint interaction. *Genes Dev* (11):1864-1872.
- Fourmann J.B., Schmitzová J., Christian H., Urlaub H., Ficner R., Boon K.L., Fabrizio P., Lührmann R. (2013). Dissection of the factor requirements for spliceosome disassembly and the elucidation of its dissociation products using a purified splicing system. *Genes Dev* (27):413-28.
- Galej W.P., Oubridge C., Newman A.J., Nagai K. (2013). Crystal structure of Prp8 reveals active site cavity of the spliceosome. *Nature* (493):638-43.
- Golas M.M., Sander B., Bessonov S., Grote M., Wolf E., Kastner B., Stark H., Lührmann R. (2010). 3D cryo-EM structure of an active step I spliceosome and localization of its catalytic core. *Mol Cell* (40):927-38.
- Gottschalk A., Neubauer G., Banroques J., Mann M., Lührmann R., Fabrizio, P. (1999). Identification by mass spectrometry and functional analysis of novel proteins of the yeast [U4/U6.U5] tri-snRNP. *EMBO J* (18):4535-4548.
- Gozani O., Feld R., Reed R. (1996). Evidence that sequence-independent binding of highly conserved U2 snRNP proteins upstream of the branch site is required for assembly of spliceosomal complex A. *Genes Dev* (10):233-243.
- Gozani O., Potashkin J., Reed R. (1998). A potential role for U2AF-SAP 155 interactions in recruiting U2 snRNP to the branch site. *Mol Cell Biol* (18):4752-4760.
- Grote M., Wolf E., Will C.L., Lemm I., Agafonov D.E., Schomburg A., Fischle W., Urlaub H., Lührmann R. (2010). Molecular architecture of the human Prp19/CDC5L complex. *Mol Cell Biol* (30):2105-19.

- Hartmuth K., Urlaub H., Vornlocher H.P., Will C.L., Gentzel M., Wilm M., Lührmann R. (2002). Protein composition of human prespliceosomes isolated by a tobramycin affinity-selection method. *Proc Natl Acad Sci U S A* 99(26):16719-16724.
- Hegele A., Kamburov A., Grossmann A., Sourlis C., Wowro S., Weimann M., Will C.L., Pena V., Lührmann R., Stelzl U. (2012). Dynamic protein-protein interaction wiring of the human spliceosome. *Mol Cell* (45):567-80.
- Heinrichs V., Bach M., Winkelmann G., Lührmann R. (1990). U1-specific protein C needed for efficient complex formation of U1 snRNP with a 5' splice site. *Science* (247):69-72.
- House A.E. and Lynch K.W. (2006). An exonic splicing silencer represses spliceosome assembly after ATP-dependent exon recognition. *Nat Struct Mol Biol* (13):937-944.
- Ismaili N., Sha M., Gustafson E.H., Konarska M.M. (2001). The 100-kda U5 snRNP protein (hPrp28p) contacts the 5' splice site through its ATPase site. *RNA* (7):182-93.
- Izquierdo J.M., Majós N., Bonnal S., Martínez C., Castelo R., Guigó R., Bilbao D., Valcárcel J. (2005). Regulation of Fas alternative splicing by antagonistic effects of TIA-1 and PTB on exon definition. *Mol Cell* (19):475-84.
- Kastner B. (1998). Purification and Electron Microscopy of Spliceosomal snRNPs. In J. Schenkel (ed.), *RNP Particles, Splicing and Autoimmune Diseases*. Springer Lab Manual, Heidelberg. 95-140.
- Kastner B., Fischer N., Golas M.M., Sander B., Dube P., Boehringer D., Hartmuth K., Deckert J., Hauer F., Wolf E. *et al.* (2008). GraFix: sample preparation for single-particle electron cryomicroscopy. *Nat Methods* 5(1):53-55.
- Kent O.A. and MacMillan A.M. (2002). Early organization of pre-mRNA during spliceosome assembly. *Nat Struct Biol* 9(8):576-581.
- Keren H., Lev-Maor G., Ast G. (2010). Alternative splicing and evolution: diversification, exon definition and function. *Nat Rev Genet* (11):345-55.
- Kim S.H. and Lin R.J. (1996). Spliceosome activation by PRP2 ATPase prior to the first transesterification reaction of pre-mRNA splicing. *Mol Cell Biol* (16):6810-6819.
- Kohtz J.D., Jamison S.F., Will C.L., Zuo P., Lührmann R., Garcia-Blanco M.A. and Manley J.L. (1994). Protein-protein interactions and 5'-splice-site recognition in mammalian mRNA precursors. *Nature* (368):119-124.
- Konforti B.B. and Konarska M.M. (1994). U4/U5/U6 snRNP recognizes the 5' splice site in the absence of U2 snRNP. *Genes Dev* (8):1962-73.
- Laemmli U.K. (1970). Cleavage of structural proteins during the assembly of the head of bacteriophage T4. *Nature* 227(5259):680-685.
- Laggerbauer B., Lauber J., Lührmann R. (1996). Identification of an RNA-dependent ATPase activity in mammalian U5 snRNPs. *Nucleic Acids Res* (24):868-75.
- Laggerbauer B., Achsel T., Lührmann R. (1998). The human U5-200kD DEXH-box protein unwinds U4/U6 RNA duplexes in vitro. *Proc Natl Acad Sci U S A* (95):4188-4192.
- Laggerbauer B., Liu S., Makarov E., Vornlocher H.P., Makarova O., Ingelfinger D., Achsel T., Lührmann R. (2005). The human U5 snRNP 52K protein (CD2BP2) interacts with U5-102K (hPrp6), a U4/U6.U5 tri-snRNP bridging protein, but dissociates upon tri-snRNP formation. *RNA* (11):598-608.
- Lam B.J. and Hertel K.J. (2002). A general role for splicing enhancers in exon definition. *RNA* (8):1233-41.
- Lamond A.I., Konarska M.M., Sharp P.A. (1987). A mutational analysis of spliceosome assembly: evidence for splice site collaboration during spliceosome formation. *Genes Dev* 1(6):532-543.

- Lauber J., Fabrizio P., Teigelkamp S., Lane W.S., Hartmann E., Lührmann R. (1996). The HeLa 200 kDa U5 snRNP-specific protein and its homologue in *Saccharomyces cerevisiae* are members of the DEXH-box protein family of putative RNA helicases. *EMBO J* (15):4001-15.
- Lauber J., Plessel G., Prehn S., Will C.L., Fabrizio P., Groning K., Lane W.S., Lührmann R. (1997). The human U4/U6 snRNP contains 60 and 90kD proteins that are structurally homologous to the yeast splicing factors Prp4p and Prp3p. *RNA* (3):926-941.
- Le Hir H. and Séraphin B. (2008). EJC at the heart of translational control. *Cell* (133):213-6.
- Lee K.M., Hsu I.a.W., Tarn W.Y. (2010). TRAP150 activates pre-mRNA splicing and promotes nuclear mRNA degradation. *Nucleic Acids Res* (38):3340-50.
- Lim S.R. and Hertel K.J. (2004). Commitment to splice site pairing coincides with A complex formation. *Mol Cell* (15):477-83.
- Lopez P.J. and Seraphin B. (1999). Genomic-scale quantitative analysis of yeast pre-mRNA splicing: implications for splice-site recognition. *RNA* (5):1135-1137.
- Lührmann R. and Stark H. (2009). Structural mapping of spliceosomes by electron microscopy. *Curr Opin Struct Biol* 19(1):96-102.
- Maeder C., Kutach A.K., Guthrie C. (2009). ATP-dependent unwinding of U4/U6 snRNAs by the Brr2 helicase requires the C terminus of Prp8. *Nat Struct Mol Biol* (16):42-8.
- Makarov E.M., Makarova O.V., Urlaub H., Gentzel M., Will C.L., Wilm M., Lührmann R. (2002). Small nuclear ribonucleoprotein remodeling during catalytic activation of the spliceosome. *Science* (298):2205-2208.
- Makarova O.V., Makarov E.M., Lührmann, R. (2001). The 65 and 110 kDa SR-related proteins of the U4/U6.U5 tri-snRNP are essential for the assembly of mature spliceosomes. *EMBO J* (20):2553-2563.
- Makarova O.V., Makarov E.M., Liu S., Vornlocher H.P., Lührmann R. (2002). Protein 61K, encoded by a gene (PRPF31) linked to autosomal dominant retinitis pigmentosa, is required for U4/U6*U5 tri-snRNP formation and pre-mRNA splicing. *EMBO J* (21):1148-1157.
- Makarova O.V., Makarov E.M., Urlaub H., Will C.L., Gentzel M., Wilm M., Lührmann R. (2004). A subset of human 35S U5 proteins, including Prp19, function prior to catalytic step 1 of splicing. *EMBO J* (23):2381-2391.
- Martin A., Schneider S., Schwer B. (2002). Prp43 is an essential RNA-dependent ATPase required for release of lariat-intron from the spliceosome. *J Biol Chem* (277):17743-50.
- Matera A.G., Terns R.M., Terns M.P. (2007). Non-coding RNAs: lessons from the small nuclear and small nucleolar RNAs. *Nat Rev Mol Cell Biol.* (8):209-20.
- Matera A.G. and Wang Z. (2014). A day in the life of the spliceosome. *Nat Rev Mol Cell Biol* (15):108-21.
- Mathew R., Hartmuth K., Mohlmann S., Urlaub H., Ficner R., Lührmann R. (2008). Phosphorylation of human PRP28 by SRPK2 is required for integration of the U4/U6-U5 tri-snRNP into the spliceosome. *Nat Struct Mol Biol* (15):435-443.
- McPheeters D.S. and Muhlenkamp P. (2003). Spatial organization of protein-RNA interactions in the branch site-3' splice site region during pre-mRNA splicing in yeast. *Mol Cell Biol* (23):4174-86.
- Meister G., Hannus S., Plottner O., Baars T., Hartmann E., Fakan S., Laggerbauer B., Fischer U. (2001). SMNrp is an essential pre-mRNA splicing factor required for the formation of the mature spliceosome. *EMBO J* (20):2304-2314.

- Möhlmann S., Mathew R., Neumann P., Schmitt A., Lührmann R., Ficner R. (2014). Structural and functional analysis of the human spliceosomal DEAD-box helicase Prp28. *Acta Crystallogr D Biol Crystallogr* (70):1622-30.
- Moore M.J. and Sharp P.A. (1993). Evidence for two active sites in the spliceosome provided by stereochemistry of pre-mRNA splicing. *Nature* (365):364-368.
- Mozaffari-Jovin S., Santos K.F., Hsiao H.H., Will C.L., Urlaub H., Wahl M.C., Lührmann R. (2012). The Prp8 RNase H-like domain inhibits Brr2-mediated U4/U6 snRNA unwinding by blocking Brr2 loading onto the U4 snRNA. *Genes Dev* (26):2422-34.
- Mozaffari-Jovin S., Wandersleben T., Santos K.F., Will C.L., Lührmann R., Wahl M.C. (2013). Inhibition of RNA helicase Brr2 by the C-terminal tail of the spliceosomal protein Prp8. *Science* (341):80-4.
- Newman A.J. and Nagai K. (2010). Structural studies of the spliceosome: blind men and an elephant. *Curr Opin Struct Biol* (20):82-9.
- Nilsen T.W. (1998). RNA-RNA interactions in nuclear pre-mRNA splicing. In *RNA structure and function* (Cold Spring Harbor, NY: Cold Spring Harbor Laboratory Press).
- Ohr T., Odenwälder P., Dannenberg J., Prior M., Warkocki Z., Schmitzová J., Karaduman R., Gregor I., Enderlein J., Fabrizio P., Lührmann R. (2013). Molecular dissection of step 2 catalysis of yeast pre-mRNA splicing investigated in a purified system. *RNA* (19):902-15.
- Pabis M., Neufeld N., Steiner M.C., Bojic T., Shav-Tal Y., Neugebauer K.M. (2013). The nuclear cap-binding complex interacts with the U4/U6-U5 tri-snRNP and promotes spliceosome assembly in mammalian cells. *RNA* (19):1054-63.
- Pena V., Rozov A., Fabrizio P., Lührmann R., Wahl M.C. (2008). Structure and function of an RNase H domain at the heart of the spliceosome. *EMBO J* 27(21):2929-2940.
- Pomeranz Krummel D.A., Oubridge C., Leung A.K., Li J., Nagai K. (2009). Crystal structure of human spliceosomal U1 snRNP at 5.5 Å resolution. *Nature* 458(7237):475-480.
- Pyle A.M. and Lambowitz A.M. (2006). Group II Introns: Ribozymes That Splice RNA and Invade DNA. *The RNA World* (Cold Spring Harbor Laboratory Press, Cold Spring Harbor, NY, ed 3)
- Query C.C., Moore M.J., Sharp P.A. (1994). Branch nucleophile selection in pre-mRNA splicing: evidence for the bulged duplex model. *Genes & development* (8):587-597.
- Ragunathan P.L. and Guthrie C. (1998). RNA unwinding in U4/U6 snRNPs requires ATP hydrolysis and the DEIH-box splicing factor Brr2. *Curr Biol* (8):847-855.
- Rappsilber J., Ajuh P., Lamond A.I., Mann M. (2001). SPF30 is an essential human splicing factor required for assembly of the U4/U5/U6 tri-small nuclear ribonucleoprotein into the spliceosome. *J Biol Chem* (276):31142-31150.
- Rappsilber J., Ryder U., Lamond A.I., Mann M. (2002). Large-scale proteomic analysis of the human spliceosome. *Genome Res* (12):1231-1245.
- Reyes J.L., Kois P., Konforti B.B., Konarska M.M. (1996). The canonical GU dinucleotide at the 5' splice site is recognized by p220 of the U5 snRNP within the spliceosome. *RNA* (2):213-25.
- Reyes J.L., Gustafson E.H., Luo H.R., Moore M.J., Konarska M.M. 1999. The C-terminal region of hPrp8 interacts with the conserved GU dinucleotide at the 5' splice site. *RNA* 5(2):167-179.
- Ritchie D.B., Schellenberg M.J., Gesner E.M., Raithatha S.A., Stuart D.T., Macmillan A.M. (2008). Structural elucidation of a PRP8 core domain from the heart of the spliceosome. *Nat Struct Mol Biol* (15):1199-1205.
- Roscigno R.F. and Garcia-Blanco M.A. (1995). SR proteins escort the U4/U6.U5 tri-snRNP to the spliceosome. *RNA* (1):692-706.

- Ruby S.W. and Abelson J. (1991). Pre-mRNA splicing in yeast. *Trends Genet* (7):79-85.
- Ruskin B., Zamore P.D., Green M.R. (1988). A factor, U2AF, is required for U2 snRNP binding and splicing complex assembly. *Cell* (52):207-219.
- Sambrook J., Fritsch E.F., Maniatis T. (1989). *Molecular Cloning. A Laboratory Manual*, 2nd ed. Cold Spring Harbor Laboratory Press, Cold Spring Harbor, NY.
- Schaffert N., Hossbach M., Heintzmann R., Achsel T., Lührmann R. (2004). RNAi knockdown of hPrp31 leads to an accumulation of U4/U6 di-snRNPs in Cajal bodies. *EMBO J* (23):3000-3009.
- Schellenberg M.J., Wu T., Ritchie D.B., Fica S., Staley J.P., Atta K.A., LaPointe P., MacMillan A.M. (2013). A conformational switch in PRP8 mediates metal ion coordination that promotes pre-mRNA exon ligation. *Nat Struct Mol Biol* (20):728-34.
- Schneider M., Will C.L., Anokhina M., Tazi J., Urlaub H., Lührmann R. (2010a). Exon definition complexes contain the tri-snRNP and can be directly converted into B-like precatalytic splicing complexes. *Mol Cell* (38):223-35.
- Schneider M., Hsiao H.H., Will C.L., Giet R., Urlaub H., Lührmann R. (2010b). Human PRP4 kinase is required for stable tri-snRNP association during spliceosomal B complex formation. *Nat Struct Mol Biol* 17(2):216-221.
- Schwer B. and Guthrie C. (1992). A conformational rearrangement in the spliceosome is dependent on PRP16 and ATP hydrolysis. *EMBO J* (11):5033-5039.
- Ségault V., Will C.L., Polycarpou-Schwarz M., Mattaj I.W., Branlant C., Lührmann R. (1999). Conserved loop I of U5 small nuclear RNA is dispensable for both catalytic steps of pre-mRNA splicing in HeLa nuclear extracts. *Mol Cell Biol* (19):2782-90.
- Semlow D.R. and Staley J.P. (2012). Staying on message: ensuring fidelity in pre-mRNA splicing. *Trends Biochem Sci* (37):263-73.
- Sha M., Levy T., Kois P., Konarska M.M. (1998). Probing of the spliceosome with site-specifically derivatized 5' splice site RNA oligonucleotides. *RNA* (4):1069-82.
- Sharma S., Kohlstaedt L.A., Damianov A., Rio D.C., Black D.L. (2008). Polypyrimidine tract binding protein controls the transition from exon definition to an intron defined spliceosome. *Nat Struct Mol Biol* (15):183-191.
- Shevchenko A., Wilm M., Vorm O., Mann M. (1996). Mass spectrometric sequencing of proteins silver-stained polyacrylamide gels. *Analytical chemistry* (68):850-858.
- Small E.C., Leggett S.R., Winans A.A., Staley J.P. (2006). The EF-G-like GTPase Snu114p regulates spliceosome dynamics mediated by Brr2p, a DEXD/H box ATPase. *Mol Cell* (23):389-399.
- Sontheimer E.J. and Steitz J.A. (1993). The U5 and U6 small nuclear RNAs as active site components of the spliceosome. *Science* (262):1989-96.
- Spingola M., Grate L., Haussler D., Ares M.Jr. (1999). Genome-wide bioinformatic and molecular analysis of introns in *Saccharomyces cerevisiae*. *RNA* (5):221-234.
- Staley J.P. and Guthrie C. (1998). Mechanical devices of the spliceosome: motors, clocks, springs, and things. *Cell* (92):315-326.
- Staley J.P. and Guthrie C. (1999). An RNA switch at the 5' splice site requires ATP and the DEAD box protein Prp28p. *Mol Cell* (3):55-64.
- Sterner D.A., Carlo T., Berget S.M. (1996). Architectural limits on split genes. *Proc Natl Acad Sci U S A* (93):15081-5.
- Tarn W.Y., Hsu C.H., Huang K.T., Chen H.R., Kao H.Y., Lee K.R., Cheng S.C. (1994). Functional association of essential splicing factor(s) with PRP19 in a protein complex. *EMBO J* (13):2421-2431.

- Teigelkamp S., Newman A.J., Beggs J.D. (1995a). Extensive interactions of PRP8 protein with the 5' and 3' splice sites during splicing suggest a role in stabilization of exon alignment by U5 snRNA. *EMBO J* 14(11):2602-2612.
- Teigelkamp S., Whittaker E., Beggs J.D. (1995b). Interaction of the yeast splicing factor PRP8 with substrate RNA during both steps of splicing. *Nucleic Acids Res* (23):320-6.
- Teigelkamp S., Mundt C., Achsel T., Will C.L., Lührmann R. (1997). The human U5 snRNP-specific 100-kD protein is an RS domain-containing, putative RNA helicase with significant homology to the yeast splicing factor Prp28p. *RNA* (3):1313-26.
- Toor N., Keating K.S., Taylor S.D., Pyle A.M. (2008). Crystal structure of a self-spliced group II intron. *Science* (320):77-82.
- Tsai R.T., Fu R.H., Yeh F.L., Tseng C.K., Lin Y.C., Huang Y.H., Cheng S.C. (2005). Spliceosome disassembly catalyzed by Prp43 and its associated components Ntr1 and Ntr2. *Genes Dev* (19):2991-3003.
- Turner I.A., Norman C.M., Churcher M.J., Newman A.J. (2004). Roles of the U5 snRNP in spliceosome dynamics and catalysis. *Biochem Soc Trans* (32):928-31.
- Valcarcel J., Gaur R.K., Singh R., Green M.R. (1996). Interaction of U2AF65 RS region with pre-mRNA branch point and promotion of base pairing with U2 snRNA [corrected]. *Science* (273):1706-1709.
- Van Heel M. (1989). Classification of very large electron microscopical image data sets. *Optik* (82):114-126.
- Van Heel M. and Frank J. (1981). Use of multivariate statistics in analysing the images of biological macromolecules. *Ultramicroscopy* (6):187-194.
- Van Heel M., Harauz G., Orlova E.V., Schmidt R., Schatz M. (1996). A new generation of the IMAGIC image processing system. *J Struct Biol* (116):17-24.
- Varia S., Potabathula D., Deng Z., Bubulya A., Bubulya P.A. (2013). Btf and TRAP150 have distinct roles in regulating subcellular mRNA distribution. *Nucleus* (4):229-40.
- Wahl M.C., Will C.L., Lührmann R. (2009). The spliceosome: design principles of a dynamic RNP machine. *Cell* (136):701-718.
- Wang E.T., Sandberg R., Luo S., Khrebtkova I., Zhang L., Mayr C., Kingsmore S.F., Schroth G.P., Burge C.B. (2008). Alternative isoform regulation in human tissue transcriptomes. *Nature* (456):470-6.
- Warkocki Z., Odenwalder P., Schmitzova J., Platzmann F., Stark H., Urlaub H., Ficner R., Fabrizio P., Lührmann R. (2009). Reconstitution of both steps of *Saccharomyces cerevisiae* splicing with purified spliceosomal components. *Nat Struct Mol Biol* (16):1237-1243.
- Wassarman D.A. and Steitz J.A. (1992). Interactions of small nuclear RNA's with precursor messenger RNA during in vitro splicing. *Science* (257):1918-1925.
- Weber G., Trowitzsch S., Kastner B., Lührmann R., Wahl M.C. (2010). Functional organization of the Sm core in the crystal structure of human U1 snRNP. *EMBO J* (29):4172-84.
- Will C.L., Schneider C., MacMillan A.M., Katopodis N.F., Neubauer G., Wilm M., Lührmann R., Query C.C. (2001). A novel U2 and U11/U12 snRNP protein that associates with the pre-mRNA branch site. *EMBO J* (20):4536-4546.
- Will C.L., Urlaub H., Achsel T., Gentzel M., Wilm M., Lührmann R. (2002). Characterization of novel SF3b and 17S U2 snRNP proteins, including a human Prp5p homologue and an SF3b DEAD-box protein. *EMBO J* (21):4978-4988.
- Will C.L. and Lührmann R. (2005). Splicing of a rare class of introns by the U12-dependent spliceosome. *Biol Chem* (386):713-724.

- Will C.L. and Lührmann R. (2011). Spliceosome structure and function. *Cold Spring Harb Perspect Biol.* 3(7):a003707.
- Wolf E., Kastner B., Deckert J., Merz C., Stark H., Lührmann R. (2009). Exon, intron and splice site locations in the spliceosomal B complex. *EMBO J* 28(15):2283-2292.
- Wolf E., Kastner B., Lührmann R. (2012). Antisense-targeted immuno-EM localization of the pre-mRNA path in the spliceosomal C complex. *RNA* (18):1347-57.
- Xie J., Beickman K., Otte E., Rymond B.C. (1998). Progression through the spliceosome cycle requires Prp38p function for U4/U6 snRNA dissociation. *EMBO J* (17):2938-2946.
- Yean S.L., Wuenschell G., Termini J., Lin R.J. (2000). Metal-ion coordination by U6 small nuclear RNA contributes to catalysis in the spliceosome. *Nature* (408):881-884.
- Zhang M.Q. (1998). Statistical features of human exons and their flanking regions. *Hum Mol Genet* (7):919-932.
- Zillmann M., Zapp M.L., Berget S.M. (1988). Gel electrophoretic isolation of splicing complexes containing U1 small nuclear ribonucleoprotein particles. *Mol Cell Biol* (8):814-21.

6. Appendix

6.1 Abbreviations

2'O-me	2'O-ribose methylated
3'ss	3'splice site
5'ss	5'splice site
A	Adenosine / ampere
aa	Amino acid
Amp	Ampicillin
APS	Ammonium peroxodisulfate
ATP	Adenosine triphosphate
BCA	Bicinchoninic acid
bp	Base pair
BP	Branch point
BPS	Branch point sequence
BSA	Bovine serum albumin
°C	Degree celsius
C	Cytosine
CTP	Cytosine triphosphate
<i>C. elegans</i>	<i>Caenorhabditis elegans</i>
Ci	Curie
cm	Centimeter
cpm	Counts per minute
Da	Dalton
dd	Double distilled
DExD/H	Consensus sequence of helicases
DMSO	Dimethyl sulfoxide
DNA	Desoxyribonucleic acid
<i>D. melanogaster</i>	<i>Drosophila melanogaster</i>
DTT	Dithiothreitol
ECL	Enhanced chemiluminescence
<i>E. coli</i>	<i>Escherichia coli</i>
EDTA	Ethylendiaminetetraacetate
EJC	Exon junction complex
EM	Electron microscopy
ESE	Exonic splicing enhancer
ESS	Exonic splicing silencer
<i>et al.</i>	<i>Et alii</i>

f	Femto
G	Guanosine
g	Gram / centrifugal force
GTP	Guanosine triphosphate
<i>H. sapiens</i>	<i>Homo sapiens</i>
h	Hour / human
HCl	Hydrochloric acid
HEPES	N-2-Hydroxyethylpiperazin-N-2-ethansulfonic acid
hn	Heterogenous nuclear
ILS	Internal-stem loop
ISE	Intronic splicing enhancer
ISS	Intronic splicing silencer
J	Joule
k	Kilo
kDa	Kilodalton
l	Liter
LB	Luria Bertani
LC	Liquid chromatography
Lsm	Like-Sm
M	Molar
m	Milli / meter
μ	Micro
min	Minutes
mM	Millimolar
mRNA	Messenger RNA
MS	Mass spectrometry
MW	Molecular weight
n	Nano
NTP	Nucleoside triphosphate
nts	Nucleotides
OD	Optical density
P	Phosphate
p	Pico
PAGE	Polyacrylamide gel-electrophoresis
PCI	Phenol-chloroform-isoamyl alcohol
pH	Preponderance of hydrogen ions
PMSF	Phenylmethylsulfonylfluoride
PPT	Polypyrimidine tract
Pre-mRNA	Precursor-mRNA
%	Percent

Py	Pyrimidine base
R	Purine base
RES	Retention and splicing
RNA	Ribonucleic acid
RNase	Ribonuclease
RNP	Ribonucleoprotein
rpm	Revolutions per minute
RRM	RNA recognition motif
RT	Room temperature
S	Svedberg unit
s	Second
<i>S. cerevisiae</i>	<i>Saccharomyces cerevisiae</i>
SDS	Sodium dodecylsulfate
Sm	'Smith', patient in which Sm proteins were first discovered
sn	Small nuclear
snRNA	Small nuclear ribonucleic acid
snRNP	Small nuclear ribonucleoparticles
SR	Serine arginine rich
TEMED	N, N, N', N'-Tetramethylethylenediamine
Tris	Tris-(hydroxymethyl)-aminomethane
tRNA	Transfer RNA
U	Uridine / unit
U snRNA	Uridine rich small nuclear RNA
U snRNP	Uridine rich small nuclear ribonucleoparticles
UTP	Uridine triphosphate
UV	Ultraviolet
V	Volt
Vol	Volume
v/v	Volume per volume
W	Watts
w/v	Weight per volume
Y	Pyrimidine base

6.2 Danksagung

An dieser Stelle möchte ich mich ganz herzlich bei all denen bedanken, die mich während dieser Arbeit unterstützt und motiviert haben.

Prof. Dr. Reinhard Lührmann danke ich für die Zeit, die ich in einer ausgezeichneten wissenschaftlichen Umgebung an diesem spannenden Projekt arbeiten durfte. Ich bedanke mich für all die Energie, die er in mein Projekt investiert hat, für seine unermüdliche Motivation und für alles, was ich von ihm als großartigen Mentor lernen durfte.

Mein ganz besonderer Dank gilt Dr. Cindy Will für die unzähligen Antworten auf all meine Fragen, die zahlreichen Diskussionen und all die Hilfestellungen, die sie mir gegeben hat. Sie hat dieses Projekt durch ihre Ideen, ihre Anregungen und ihre konstruktive Kritik sehr bereichert.

Ein herzliches Dankeschön geht an die Mitglieder meines Thesis Committees und die weiteren Mitglieder meines Prüfungsausschusses: Prof. Dr. Henning Urlaub, Prof. Dr. Markus Zweckstetter, Prof. Dr. Ralf Ficner, Prof. Dr. Holger Stark und Dr. Claudia Höbartner.

Ein großes Dankeschön geht auch an Dr. Berthold Kastner und Dr. Norbert Rigo für die angenehme Zusammenarbeit und ihre Hilfe zur Elektronen-mikroskopischen Untersuchung der Spleißosomen.

Dr. Dmitry Agafonov danke ich für seine Hilfe bei der Analyse meiner Proben mittels 2D Gelelektrophorese und die vielen konstruktiven Anmerkungen.

Monika Raabe und Uwe Pleßmann danke ich für die Durchführung der vielen MS-Analysen.

Meinen Kollegen Cornelius, Norbert, Stefanie, Nicolas, Thomas, Julia und Peter gilt ein besonderer Dank. Sie haben mich vom ersten Tage an in ihrer Mitte aufgenommen und sind mir schnell sehr ans Herz gewachsen. Danke für die tolle Zeit und all den Spaß, den wir zusammen hatten!

Ein großes Dankeschön geht auch an Gabi, Irene, Uschi, Gertrud, Claudia, Kami, Juliane und all den anderen helfenden Händen der Abteilung, die nicht weniger wichtig waren für die erfolgreiche Durchführung meiner Doktorarbeit.

Aus tiefstem Herzen bedanke ich mich bei allen lieben Menschen, die mich in den letzten Jahren auch außerhalb des Labors begleitet haben. Zu Beginn bedanke ich bei meinen Freunden, die mich nicht nur tatkräftig unterstützt haben, sondern mich stets aufbauten und für die erforderliche Abwechslung sorgten.

Leo danke ich für ihre unzähligen aufbauende Worte und die großartige Unterstützung, die sie mir während dieser Arbeit gestiftet hat.

Meinem Bruder Benjamin danke ich für die unzähligen Ratschläge und die große Hilfe, die er mir ein Leben lang hat zukommen lassen. Er ist mir ein großes Vorbild in allen Lebenslagen.

Insbesondere möchte ich mich bei meinen Eltern Günter und Jutta bedanken, die in jeglicher Hinsicht den Grundstein für meinen Weg gelegt haben. Ohne ihr unerschöpfliches Vertrauen, ihr grenzenloses Verständnis und ihre unermüdliche Hilfe wäre mein Studium und diese Doktorarbeit niemals möglich gewesen. Danke.

6.3 Curriculum vitae

Carsten Boesler

Date of birth: March 31th 1986

Place of birth: Homberg (Efze), Germany

Education

1992-1998	Georg-August-Zinn-Schule Morschen
1998-2002	Burgsitzschule Spangenberg
2002-2005	Geschwister-Scholl-Schule Melsungen, Abitur July 2005

University

2005-2010	Diploma in biology, Universität Kassel Major subject: Genetics 1. Minor subject: Biochemistry 2. Minor subject: Cell biology Oral examination: December 2009 Diploma thesis: „rRNA in <i>Dictyostelium</i> “ at the Heisenberg Research Group Ribogenetics, Darmstadt January-September 2010 Supervisor: PD. Dr. Christian Hammann
-----------	--

PhD

2010-2014	PhD project in the laboratory of Prof. Dr. R. Lührmann, Department of Cellular Biochemistry, Max Planck Institute for Biophysical Chemistry, Göttingen, Germany Title: „Requirements for pre-catalytic B complex formation during exon- and intron-defined spliceosome assembly“
-----------	---

Publication

Boesler C., Kruse J., Söderbom F., Hammann C. (2011). Sequence and generation of mature ribosomal RNA transcripts in *Dictyostelium discoideum*. *The Journal of Biological Chemistry* (20): 17693-17703.

Meetings

“19th Annual meeting of The RNA Society”, 2014, Quebec City (Kanada)

Talk with the title: **“An early assembly intermediate containing tri-snRNP forms during both exon- and intron-defined splicing, and its conversion to a stable B complex involves structural rearrangements triggered by tri-snRNP/5’splice site interaction”**.

“10th International PhD student symposium Horizons in Molecular Biology”, 2013, Göttingen

Poster presentation with the title: **“Structure and composition of exon definition complexes”**.